BIOMATERIAL AND GENETIC TOOLS TO INFLUENCE NEURONAL NETWORK FORMATION, EXCITABILITY, AND MATURITY AT THE ELECTRODE INTERFACE

By

Mónica B. Setién-Grafals

A DISSERTATION

Submitted to
Michigan State University
in partial fulfillment of the requirements
for the degree of

Biomedical Engineering – Doctor of Philosophy

2020

ABSTRACT

BIOMATERIAL AND GENETIC TOOLS TO INFLUENCE NEURONAL NETWORK FORMATION, EXCITABILITY, AND MATURITY AT THE ELECTRODE INTERFACE

By

Mónica B. Setién-Grafals

Understanding brain function remains a grand challenge of our time. Likewise, when neurodegeneration occurs, repair efforts are limited due to the highly heterogeneous and interconnected nature of the cerebral cortex. The drive to better understand normal brain function and pathological states has intensified demand for new technologies which can interrogate the nervous system with enhanced spatiotemporal resolution. Implanted brain electrodes are being used and developed to provide a deeper understanding for neurological injury and neurodegeneration. However, issues with biological integration come into play and potentially interfere with signal stability over time. Here, this work provides innovative tools that can be used to interface and control the tissue-electrode interface. In particular, we are interested in exploring surface chemistries, genetic tools, and electrode materials which favor neural regeneration around implanted electrodes.

The research presented in this dissertation describes the exploration of biomaterial and genetic tools for interfacing the tissue-electrode interface: (1) characterization of surface chemistries presented to differentiating neural progenitors, and an understanding of the conditions which promote neurite outgrowth and electrophysiological maturation, (2) a blue-light inducible gene expression system, which could potentially be used to control gene expression at the implanted electrode interface, and (3) testing the impacts of "next-generation" electrode materials, such as diamond, as candidates for neural interfacing. Chapter 2 uncovers the study of various

common substrates and their effects on rat neural progenitor cells, which can be used to create unique morphologies. Chapter 3 explores the use of an optogenetic system from a bacterial transcription factor (EL222) that allows for blue light-dependent transcriptional activation. Here, we validated the use of EL222 for spatial patterning of fluorescent reporter genes and developed stable expression in HEK293 cells, which can be used long-term for developing approaches for light-driven regeneration of neural circuitry. Chapter 4 reveals material and genetic factors that can affect cell structure and function. Here, we report the results of an initial characterization of the biocompatibility of the novel diamond-based materials, including conductive boron-doped polycrystalline diamond (BDD) and insulating polycrystalline diamond (PCD). The results presented will inform the transfer of the novel diamond substrate materials to sensing applications in the *in vivo* environment, where we expect to leverage the positive performance characteristics of the diamond materials displayed *in vitro*.

Taken together, these chapters offer significant development of material and biological tools and that will help manage and mitigate challenges presented at the tissue-electrode interface. Future directions aim at exploring synergistic effects of electrode material and optogenetic control for controlling excitability and identity of cells at the interface, effectively bridging the divide between electronics and tissue.

To my parents and my beloved family: my mom Claribel, my late father Rafael, my sister Paola, and my other half, Mateo, whose unyielding love, support and encouragement have proved invaluable.

ACKNOWLEDGEMENTS

I would firstly thank my advisor, Dr. Erin Purcell, whose incredible guidance and support has enabled me to be in this position. When I first met her, her passion for neural engineering was vibrant and since joining the REIL lab, as her second graduate student, she quickly became a mentor and motor for my achievements as a student and professional. She devoted immeasurable time and energy to teach me laboratory, research, and writing techniques and tools, while pushing me to be and do my best. She has provided me with teaching and mentoring experiences in the classroom and in the lab, while also furthering my professional skillset by encouraging conference attendance and participation, as well as collaboration with multidisciplinary teams. Since day one, she has been nothing but supportive of my goals without question. Without her leadership and persistent help this dissertation would not have been possible. I would also like to thank Dr. Wen Li, Dr. Ripla Arora, and Dr. Zhen Qui, my committee, who has provided great support and advice throughout my PhD candidacy.

In addition, a thank you to Dr. Steve Suhr and Dr. Marie-Claude Senut for their invaluable guidance and support for many experiments and manuscripts since the beginning. Steve has been there through all the ups and downs and his expertise in molecular biology and beyond have shaped key elements of my research shown here. Marie-Claude has provided me with key techniques and insights, for which my chapter on neural progenitor cells could have not been possible. Together, as a power couple, they have taught me, not only what being an extraordinary scientist is, but also what life is all about.

Next, I would like to thank individuals who directly contributed my work. Nathan Blanke, who provided exceptional MATLAB scripts for data analysis, Arduino codes, and 3D

printed parts for Chapter 3, as well as many insights, I'm grateful for your hard work. Kylie Smith contributed to many aspects of my work by quickly mastering various techniques in the lab. Her contributions were invaluable; I am very grateful and eager to see your own dissertation soon. Kaleb Howard contributed to data analysis for Chapter 2, Hasan Fiaz contributed to data analysis for Chapter 4. Dr. Wasif Khan (of Dr. Li's group) was an invaluable contributor and collaborator for the micro-LEDs development used in the work shown here.

I would like to thank the rest of REIL lab who over the years have provided intellectual contributions formally during our lab meeting discussions or informally during lunch or late days at the lab. Especially, Joseph Salatino, who guided me through many aspects of the BME program and the lab, Cort Thompson who has been here since day zero, providing great feedback and support, and Bailey Winter, who always showed up with a smile and a story to tell.

I wish to express my gratitude towards Dr. Percy Pierre, who made it possible for me to be here today. My cousin, Emmanuelle Merced, who introduced me to him, I'm forever grateful for the opportunity to learn about the BME program at MSU.

Finally, I would like to thank my entire family and extended family for their outstanding love and support.

TABLE OF CONTENTS

LIST OF TABLES

LIST OF FIGURES

1. CHAPTER 1 | Introduction

1.1 Principles of neural engineering

1.1.1 A brief history of neurophysiology

Physiologists in the 18th century observed "fine vessels" within a nerve as they explored the mechanisms of how nerves function. In 1794-1797, Luigi Galvani first demonstrated the propagation of an action potential by stimulating two frog legs attached by sciatic nerves, which resulted in a contraction for both legs once the nerve was in contact with the nerve or muscle of the second leg. Later, Ramón y Cajal discovered that a bird's brain was composed of individual cells touching each other by means of a staining protocol named after its developer, Golgi's method (Golgi, 1875). This experiment led to the concept that the nervous system is composed of neurons that behave as biochemically distinct cells: the "neuron doctrine" (Ramón y Cajal, 1888).

Around the same period, basic science experiments began to interrogate the function of neurons in parallel with structural studies. The first resting action potentials were recorded from frog sciatic nerves by using a differential rheotome (Bernstein, 1868). In 1939, Hodgkin and Huxley performed the first intracellular recording of a single neurons in the squid giant axon and a glass microelectrode. While using voltage clamp, Hodgkin and Huxley also manipulated the quantities present of different ions in the extracellular fluid leading to the determination of exact sodium and potassium ions that contribute during an action potential (Hodgkin and Huxley, 1952). This fundamental work provided a foundation for invasive and non-invasive electrodes to be developed and utilized to record or modulate neural activity with high temporal resolution in humans.

1.1.2 Brain-machine interfaces and invasive recordings

Electrophysiological signals became key in exploring the function of the motor cortex and for using its output to control devices externally. This was made possible due to advances in microelectrode technologies in combination with the use of extracellular electrophysiology. Multi-electrode arrays were developed in the 1950s to record and modulate neural activity (Green, 1958; Strumwasser, 1958) and are continuously evolving towards chronic, large-scale recordings and stimulation paradigms (Krüger and Bach, 1981). Neural interface technologies were employed to be a part of researchers' toolkit for studying how the brain functions. Early investigators believed that the primary motor cortex was the location where muscle activation initiated (Carlson and Devinsky, 2009; Ferrier, 1873). It was later discovered by Georgopoulos and his colleagues (Georgopoulos et al., 1982) that the discharge pattern of cortical neurons was directionally tuned by recording the activity of single cells from the motor cortex of monkeys while they made movements with their arm in different two-dimensional directions.

Shortly after, the population vector method was developed to investigate the relationship between the neural activity in the motor cortex and the direction of arm movements in two- and three-dimensional spaces. This allowed the movement trajectory to be extracted from a recording of neural activity and provided a framework for future neuroprosthetic control (Georgopoulos et al., 1986). Monkeys were trained to make point-to-point movements from a center starting position while neurons were recorded during the task. With this experiment, it was discovered that neurons have mean discharge rates that were highest for the one preferred direction and tapered off in directions away from the preferred direction. Additionally, in 1978, Schmidt et al. successfully implanted chronic microelectrodes into monkeys' motor cortex and demonstrated that they were

capable of controlling firing rates (Schmidt et al., 1978), which was a key step in the development of brain machine interfaces (also known as neural prosthesis).

Advances in microfabrication led silicon probes to be standard tools for in vivo electrophysiology. The Michigan array was created as a multielectrode array to access extracellular recordings at desired cortical depths due to it planar shape and multiple electrode sites placed along the shank (Hoogerwerf and Wise, 1994) (Figure 1C). The "Utah Intracortical Electrode Array" (UIEA) was developed shortly thereafter in 1992 (Rousche and Normann, 1999). This Utah multielectrode array has the capacity to access the columnar structure of the cerebral cortex for various applications and aimed at improving depth resolution of the electrode. These devices have provided a leading path for recording neural activity and decoding of information that leads to accurate predictions of arm movements that are used in brain machine interfaces (BMIs) (Figure 1B).

The first clinical study of brain-machine interfaces, famously known as BrainGate, were first reported in 2006 were a human with tetraplegia was able to control a computer cursor by thinking about the action (Hochberg et al., 2006); by 2012 researchers were able to restore 7-degres of freedom of a paralyzed human (Hochberg et al., 2012). By 2017, BrainGate researchers have enabled arm movement on a quadriplegic man via functional electrical stimulation of the peripheral muscles and nerves while his movements were controlled by an intracortical brain-computer interface (Ajiboye et al., 2017). Previous pivotal work describing cosine tuning of neurons (Churchland and Shenoy, 2007), alongside the detection of sensory feedback for motor

cortex modulation (Hatsopoulos and Suminski, 2011; Suminski et al., 2010) led to the first BrainGate studies that continue to this date.

Implantable devices continue to be emerging tools for clinical settings to enable direct communication between the brain and machine being controlled. Neural probes for research applications allow recordings of neural activity, which pave the way for understanding cellular pathways at the electrode-tissue interface (Hochberg et al., 2006; Laxton et al., 2010; Moore and Shannon, 2009; Rosin et al., 2011; Simeral et al., 2011). Microelectrode arrays demonstrate to be of great potential for understanding and treating neurological disorders, however, issues remain regarding stability and long-term recording due to foreign body response that occurs after implantation as well as mechanical and electrical failures of the electrode itself (Eles et al., 2018; Purcell et al., 2009; Salatino et al., 2017a). Signal loss over time is a part of the difficulties of electrode recordings aligned with low amplitude signals, which can shift often day to day (Perge et al., 2013; Prasad et al., 2012).

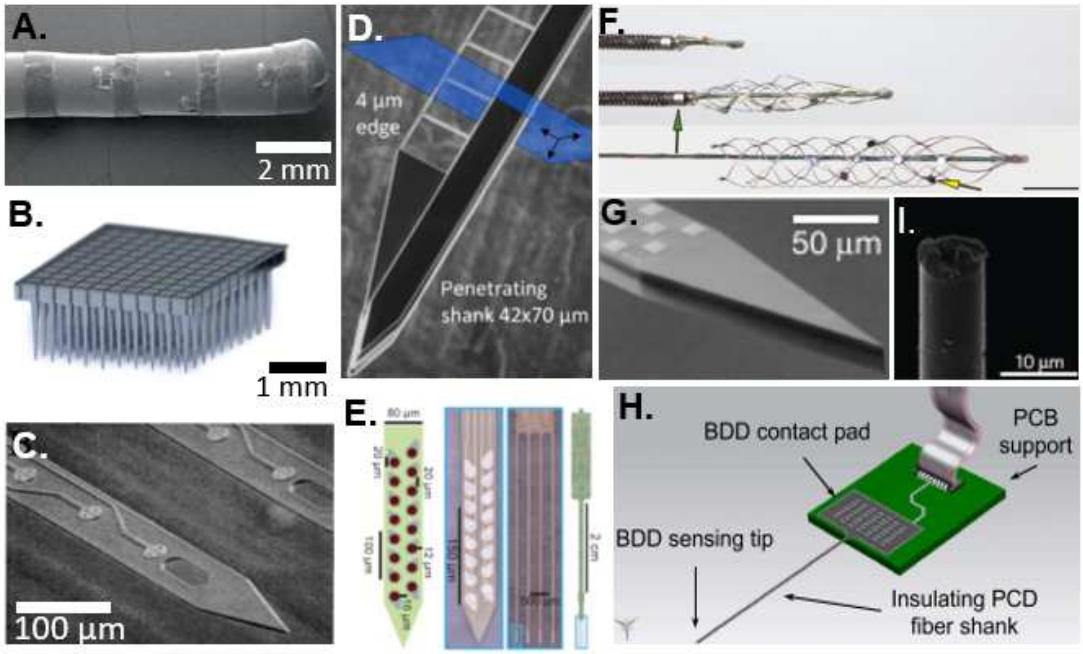

Figure 1. Implantable device design technologies for neural interfaces. (A) Human deep brain stimulation lead implant (Moss et al., 2004). (B) Blackrock Utah intracortical array (Nordhausen et al., 1996). (C) Michigan array (Kipke et al., 2003). (D-H) Next-generation devices: (D) (Seymour and Kipke, 2007) (E) (Chung et al., 2019) (F) (Oxley et al., 2016) (G) (Jun et al., 2017) (I) (Kozai et al., 2012) (H) (Rusinek et al., 2018).

1.1.3 Tissue response to implanted electrodes

One of the primary problems that emerge with implanted electrodes is signal recording instability and degradation over time which is likely to be a multifaceted problem comprised of mechanical and electrical failure of the electrode itself (Kozai et al., 2015; Nicolelis, 2001), as well as the foreign body response. This biological response is the chronic inflammatory response that occurs around the implanted microelectrode array which causes neurodegeneration due to blood brain barrier disruption and also reduction in the number of neurons that can be recorded from. This effect is known as the foreign body response, which is believed to be a source of signal

instability and loss that occurs when microglia and astrocytes encapsulate the device (gliosis) while local neurons density is reduced, preventing signal from being recorded via isolation of the device (Figure 2) (Biran et al., 2005; Salatino et al., 2017a). This glial sheath creates a diffusion barrier to ion flow and increases impedance (Prasad et al., 2012; Roitbak and Syková, 1999) and the distance between the neurons and the electrode sites (Liu et al., 1999). It has been estimated that a 40% loss of neuronal density within 100μm of the device occurs in the first month on implantation (Biran et al., 2005; E K Purcell et al., 2009). For neural implants to be useful in research and clinical settings, stability of long-term recordings from a large neuronal population of various brain regions must be achieved in a reliable and reproducible fashion (Lebedev and Nicolelis, 2006).

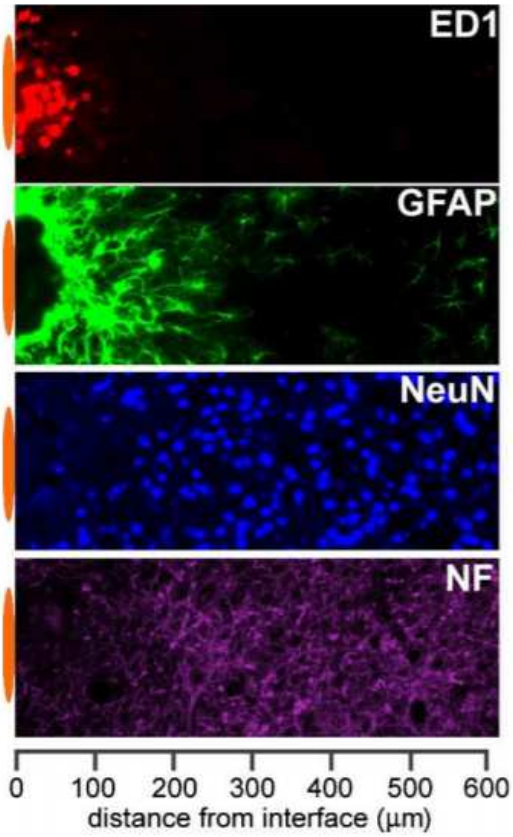

Figure 2. Histological images showcasing neuronal loss and gliosis due to foreign body response of implanted microelectrode in a rat brain at 4-week post-implantation. Inflammatory (ED1) and astrocytic (GFAP) markers are shown surrounding the electrode. NeuN+ and neurofilament (NF) markers are reduced closer to the device orange oval) (Figure reproduced with permission from Biran 2005.

1.1.4 Electrode material compatibility and safety

Despite significant advances in the field of device fabrication, several challenges remain such as material biocompatibility and safety. Next-generation microelectrode arrays have been designed to be smaller and softer, composed of more biocompatible materials to improve integration with the brain environment, such as diamond (Rusinek et al., 2018) , flexible parylene-C (Hara et al., 2016; E K Purcell et al., 2009; Seymour and Kipke, 2007; Xu et al., 2015) and flexible polyimide (Rousche et al., 2001) which in turn increases spatial resolution of neuronal sampling and overall longevity of neural recordings. However, the field continues to lack guiding principles for the selection of materials and geometries of devices that are better suited for brain tissue implantation (Thompson et al., 2020).

There are modifications strategies that can take place to develop electrodes that allow for better integration of the electrode to the tissue-electrode interface by helping reduce the foreign-body response and reducing impedance. One way to modify electrode probes is by performing surface modifications or coatings to vary surface hydrophilicity, chemistry, and surface topography. Materials used as coatings include hydrogels (Fattahi et al., 2014), laminin, anti-inflammatory surface molecules (He et al., 2007; Kolarcik et al., 2012), silk (Tien et al., 2013), synthetic scaffolds (Mammadov et al., 2013), polymer nanoparticles for reducing inflammation (Abidian and Martin, 2009; Green and Abidian, 2015; Mercanzini et al., 2010) and astrocytic extracellular matrix (Oakes et al., 2018). Many other strategies have emerged to improve biocompatibility by reducing gliosis, inflammation and impedance and remain as contender strategies to work synergistically with other modifications to potentially increase electrode biocompatibility.

Surface area of the electrodes and stiffness play important roles in determining effective integration of the electrode to the brain. Key features include Young's modulus, bending stiffness, and cross-sectional area. Stiffer materials, such as silicon, can increase inflammatory response greatly when compared to softer materials (Moshayedi et al., 2014). A mismatch in Young's modulus is present in comparison to the brain tissue (~10^{-5} GPa) and silicon (~10^{2} GPa), which increases gliosis and inflammation. Flexible, more adaptive materials provide a reduction in gliosis and inflammation as seen with compliant implants (Luan et al., 2017; Ware et al., 2014, 2012). Additionally, reduced cross-sectional area has been shown to increase biocompatibility by reducing gliosis and maintaining neuronal population (Kozai et al., 2012; Seymour and Kipke, 2007). Devices are moving towards becoming smaller and more flexible; however, issues remain to achieve seamless electrode-tissue interface integration. There is great potential for developing technologies that combine multiple modifications mentioned here and beyond to achieve better compatibility and chronic stability of the electrode (Thompson et al., 2020).

1.2 Regenerative electrode interface

1.2.1 Neural stem cells for seamless integration of electrode interface

Neural stem cells (NSCs) and neural progenitor cells (NPCs) have great potential as therapeutics for brain tissue injuries by minimizing the mismatch between the electrode and brain tissue, which in turn can also improve biocompatibility (Azemi et al., 2010). More specifically, stem cell-seeding for the tissue-electrode interface has been shown to improve the integration of the probe with brain tissue (Purcell et al., 2009). NPCs have been shown to migrate to locations of microglia inflammation and differentiate preferentially to oligodendrocytes (Aarum et al., 2003) and to neurons (Aloisi, 2001), while others have shown their neurotrophic ability by promoting

neuronal survival by minimizing gliosis (Lu et al., 2003; Ourednik et al., 2002). Overall, an electrode surface with NPCs may less foreign to the brain tissue, minimizing the foreign body response, and could also benefit the injury site by providing release of neurotrophic factors for neuronal survival improvement (Azemi et al., 2010; Green et al., 2013; Richter et al., 2011).

Efforts from different research groups have demonstrated the idea of "living electrodes" which refers to embedding devices with neural cells to provide a more "natural" cascade of events for better integration by using different electrode coating technologies (Adewole et al., 2018; Azemi et al., 2010; Goding et al., 2017; Serruya et al., 2018). A layered construct were a hydrogel scaffold holds neural progenitor cells had been executed (Green et al., 2013), however there are some challenges with this idea regarding mechanical and biological properties of the scaffold and neural outgrowth control. Additionally, a degradable biosynthetic polymer scaffold had been developed with variable moduli that can be tuned to provide desired flexibility while holding bioactive molecules for cellular growth (Aregueta-Robles et al., 2014). More recently, another layered construct has been developed which uses a combination of conductive hydrogel and a biodegradable synthetic hydrogel that aids with cell encapsulation at the surface of the device while degrading over a 21 day period (Goding et al., 2017).

The idea of a "living electrode" has the potential to provide functional synapses between devices and cells in the region of interest allowing for a seamless communication of the neural interface. New ideas for stem cell harvesting and encapsulation are needed for an increase survival of cells (Goding et al., 2017). Various sources for neural stem cells are available, including direct isolation from primary central nervous system tissue, such as fetal (Okabe et al., 1996) and adult

(Reynolds and Weiss, 1992) brains as well as spinal cord tissue (Shihabuddin et al., 1997); transdifferentiation from somatic cells such as skin fibroblasts (J. Kim et al., 2011); and lastly from induced pluripotent stem cells, which can be developed into large quantities and enable basic science research (Takahashi et al., 2007; Kazutoshi Takahashi and Yamanaka, 2006; Yamanaka, 2009).

1.2.2 Induced pluripotent stem cells (iPSCs) and their use in neural engineering

Yamanaka et al. reported in 2006 the generation of pluripotent stem cells from mouse somatic cells by using a concoction of four transcription factors (Oct3/4, Sox2, Klf4, and Myc). This discovery of these embryonic stem cells (ESCs) resembling cells has in turn contributed to the growth of stem cell research and are now used for various applications such as disease modeling, autologous cell therapy, and as substrates for different screens (Bahmad et al., 2017). Additionally, efforts have been made to generate defined lineages of neural cells from iPSCs. Recently, stem cell therapy for neurodegenerative diseases and neural disorders aims to generate patient- and disease- specific neural stem cells. Stem cell therapy is a promising approach for treating neurodegenerative diseases which requires generation of iPSC derived NSCs and is considered to be a revolutionary step towards personalized medicine (Ferreira and Mostajo-Radji, 2013). Many challenges remain regarding the ability to control cellular fate, which can vary depending on genetic and molecular mediators as well as environmental factors. By controlling and guiding stem cell into desired lineage, researchers can better mimic the desired environment *in vivo* by utilizing different tissue engineering and fabrication techniques. Cellular phenotypic responses can initiate a cascade of pathways that are very specific and need to be monitored for the intended application (Kshitiz et al., 2012).

1.2.3 Interfacing neural networks with light using optogenetic switches

Advances in neuroscience, molecular biology, and neural engineering have set the stage for creating new methods for controlling the gene expression and maturation of neural cells. Before optogenetics, chemically inducible systems first made it possible for researchers to derive neurons from stem cells by overexpressing proneural genes (Gossen and Bujardt, 1992). In 1999, Sir Francis Crick predicted the use of light for identification of neuron types by turning the firing activity on and off (Crick, 1999). Shortly after, in the early 2000s the discovery of channelrhodopsins-1 and -2 led to the development of optogenetics as a tool were naturally occurring photosensitive proteins from other organisms are engineered as protein switches with genetic encoding that allows to control cellular signaling and behavior (Boyden et al., 2005; Deisseroth, 2011). Light proves to be a superior tool compared to chemical methods for manipulation of gene expression due to its ease of availability, high flexibility, low toxicity to cells, and high spatial and temporal resolution. Thanks to these powerful characteristics, optogenetic tools enable researchers to systematically examine biological processes, which helps researchers gain a deeper understanding of the cellular mechanisms.

To understand what is occurring at the electrode-tissue interface, spatiotemporal resolution of gene expression needs to be high and induction needs to be localized. During the last decade, there have been significant advances thanks to the introduction of optogenetics. Optogenetics was first defined as the use of light-sensitive proteins for activating or inhibiting expression in neurons. From this discovery, many optogenetic systems have become widely available. Alongside, technologies for *in vivo* stimulation have also been developed. Despite many efforts, several limitations remain in developing the ideal optogenetic tool for gene expression control. Below, a

summary explores recent advances in optogenetics switches including phytochromes (PHY), cryptochromes (CRY), and light-oxygen-voltage (LOV)-sensing domains including EL222 and VVD systems.

The PhyB-PIF system takes advantage of the red/far-red light reversible interaction of PhyB and PIF that can be switched between *on* and *off* states (Muller et al., 2013) A shortcoming of this system is that it requires an exogenous non-protein chemical compound to be delivered. However, it offers an advantage over other systems for using red light for greater depth of penetration, making it suitable for *in vivo* applications. This system offers a high spatiotemporal control and has proved useful in reshaping and directing cell morphology of mammalian cells (Levskaya et al., 2009). Additionally, the PhyB/PIF system was the first to prove multi-chromatic control of gene expression in mammalian cells, allowing for a maximum of three genes to be light-responsive (Muller et al., 2013).

The CRY2-CIB1 system has a photosensitive transactivator that dimerizes when exposed to a specific wavelength of light. This process allows the binding of the transactivator to its response element, enabling gene expression (Wang et al., 2012). This system has a spatial and temporal resolution and reversibility in the millisecond range (Konermann et al., 2013). The CRY2-CIB1 system was adapted to target endogenous genes and up to 20-fold of gene expression was seen and has an advantage by its ability to target endogenous genes.

A light-switchable gene expression system named VIVID uses a genetically encoded light-switchable transactivator (VVD) which was shown to be very stable in the photoactivated state

(Zoltowski et al., 2013). VVD is a FAD-binding-light-oxygen-voltage (LOV)-domain that is derived from the fungus *Neurosppora crassa.* This system is extremely sensitive to blue light and is capable of being activated with pulsing light instead of continuous illumination, thus decreasing any light-toxicity effects (Wang et al., 2012). However, this system offers slow kinetics, limiting its use for gene expression applications.

The EL222 system was first developed by Motta-Mena et al. in 2014 and it is a light-sensitive transcription factor from the marine bacterium *E. litoralis*. This transcription factor is composed of a helix-turn-helix (HTH) DNA-binding domain and a LOV domain. The LOV-domain attached to the DNA-binding domain under dark conditions, which inhibits dimerization of the transcription factor, meaning no specific DNA-binding takes place. When blue light is present, EL222 is homodimerized and binds specifically to the DNA sequence (C120) for initiation gene expression regulation. This interaction is spontaneously reversed in the dark, rendering EL222 inactive ($\tau \sim 11$ s at 37 °C) (Nash et al., 2011; Rivera-Cancel et al., 2012; Zoltowski et al., 2011). Since then, many variants of this system have been established for different lifetimes ranging from seconds to thousands of seconds and have shown successful reversibility of kinetics (Baaske et al., 2018; Reade et al., 2017). Additionally, this optical system has demonstrated the highest success amongst other inducible systems when adapting from an *in vitro* to an *in vivo* application (Zoltowski et al., 2013).

1.2.4 LED-based optical neural implants

Optical induction systems provide great advantages to study neural networks, and a variety of tools have been developed to optically interface brain tissue *in vivo*. The key component for applying these systems to *in vivo* applications lie in utilizing devices that can intersect the brain

and provide rich readouts while minimizing glial encapsulation of the device. Optical instrumentation needs to be designed to deliver precise illumination to brain regions of interests to influence changes in targeted tissue. *In vivo* light delivery is quite challenging, primarily due to how light is easily diffused through tissue. This requires the light source to be very close to the region of the brain the researcher is targeting (Carter and De Lecea, 2011). For this, an implant through the skull into the brain region of interest is required, thus although make the process more complex, makes deep brain structures more accessible (Matveev et al., 2015).

The first approaches of using light for *in vivo* studies was possible using optical fibers. Recently, wireless optofluidic systems were developed which offers light delivery capabilities in addition to pharmacological mediation or fluid delivery (Jeong et al., 2015; Kim et al., 2013; Liu et al., 2015). By combining optogenetic tools with recording capabilities researchers have the possibility of identifying labeled neurons, characterizing and classifying neuron types and testing their roles in local circuits (Royer et al., 2010). To study neural circuits with light, electrical recording methods offer the greatest temporal resolution and frequency range that can easily complement optical stimulation (Seymour et al., 2017). Using implantable optical fibers are a great tool for stimulating with light, however many do not offer a measure for readout of activity. To overcome this issue, optrodes were developed (Figure 3).

Optical electrode probes, or optrodes, contain an optical stimulator consisting of a light guide optic fiber and a microelectrode for simultaneous light delivery and data recording at the single-cell level resolution (Royer et al., 2010). A wireless optrode has recently been developed in the form of a head stage that offers a high channel count that can provide simultaneous optical stimulation and recording (Gagnon-Turcotte et al., 2017). Additionally, surface electrodes have

had an emerging upcoming such as the NeuroGrid which is a neural interface device that is capable of recording LFPs and spikes from cortical neurons while conforming to the surface of the brain (Khodagholy et al., 2015). More recently, a flexible, small (9.8 mm diameter) wireless subdermal implant offers a reduction in invasiveness due to implantation while minimizing collision of the hardware with its environment (Shin et al., 2017).

Novel technologies have played a notable role in the advancement of light delivery. Such technologies include a fiberscope, which is a microscope coupled to fiber optics that contain a micro-objective for neuronal activation while simultaneously imaging by epifluorescence, structured illumination, or scan-less confocal microscopy, and recording cellular activity (Szabo et al., 2014). Injectable optoelectronics for wireless optogenetics have also been developed (Kim et al., 2013). This ultrathin, multifunctional injectable device is mounted in an injection needle that can be inserted into soft tissue and inserted while being minimally invasive. It has various components including LEDs, thermal, optical and electrophysiological sensors and actuators, which can be configured in a single or multi-layer organization. Injectable devices have a fast upcoming in the field of electronics and provide sophisticated capabilities for interfacing biology (Kim et al., 2013; Liu et al., 2015).

Recently, a new avenue for optogenetic applications has been unraveled that consists of using upconversion nanoparticles (UCNPs). Researchers developed lanthanide doped UCNPs that can transform near infrared (NIR) light into visible light. This innovation can reach deeper areas of the brain noninvasively by using a laser outside the skull. Future research will need to address

chronic interaction of these particles with brain tissue in order to assess biocompatibility (Chen et al., 2018).

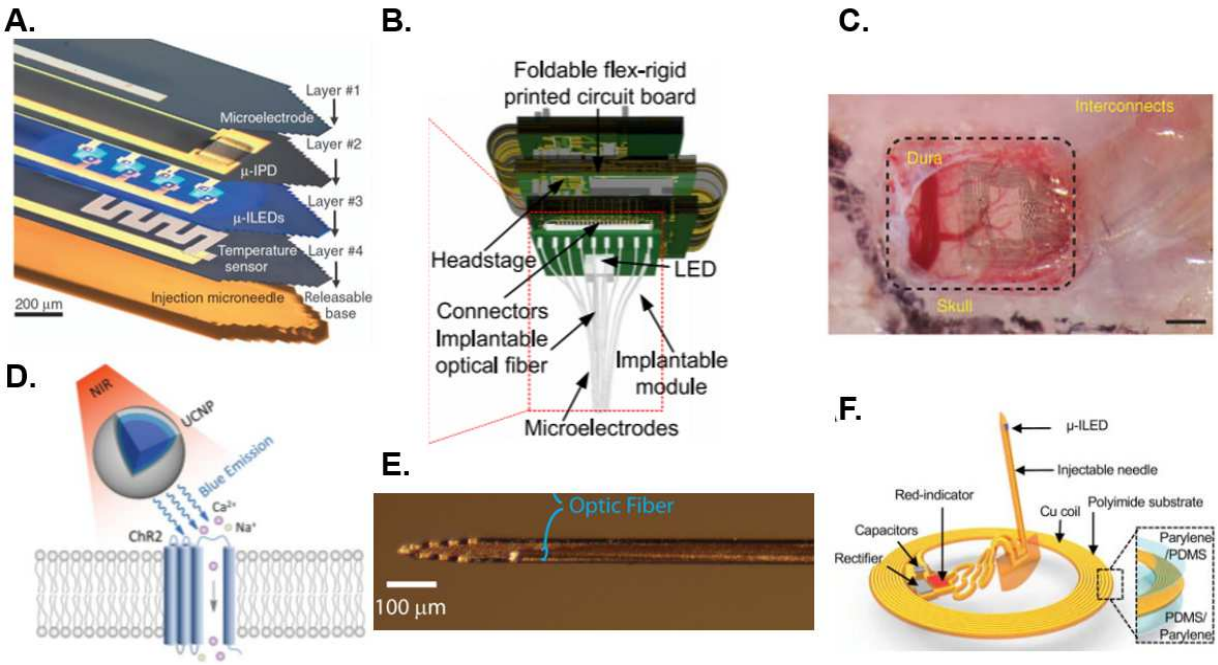

Figure 3. Next generation device design aimed at combining recording capabilities with light. (A) Injectable, cellular-scale optoelectronics (Kim et al., 2013). (B) Wireless headstge for optogenetics and neural recordings (Gagnon-Turcotte et al., 2017). (C) NeuroGrid (Khodagholy et al., 2015). (D) Upconversion particles (Chen et al., 2018) (E) Multiarray with optical capabilities (Royer et al., 2010). (F) Wireless subdermal optoelectronics (Shin et al., 2017).

1.2.5 Understanding and Controlling Gene Expression Surrounding Electrodes: Future Vision

The high interconnectedness and heterogeneity of the brain although provide our high functionality, pose a challenge for brain repair efforts and *in vivo* modeling. Precisely controlling neuronal identity and activity proves to be invaluable in deciphering the function of neuronal circuits and regenerating lost circuitry. Many efforts from neuroscience, engineering, and biology have provided insights into ways of controlling neuronal gene expression. Additionally, new approaches for both understanding and controlling the reactive tissue response are being developed

by utilizing optical induction of proneural gene expression control and by reprogramming the identity of glia at the interface (Winter et al., 2017). Coupling implanted electrodes with optical induction of gene expression could influence integration in two ways: (1) it could be a tool for influencing cell fate in stem cell-seeded probes, or (2) it could be used to directly influence gene expression in native tissues surrounding devices.

On the first point, previous studies have shown that the overexpression of proneural genes can lead to neural differentiation. *Neurogenin-2* (Heinrich et al., 2010) and *NeuroD1* (Guo et al., 2014) in astroglia can lead to glutamaergic neurons, while the combination of *Ascl1* and *Dlx2* proneural genes can lead to GABAergic neurons for brain repair after neurodegeneration (Heinrich et al., 2010). Coupling gene expression with light has also been explored recently, demonstrating the precise spatiotemporal capacity that light provides (Konermann et al., 2013; Motta-Mena et al., 2014). By controlling stem cell differentiation fate at the interface with an optoelectrode array, proneural gene optogenetic control can allow for a seamless electrode interface allowing for long-term recording capabilities.

On the second point, current research regarding cellular responses that contribute to electrode failure aims at the evaluation of cell types that surround the device. Additionally there has been some research looking at the gene expression profile that these cells express at the interface to better understand the tissue-electrode interface (Bedell et al., 2020). It has been shown previously that histological markers for inflammation are present such as upregulation in GFAP gene expression as a result of activated astrocytes (Buffo et al., 2010; Griffith and Humphrey, 2006; Polikov et al., 2005). Additionally, VGLUT1 had been shown to decline while VGAT was

shown to decrease over time demonstrating a shift toward reduced excitatory and increased inhibitory expression (Salatino et al., 2017b). Research has also shown that NOXa1 relative gene expression decreases compared to control, indicating oxidative stress present (Ereifej et al., 2018). Gene expression profiling and control is crucial to further comprehend and mitigate gliosis. By genetically manipulating the identity of a specific cell type at the electrode site the goal is to seamlessly integrate the electrode to the tissue for long-term recordings which will help to understand and control the reactive tissue response to brain implants.

1.3 Solutions to challenges and objectives of this work

Optogenetics advances provide a unique neuromodulation technique that allows optical control of genetically targeted specific cells that express light-sensitive opsin proteins with sub-

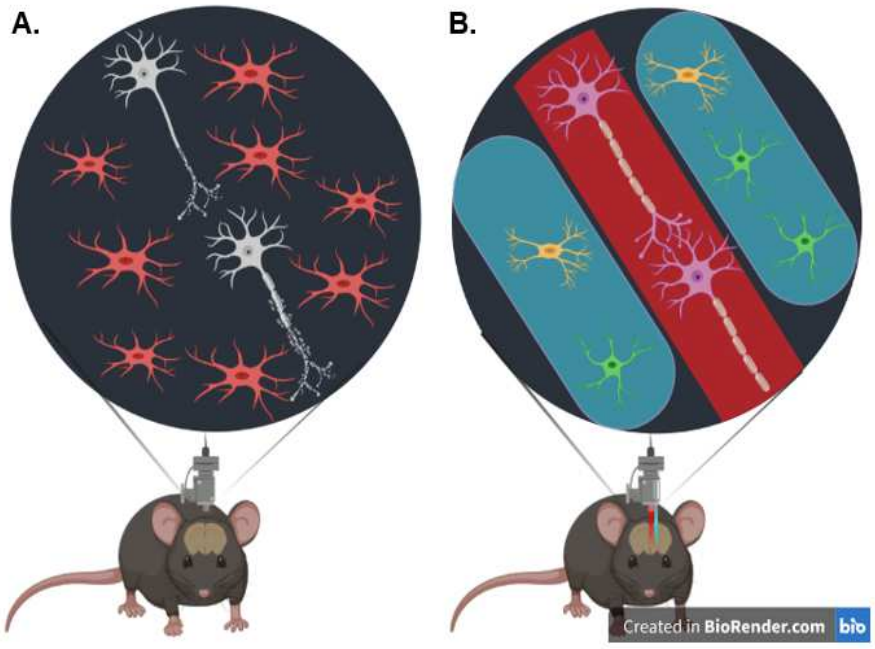

Figure 4. Controlling biological activity with light will bridge connectivity to recreate the native circuitry similarly to preimplantation. (A) Reactive glia (red) and damaged neurons (grey) are present surrounding the implantation site of the optofluidic device. (B) Delivery of virus for optogenetic stimulation takes place and light illumination (red and blue) helps to restore circuitry present pre-implantation showcasing healthy neurons (pink), neuroprotective astrocytes (green) and quiescent microglia (yellow).

millisecond temporal precision. Future work will involve the integration of micro-LEDS, neurotransmitter detection, and neuroelectrical signal recording. Due to the brain's composition of highly dense neuron population, the analysis of neuronal signaling requires high-resolution in space and in time to be neuron-specific and perturb the circuitry in a controlled environment. To be successful with neural recordings, a combination of genetic engineering-assisted optical stimulation and parallel electrical recording of neuronal activities (optoelectrophysiology) is a promising tool for studying neuronal circuits (Figure 4).

1.4 Structure of dissertation

The dissertation has five chapters including the introduction were main topics and historical background is provided in Chapter One. A study of substrates and their effects on neural progenitor cells is presented in Chapter Two. Chapter Three includes a study of a blue-light optogenetic system for spatial control of gene expression. Chapter Four discusses material and genetic factors that can contribute to the control of cell fate, structure, and function. Lastly, Chapter Five, presents a summary of results, final conclusions and closing remarks, alongside ongoing work and future directions and the dissertation ends.

1.5 Research Questions and Objectives

The overall goal of this dissertation is to (1) explore methods that aim at revealing the influence of electrode material properties in the structural and functional maturation of primary rat cortical neurons and rat neural progenitor cells *in vitro,* and (2) to characterize an optical gene expression system for precise control of neural expression by identifying key optimization parameters of the

optogenetic system to couple the system with proneural gene expression with micro-LED coupled-arrays. In the efforts of achieving these goals the study asks the following scientific questions:

- Is there a difference among substrate coatings and electrode materials in reference to structure and maturation of rat neural progenitor cells and rat primary neurons?
- What is the impact of a given electrode material on cellular structure and function?
- How can we optimize an optogenetic system for precise modulation of gene expression with micro-LEDs?

These questions are answered through the reach of the following objectives:

- Compare different substrate materials for deriving neurons from rat iPSCs.
- Compare different electrode materials *in vitro* by looking at the immunochemistry and electrophysiology of rat neural progenitor cells and primary rat cortical neurons.
- Characterization and optimization of a blue-light optogenetic system, EL222, for enhancing response characteristics of the system.
- Construct a stable cell line with the optimized optogenetic system to explore effects of blue light duration and intensity on the system's response characteristics.
- Develop methods to achieve and analyze a spatial response due to light which aims at achieving a spatial gradient of gene expression for future work regarding perturbation of residual neurons or reactive astrocytes at the tissue-electrode interface.

The outcomes of this research will provide insight to the neural engineering community by first generating an optimized optical gene expression system to achieve spatial control of gene

expression along a gradient of optical power to reconstruct damaged neural circuitry in the brain. Secondly, identifying if intrinsic properties of a material can affect excitability, maturity and network formation of neurons and neural progenitor cells *in vitro,* can allow for informed material selection for long-term implantation *in vivo*. Together, the studies provide a foundation for progress toward realizing a regenerative electrode interface.

2. CHAPTER 2 | Differentiation and Characterization of Neurons Derived from Rat iPSCs

2.1 Abstract

Background

Induced pluripotent stem cells (iPSCs) may be an advantageous source of neuronal cells to repair damage due to neurological disorders or trauma. Additionally, they are promising candidates to develop models to study underlying mechanisms of neurodegenerative diseases. While successful neural differentiation of iPSCs has been reported in mice, protocols detailing the generation of neural cells from rat iPSCs are relatively limited, and their optimization by manipulating cell culture methods has remained unexplored.

New Method

Here, we describe and compare the effects of four distinct, commonly used substrates on the neuronal differentiation of rat iPSC (riPSC) derived-neural progenitor cells. Our approach is to use substrate coating as a method to enrich differentiated riPSCs for neuronal subtypes with the desired morphology and maturity. We use a combination of electrophysiology, immunofluorescence staining, and Sholl analysis to characterize the cells generated on each substrate over a nine-day time course.

Results

The surface coating presented by the cell culture substrate influences the polarity and arborization of differentiating neurons. Polyornithine-laminin coating promoted neuronal arborization and maturation, while Geltrex favored bipolar cells which displayed indicators of functional immaturity. Poly-D-lysine substrate was associated with limited neurite outgrowth and arborization. Gelatin was the least favorable substrate for the growth and differentiation of our cells.

Comparison with Existing Method

Rat-derived neural progenitor cells have been previously derived; however, our methods to use substrate coatings to influence morphological and electrical maturity have not been explored previously.

Conclusion

Substrate coatings can be selected to enrich differentiated riPSCs for unique neuronal morphologies.

2.2 Introduction

Induced pluripotent stem cells (iPSCs) have the capacity to engage in self-renewal and differentiate into specified lineages, allowing the development of pluripotent cell-based models of human disease (Tabar and Studer, 2014; K Takahashi and Yamanaka, 2006). Although the rat is a species with a long history of use in laboratory research, the derivation of stem cells from rats has been far outpaced by the development of mouse stem cell lines (Liao et al., 2009). While the isolation of mouse embryonic stem cells was first reported in the early 1980's (Martin, 1981), attempts to establish similar results in alternative rodent species were largely unsuccessful until nearly thirty years later (Buehr et al., 2008; Demers et al., 2007; Li et al., 2009; Ueda et al., 2008). In parallel, Yamanaka and colleagues reported their seminal finding that a cocktail of transcription factors could reprogram adult mouse somatic cells to pluripotency (iPSCs) (K Takahashi and Yamanaka, 2006). The successful generation of rat iPSCs (riPSCs) was reported soon thereafter (Chang et al., 2010; Hamanaka et al., 2011; Li et al., 2009; Liao et al., 2009; Merkl et al., 2013). Nonetheless, the reported methods available for the derivation and optimization of differentiation conditions for riPSCs remain relatively limited.

Irrespective of the species of origin, achieving adequate control of the fate and function of cells differentiated from iPSCs remains a significant challenge. With exposure to specific small molecules, reprogramming factors, or substrate cues, iPSCs can be directed to produce target phenotypes, including neural cells and their subtypes (Kim and de Vellis, 2009; Tabar and Studer, 2014). As such, iPSCs are promising candidates to repair the damage resulting from neurodegenerative diseases and trauma (Avior et al., 2016). However, suboptimal maturation, survival, and spatiotemporal control of cellular differentiation and integration with host tissues remain significant hurdles to effective repair (Tabar and Studer, 2014; Tong et al., 2010). Regeneration of damaged neuronal tissues will require the identification of intrinsic and extrinsic cues which recapitulate developmental pathways to produce the desired neuronal phenotype, as well as the optimization of strategies to control innervation into native neural circuitry. Given the historically reduced emphasis on the development of riPSCs as an input cell source, studies which report the appropriate cues favoring the neuronal specification of these cells are particularly scarce.

There are compelling advantages to the use of rats as model systems for understanding brain function and disease: rats are more amenable to learning cognitive tasks in behavioral studies, they are more appropriate subjects for surgical manipulations based on their size, and they may serve as better models of certain human disease states (Iannaccone and Jacob, 2009). Here, we report novel methods to derive neurons with unique morphologies from riPSCs. We found that substrate conditions influence the polarity and arborization of differentiating neurons, providing new light on the methods which may be used to obtain enriched populations of riPSC-derived neurons with particular morphologies. Furthermore, we distinguish the impact of substrate cues on

the morphology versus the function of differentiated neurons: even after differentiation into morphologically "mature" neurons, additional cues are required to establish *functionally* mature neurons. The data presented here provide new methods to derive, differentiate, and selectively produce neurons with the desired morphology from riPSCs.

2.3 Materials and Methods

2.3.1 Generation and culture of rat induced pluripotent stem cells (riPSCs)

RiPSCs were derived from embryonic (E16) Fischer 344 rat fibroblasts that were reprogrammed by retroviral expression of *Oct4*, *Sox2*, *Klf4*, *CMyc* and *SV40 LT-Ag* (Liao et al., 2008; Liskovykh et al., 2011). RiPSCs were then trypsinized and maintained on a feeder layer of irradiated mouse embryonic fibroblasts (MEFs, Globalstem, Life Technologies) in stem cell medium. The riPSC medium consisted of 50% N2 medium (1% N2 supplement, 2.5% BSA, 1% penicillin/streptomycin, 0.3% β-Mercaptoethanol in DMEM/F12), 50% B27 medium (2% B27 supplement, 1% penicillin/streptomycin, 1% L-Glutamine in Neurobasal medium) supplemented with 3 μM GSK3αβ inhibitor CHIR99021 (Cayman chemical), 1 μM MEK inhibitor PD0325901 (Cayman chemical) and 10 μg/mL rat leukemia inhibitory factor (LIF) (Millipore) (Liskovykh et al., 2011; Makanga et al., 2015). Cells were maintained in a humidified incubator at 37ºC with 5% CO_2 and the medium was changed daily. Colonies with typical iPSC morphology were passaged every 4-7 days by mechanical dissection and subsequent transfer to MEFs. The pluripotent state of riPSCs was assessed by quantitative real time PCR (qRT-PCR) analysis and immunofluorescence detection for the pluripotency markers *Oct4, Octalat, Sox2,* and *Nanog (*Figure 10).

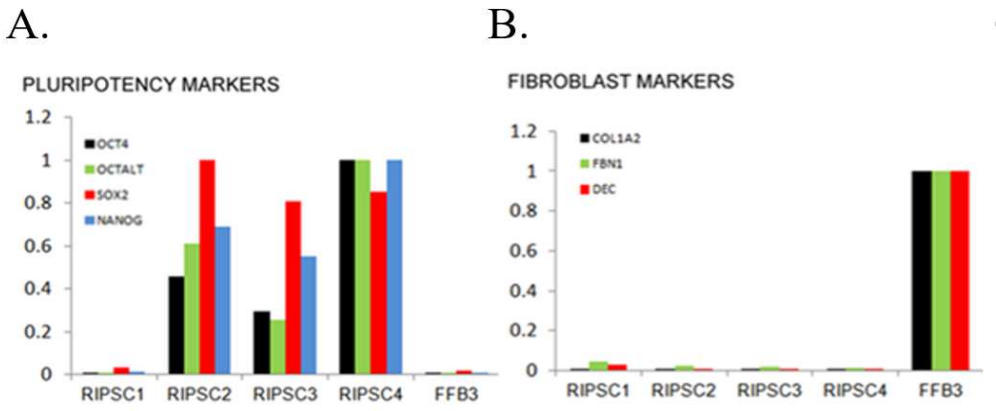

Figure 5. RT-PCR testing for pluripotency, fibroblast, and diagnostic markers for four initial riPSCs lines developed. (A) Pluripotency markers tested were highly expressed in riPSCs line 4, although Sox2 was slightly higher in riPSC line 2. Line 1 showed close to zero pluripotency markers, indicating a failure to achieve iPSC status. (B) Fibroblast phenotype markers were tested for all lines. RiPSC line 1 showed slight retention of fibroblast marker expression; however, all lines demonstrated clear downregulation of fibroblast markers in comparison to control (FFB3). The cell line used in the present study was riPSC4.

2.3.2 Derivation of neural precursor cells (NPCs) from riPSCs

For neural induction, mechanically dissected riPSC colonies were grown for 4 days as embryoid bodies (EBs; Liskovykh et al., 2011; Merkl et al., 2013) on non-adherent plates in LIF-depleted riPSC medium, followed by 3 days in the same medium supplemented with 1-3 µM retinoic acid (Sigma/Millipore) (Figure 5) EBs were then transferred to fibronectin-coated plates (10-20 µg/mL, Life Technologies) and further cultured in N2 medium. N2 medium was composed of 1% N2 supplement, 1% penicillin/streptomycin in DMEM/F12 (Life Technologies) supplemented with 25 µg/mL of rat epidermal growth factor (rEGF; Prepotech) and rat basic fibroblast growth factor (rFGF; Peprotech).

2.3.3 Influence of culture substrate on the neuronal differentiation of riPSC-derived NPCs

Cell culture substrates can have a profound impact on cell attachment, morphology, growth and differentiation(Gordon et al., 2013). Here, we tested four substrates that are commonly used

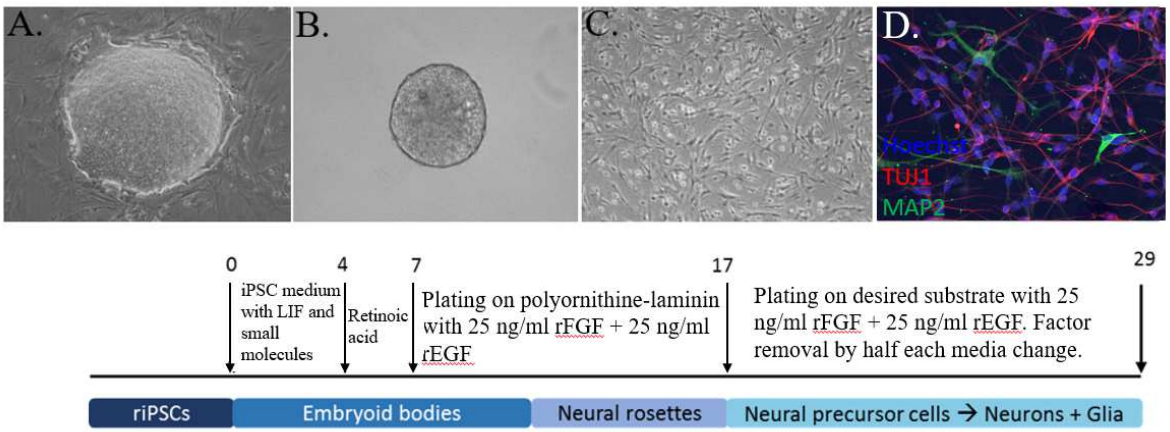

Figure 6. RiPSCs derivation into rNPCs and initial characterization of pluripotency. (A) Image of riPSCs colony. (B) Image of a rat-derived embryoid body. (C) NPCs expanding on polyornithine-laminin. (D) Immunohistochemical staining of TUJ1, MAP2, and Hoechst of differentiated rNPCs on polyornithine-laminin for Day 5.

in cell culture and exhibit different surface characteristics and cues for supporting cellular adhesion and differentiation (summarized in Supplementary Table 1). Neuronal differentiation of riPSC-derived NPCs was achieved by plating cells at a 100,000 cells/well density. To evaluate the effects of different culture substrates on their neuronal differentiation potentials, riPSC-derived NPCs were plated and grown on plastic coverslips (Thermanox, ThermoFisher) pre-coated with either 10 µg/mL polyornithine/5 µg/mL laminin ("poly-lam"; Life Technologies), 0.1% gelatin (Sigma-Aldrich) in dH_2O, 0.3% Geltrex (Life Technologies) in DMEM, or 1 mg/mL poly-D-lysine in dH_2O (Sigma). Cells were cultured in N2 medium until they reached 80-90% confluency, at which time, neuronal differentiation was initiated by supplementing the N2 medium with 20 ng/mL rat brain derived neurotrophic factor (BDNF, Peprotech), 200 ng/mL ascorbic acid (Sigma-Millipore) and 100 ng/mL cAMP (Sigma/Millipore), while progressively decreasing rEGF and rFGF concentrations. Experiments were done in duplicates with gelatin and polyornithine-laminin performed in triplicates to reach a sufficient sample size for all conditions. Statistical analysis verified that differences between culture replicates were non-significant (t-test, SPSS).

2.3.4 Whole cell patch-clamping electrophysiology

The electrical properties of riPSC-derived neurons were assessed by whole-cell patch clamp electrophysiology at 1, 5, and 9 days (D1, D5, D9, respectively) following initiation of neuronal differentiation. To this end, thin-wall borosilicate glass pipettes of 7-15 MΩ resistance were pulled on a P-97 micropipette puller (Sutter Instrument). In some cases, pipettes were pulled at a higher resistance of 15 MΩ to achieve successful cell sealing, which was more challenging than primary neurons. Pipettes were filled with an internal solution consisting of 135 mM potassium gluconate, 10mM HEPES, 7mM NaCl, 2mM $MgCl_2$, 2mM Na_2ATP, and 0.3mM NA_2GTP (pH= 7.3) (Thompson et al., 2017) . Cells were immersed in a carboxygenated physiological solution of 126 mM NaCl, 26 mM $NaHCO_3$, 2.5 mM KCl, 2 mM $CaCl_2$ $2H_2O$, 2 mM $MgSO_4$ $7H_20$, 1.25 mM NaH_2PO_4, and 10 mM Glucose (pH=7.4) and visualized under a 40x water immersion objective on an upright microscope (Nikon FN-1) equipped with a Q-imaging camera. Cells exhibiting a phase bright soma with growing process(es) were selected for analysis, and recordings were made with an Axopatch 200BAmplifier, digitized with a Digidata 1550A data acquisition system using Clampex 11 (Molecular Devices). Cells were sealed with resistances of > 1GΩ and subsequently stimulated following break-in with step injections of 0.1 nA from a holding potential of ~-60-80mV. In some cases, cells were held at more negative potentials to release sodium channel inactivation and facilitate spiking (-90--100mV). Recordings from ~10 cells per condition per time point were analyzed. For reference, spikes from embryonic rat cortical neurons were recorded using culture and recording methods as previously described (Thompson et al., 2017).

2.3.5 Immunofluorescence staining protocol

For immunofluorescence staining, cells were fixed in 4% paraformaldehyde (Sigma) for 15 minutes and washed twice with phosphate-buffered saline (PBS). Cells were blocked in 10% normal goat serum (Vector Labs) in 0.3% Triton-X-100 (10%NGST) and incubated overnight at 4°C with primary antibodies diluted in 5% NGST. Antibodies for cellular characterization included the neuronal markers rabbit anti-TUJ1 (1:500; Abcam) and mouse anti-MAP2 (1:250; Millipore Sigma). Following rinses in 5% NGST, cells were incubated with secondary anti-rabbit or anti-mouse antibodies conjugated to Alexa Fluor 594 or Alexa Fluor 488 (1:200; Abcam) for 2 hours in the dark at room temperature. Nuclei were stained with Hoechst dye (1:1000; Life Technologies). Following four rinses in PBS, cell-coated coverslips were mounted on slides using ProLong Gold (Life Technologies). Specificity of the immunofluorescence staining was determined by replacing primary antibodies with 5% NGST. Immunostained cells were examined with an Olympus FluoView 1000 Filter-based Inverted Laser Scanning Confocal Microscope using the FluoView software (Olympus) under 20x magnification.

2.3.6 Imaging and data analysis

Electrophysiology data was analyzed using Clampfit as part of pCLAMP 11 software suite. Every spike or spike-like event was counted and analyzed by measuring its amplitude (in mV) and its duration (width) at half-amplitude. The percentage of TUJ1- and MAP2-positive NPC-derived neurons was quantified at D1, D5, and D9 of the differentiation protocol by an operator blind to the experimental conditions. For each coverslip, five fields were randomly chosen and imaged on a Nikon Eclipse TE2000-U inverted microscope or a Nikon A1 TIRF microscope at magnification 20x. Exposure settings were kept constant during imaging. For each imaged field, the number of

cells staining for TUJ1 or MAP2 was recorded. ImageJ software (Schneider et al., 2012) was also used for counting Hoechst-stained nuclei using the automated counting protocol (Labno, n.d.). The total number of cells positive for either TUJ1 or MAP2 was expressed as a percentage of the total number of Hoechst-positive cells.

The morphological complexity of TUJ1- and MAP2-positive neurons derived from riPSCs were assessed using Sholl analysis as previously published (Sholl et al., 1953; Gensel et al., 2010). Briefly, the method consists of counting the number of times a neurite crosses rings of increasing radius length (10 μm) that are centered on the cell soma. For each experimental condition, about 20 neurons with clearly identifiable neurites were randomly selected and the average sum of crossings, average total number of branching and average maximal neuritic distance were recorded for each neuron. For each coverslip, five fields were randomly chosen and imaged on a Nikon Eclipse TE2000-U inverted microscope at 40x magnification. If needed, multiple images were stitched together manually to properly identify neurites.

2.3.7 Statistical analysis of the data

Statistical significance between the different experimental conditions was determined by one-way analysis of variance (ANOVA) followed by a post-hoc Tukey HSD using SPSS software (IBM). All data are expressed as mean ±SEM. Statistical significance was set at $p \leq 0.05$.

2.4 Results

2.4.1 Observations of substrate effects on the morphology and differentiation of immature neurons generated from riPSCs-derived rNPCs at D1, D5 and D9

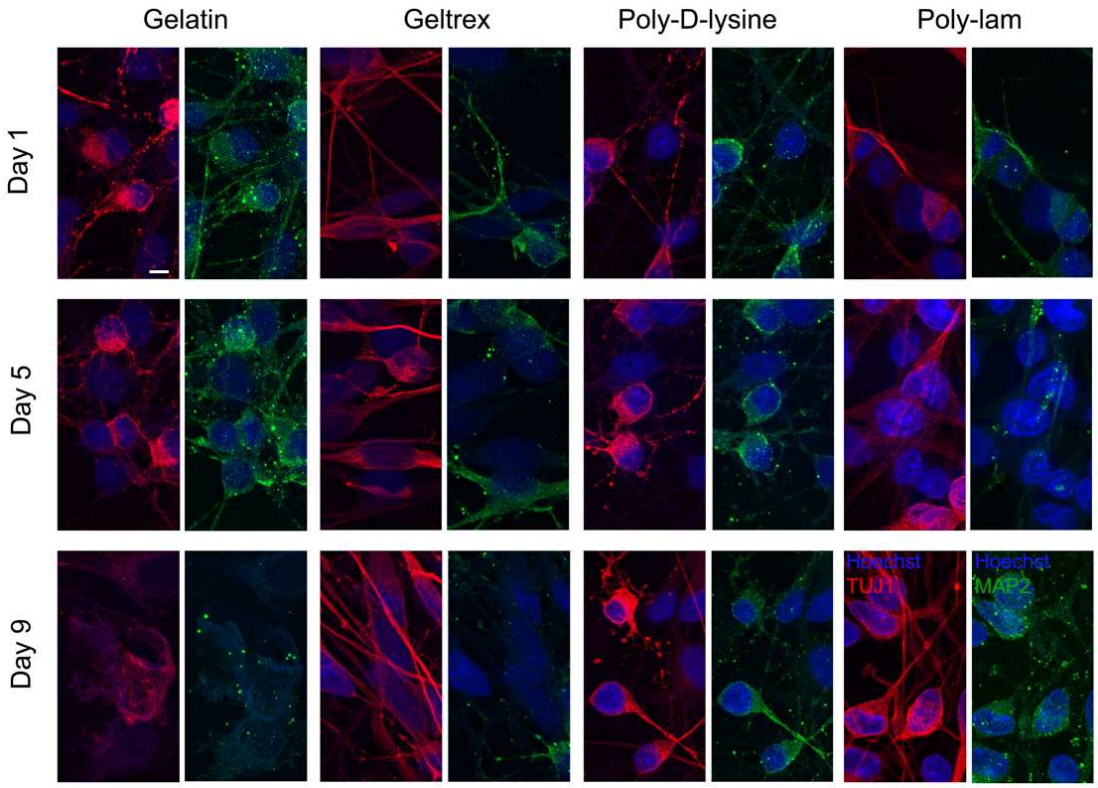

Figure 7. High-magnification images of cells plated on various substrates at days 1, 5, and 9. Observations indicate that TUJ1 (red) and MAP2 (green)-positive cells differ in their morphology by substrate and time point. Cell plated on Geltrex display bipolar morphology for TUJ1-positive cells. Cells on gelatin showed rounded morphology with short neurites. Poly-D-lysine shows mostly MAP2 positive cells that appear immature. Cells on poly-lam displayed rounded cells that developed extended neurites throughout the time points. Scale = 10 µm. Hoechst is shown in blue.

As illustrated in Figure 6, cells positive for TUJ1 and MAP2 were present on all substrates tested. However, depending on the substrate, clear differences in neuronal morphology and differentiation were immediately evident. The greatest percentage of TUJ1-positive cells was observed on polyornithine-laminin ("poly-lam") substrates at D9 (Figure 7A), while the greatest percentage of MAP2-positive cells was observed on poly-D-lysine (Figure 8A) when compared to

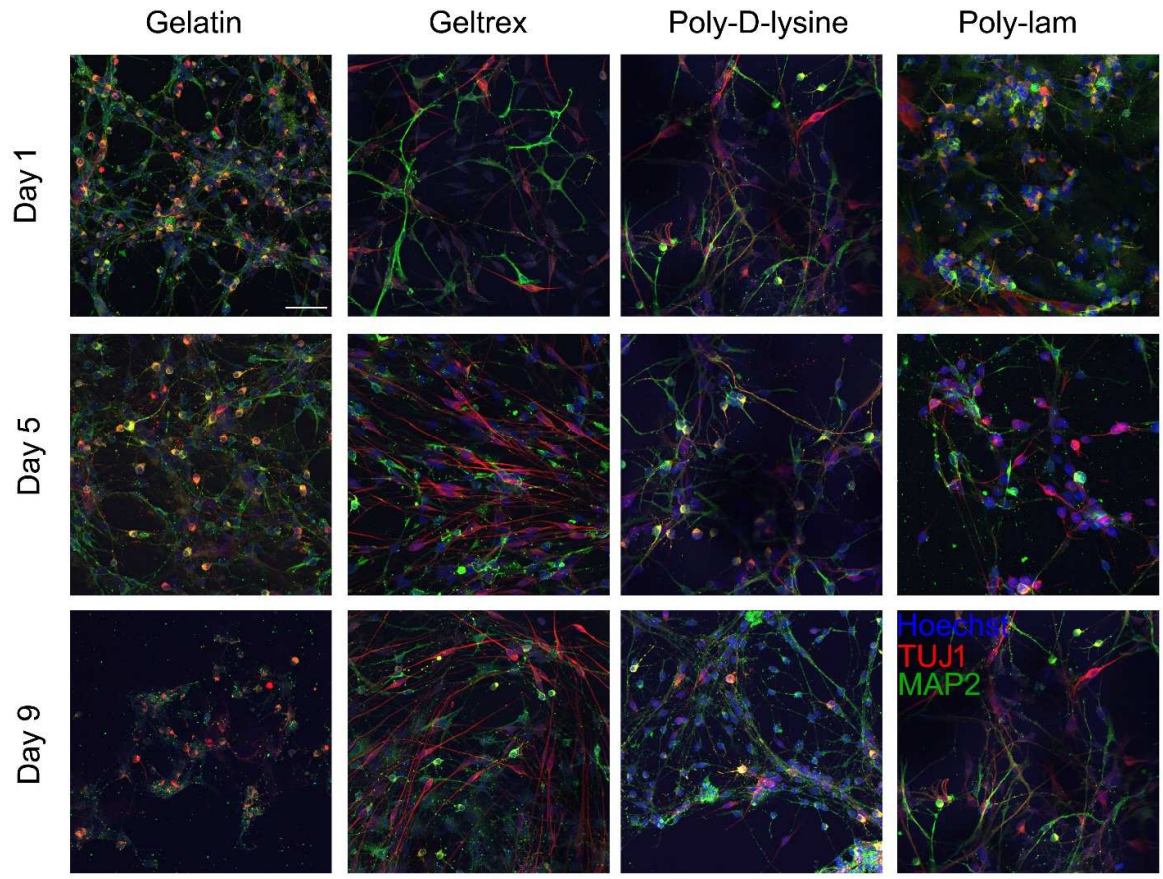

Figure 8. Representative images of cells plated on various substrates at days 1, 5, and 9 of differentiation. Observations indicate that TUJ1 (red) and MAP2 (green)-positive cells differ in their morphology by substrate and time point. Cell plated on Geltrex tended to display bipolar morphology for TUJ1-positive cells. Cells on gelatin showed rounded morphology with short neurites. Poly-D-lysine shows mostly MAP2 positive cells that appear immature. Cells on poly-lam displayed rounded cells at D1, which tended to develop extended and branched neurites by D9. Scale = 50 µm.

gelatin and Geltrex for D1 ($p < 0.013$) and for all substrates for D9 ($p < 0.001$). TUJ1-positive cells on poly-lam displayed longer neurites with increased branching in comparison to other substrates, particularly by D9 (Figure 7, Figure 8). Immature neurons on poly-lam appeared to be

rounded with few short neurites at D1 and D5; however, by D9, these neurites became more extended and arborized (Figure 7 and Supplementary Figure 13). TUJ1-positive cells on Geltrex had more elongated soma and neurites than any other substrate, with a bipolar morphology that appeared to grow in an aligned pattern (Figure 6).

Cells plated on gelatin exhibited a rounded appearance with short and blunted neurites, with most cells exhibiting unipolar morphology. Growth and differentiation were least robust on this substrate: neurites appeared to retract at D5, and cells are almost completely depleted on gelatin by D9 (Figure 6). Cells seeded on poly-D-lysine displayed several neurites surrounding the soma, although processes were shorter than those associated with Geltrex and poly-lam. At D1, there was a larger number of TUJ1-positive cells compared to MAP2-positive neurons for all the substrates tested, except for the poly-D-lysine substrate (Figure 7, Figure 8).

2.4.2 Sholl analysis of the effects of cell culture substrates on the morphology of TUJ1-positive cells highlight neurite outgrowth on polyornithine-laminin and Geltrex substrates

Differentiation on the different substrates resulted in neuronal cells displaying unique patterns of TUJ1-positive neurite complexity as assessed by Sholl analysis (Figure 7B-E). Neurites extended from TUJ1-positive cells plated on Geltrex and poly-lam substrates exhibited the longest neurites (highest maximal distance). Branching analysis trended towards poly-lam showing an increase in branching compared to gelatin, poly-D-lysine and Geltrex (data not shown). At D1 and D5, Geltrex and poly-lam consistently outperformed gelatin and poly-D-lysine substrates in their promotion of neurite outgrowth. Geltrex and poly-lam exhibited an increase in neurite crossings compared to poly-D-lysine ($p < 0.001$ for D1; $p < 0.001$ for D5). Additionally, Geltrex showed a significant increase in the total number of neurites when compared to gelatin ($p < 0.001$) at D5 (Figure 7D). At D9, an increase in neurite outgrowth occurred with poly-D-lysine ($p < 0.001$). Together, these data suggest that each substrate has unique properties that may alter the

differentiation and maturation of rNPCs, where poly-lam exhibited the greatest number of neurite crossings and branching compared to all other substrates tested.

2.4.3 Sholl analysis of the effects of cell culture substrates reveals reduced MAP2-positivity and outgrowth on polyornithine-laminin substrate

Early neurons derived from rNPCs seeded on all four different substrates demonstrated effects that were unique to MAP2-positive cells. MAP2 positive cells were enriched on poly-D-

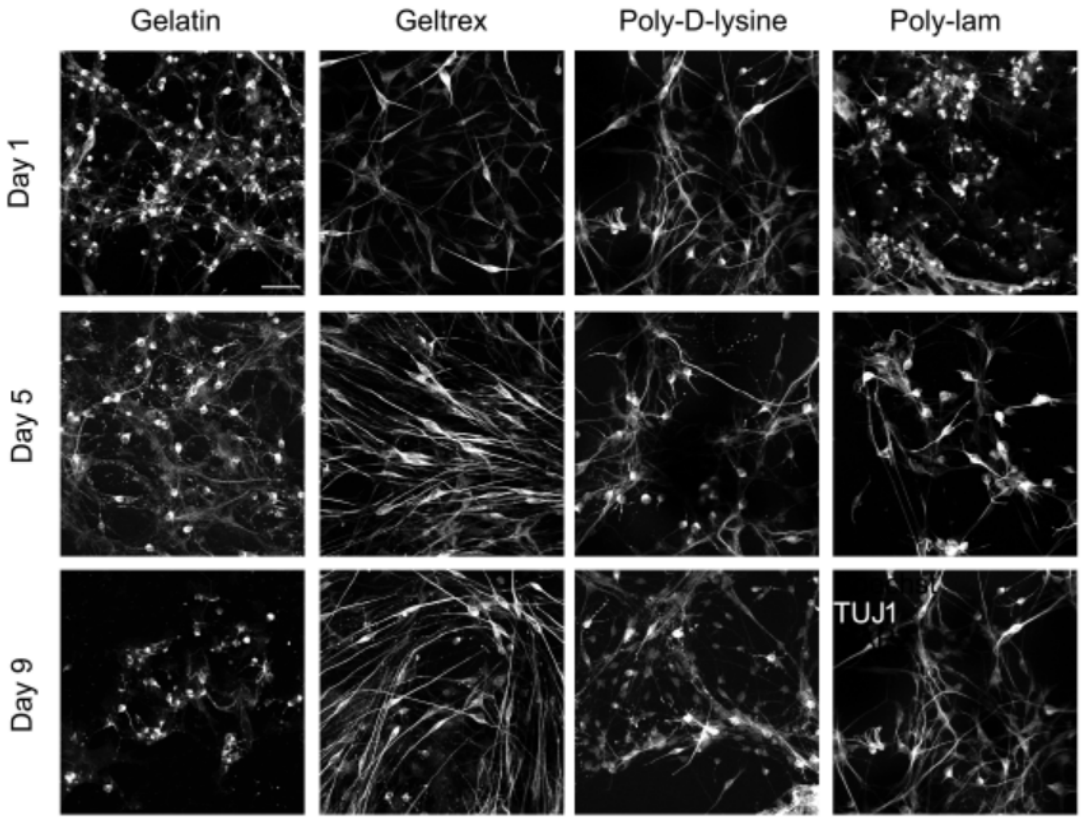

Figure 9. Representative images of TUJ1-positive cells plated on various substrates at days 1, 5, and 9 of differentiation. Observations indicate that TUJ1-positive cells exhibit different morphology by substrate and time point. Scale = 50 μm.

lysine substrates as a percentage of the cellular population (Figure 8A). Sholl analysis of neurite architecture was also performed on MAP2-positive cells (Figure 8B-E). Whereas TUJ1-positive neurite outgrowth and branching was favored on poly-lam by D9, MAP2-positive neurite outgrowth generally was favored on substrates other than poly-lam. Neurites extended from

MAP2-positive cells plated on gelatin and Geltrex exhibited the highest average maximal distance from tested substrates (Figure 8B). Average number of branching favored poly-D-lysine and Geltrex; Geltrex outperformed all other substrates for D5 ($p < 0.002$), while poly-D-lysine increased branching number for D9 compared to Geltrex ($p < 0.01$). Additionally, analysis of average number of crossings revealed that gelatin and Geltrex outperformed poly-D-lysine ($p < 0.014$) and poly-lam for D1 ($p < 0.017$). At D5 (Figure 8D), MAP2-positive cells differentiated on

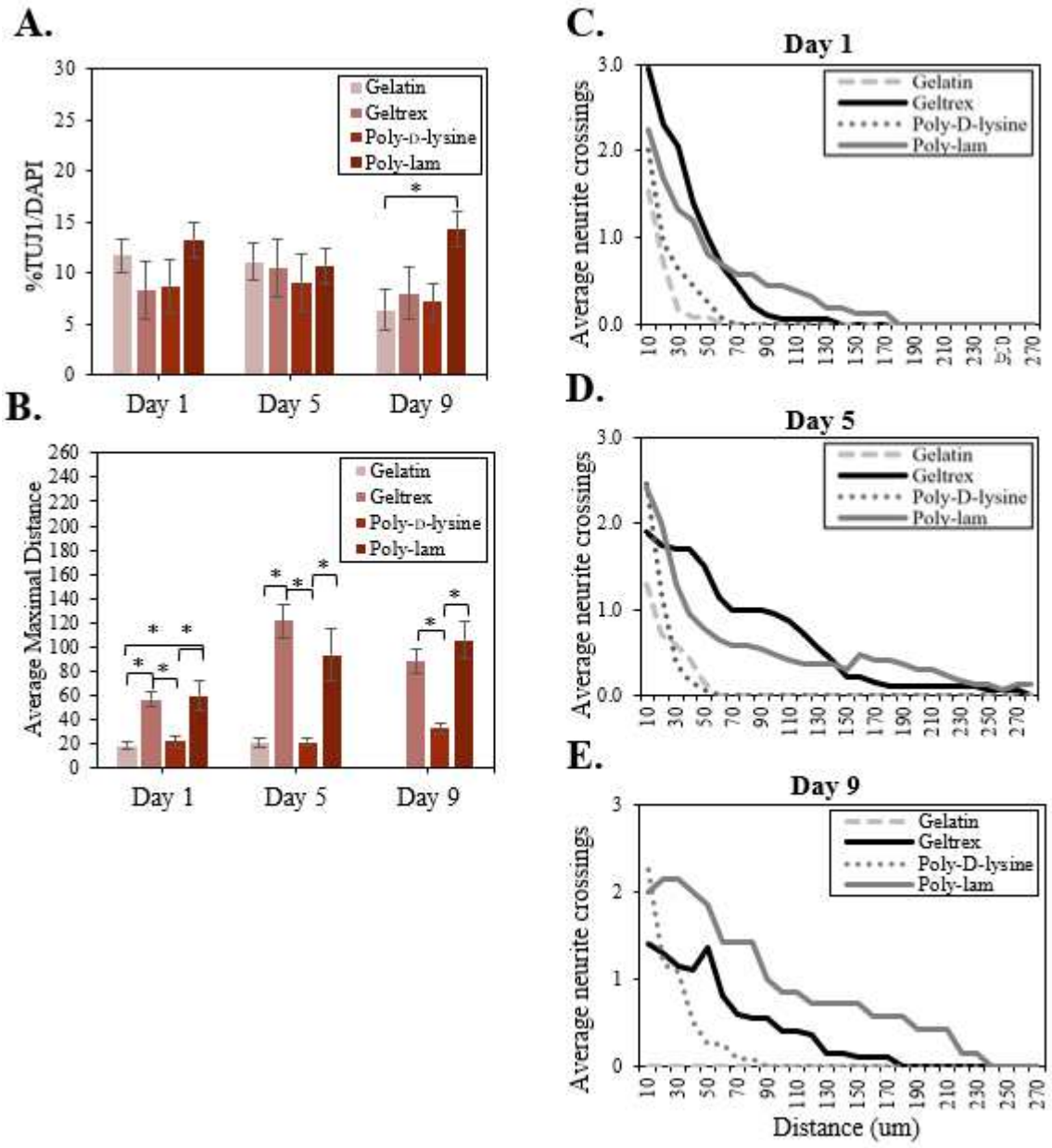

Figure 10. Quantitative analysis of TUJ1-positive cells generated from riPSC-derived NPCs. (A) The percentage of TUJ1-positive cells over total number of cells indicates increased neuronal differentiation on poly-lam by D9. (B) Average value for maximal distance a neurite reached during Sholl analysis shows increased neurite elongation on Geltrex and poly-lam substrates in comparison to gelatin and poly-D-lysine. Histogram values are means ± SEM (n ~ 20; ANOVA). *Statistical significance set at $p < 0.05$. (C-E) Sholl analysis of the average neurite crossings in neurons (TUJ1-positive) derived from rNPCs (n ~ 15).

Geltrex displayed a significant increase in neurite crossings as compared to gelatin ($p < 0.001$), poly-D-lysine ($p < 0.006$), and poly-lam ($p < 0.001$). At D9, both gelatin and Geltrex showed a significant increase in the total number of neurites when compared to poly-lam ($p < 0.001$). Overall, the promotion of MAP2-positive expression and neurite extension was less robust on poly-lam than other the other substrates tested; this result was notable for its opposing effect to TUJ1 results (Figure 6-7).

2.4.4 Spiking activity is similarly limited across substrates, although spikes recorded on Geltrex demonstrate longer duration

Overall, spiking activity was limited for all rNPCs-derived neurons independently from the substrates they grew on, indicating functional immaturity of the differentiated cells. Single spikes

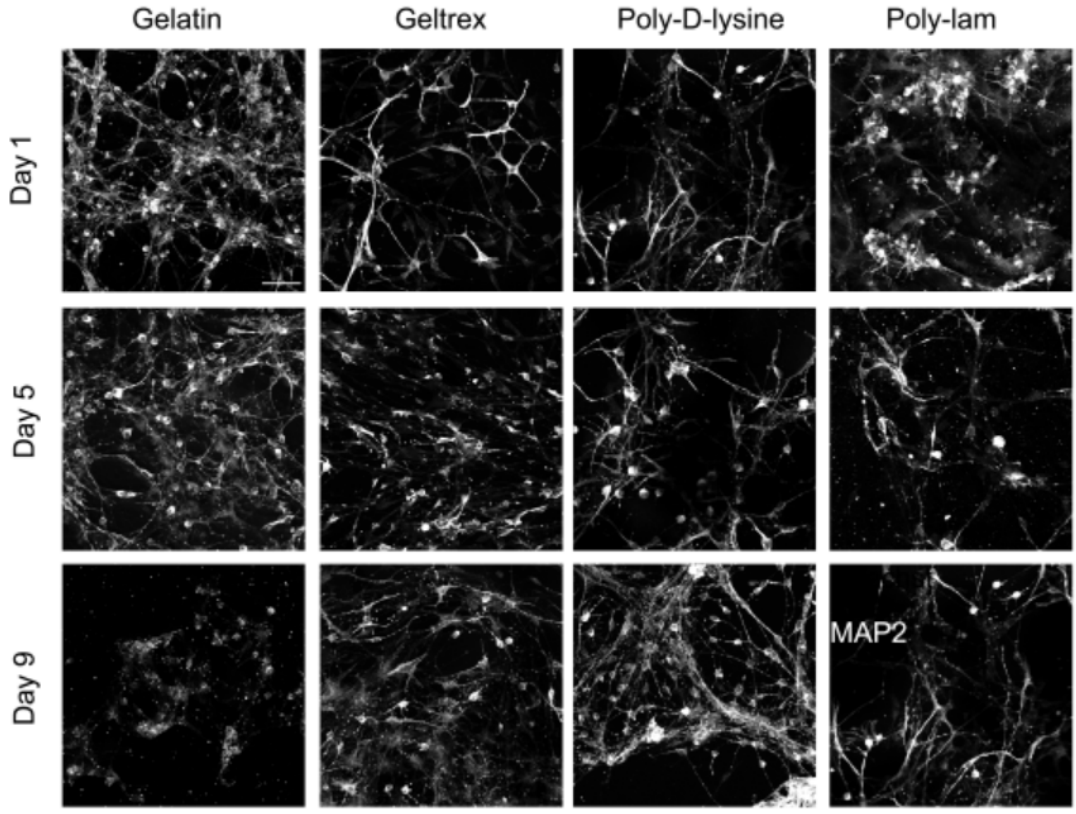

Figure 11. Representative images of MAP2-positive cells plated on various substrates at days 1, 5, and 9 of differentiation. Observations indicate that MAP2-positive cells exhibit different morphology by substrate and time point. Scale = 50

were obtained across substrates and time points (Figure 9A), with a single instance of a spike train observed on poly-lam (Figure 9B). As a benchmark for comparison, embryonic (E18) rat cortical neurons display robust responses to injected current using similar electrophysiology protocols (Figure 9C). Nonetheless, poly-lam and Geltrex resulted in increased probability of spiking compared to poly-D-lysine and Geltrex. To further analyze excitability, the spike width (duration) at half-amplitude values were measured for each cell that spiked (decreased half-amplitude values indicate briefer, more mature spiking characteristics) (Figure 9D). Geltrex favored increased half-amplitude width at D1 when compared to gelatin ($p = 0.001$), poly-D-lysine ($p = 0.045$), and poly-lam ($p = 0.002$). At D5, Geltrex sustained increased half-amplitude width, being statistically significant when compared to gelatin ($p = 0.004$) and poly-lam ($p = 0.011$). However, at the latest time point there were no substrate-related effects on this measurement. Excitability of immature neurons was limited regardless of the substrate tested, and none of the substrates demonstrated an obvious positive effect on electrical maturation. Spikes from cells seeded onto poly-D-lysine were especially challenging to elicit, resulting in limited observations (Figure 9A).

2.5 Discussion

In this study, the effects of cell substrates on the morphological and functional features of differentiating rat neurons for the derivation and differentiation of rNPCs based on unique substrate conditions (summarized in Supplementary Table 1) have been characterized. Conditions for differentiation were optimized by screening various substrates to promote optimal growth and adhesion for neuronal differentiation. Electrophysiology, immunofluorescence detection of neuronal markers, and Sholl analysis were used to characterize neuronal differentiation of rNPCs by validating excitability and maturity. Our results indicated the following: (1) that poly-lam coating promoted optimal neuronal differentiation based on Sholl analysis, TUJ1 expression, and

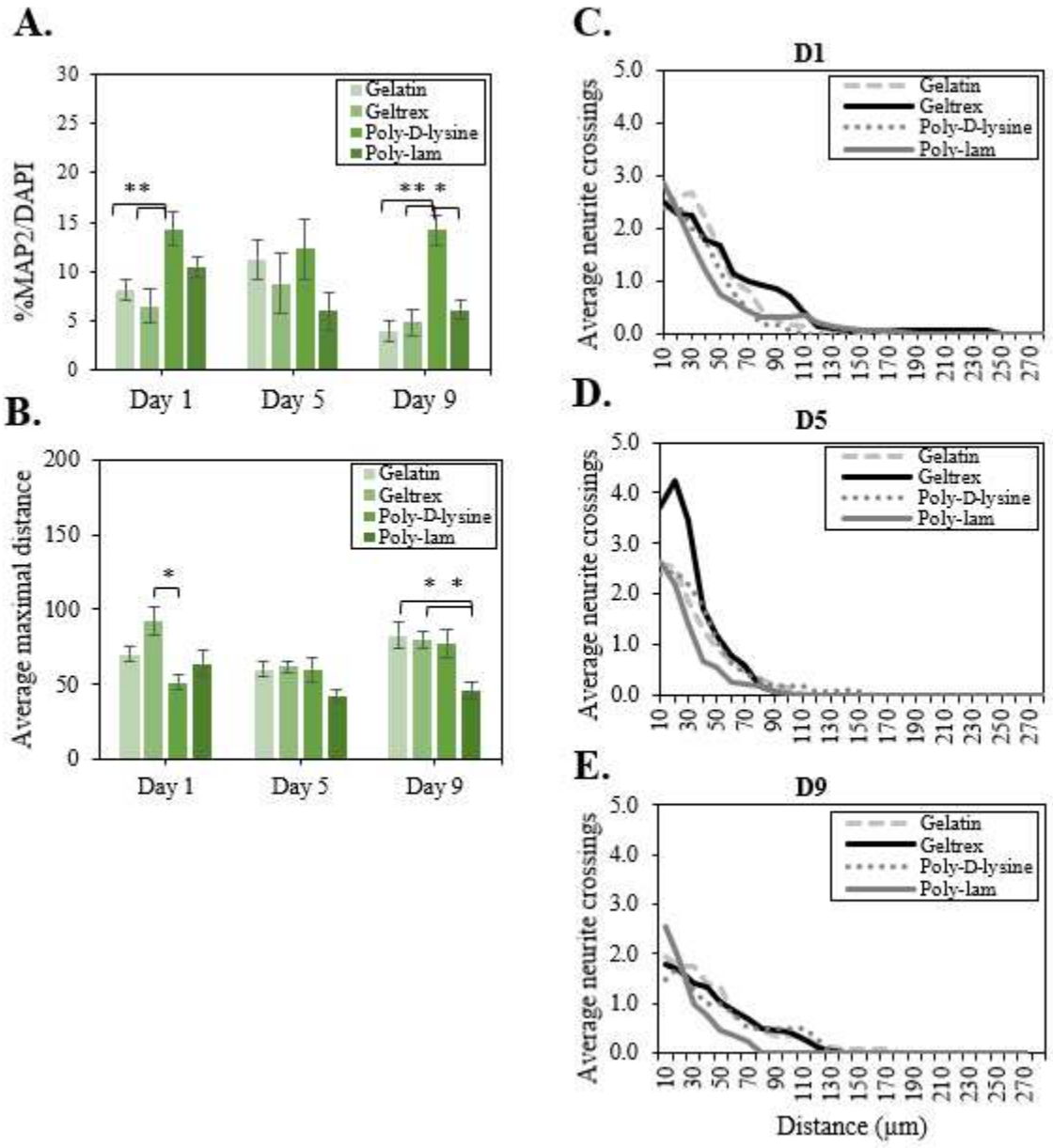

Figure 12. Quantitative analysis of MAP2-positive cells generated from riPSC-derived NPCs. (A) The percentage of MAP2-positive cells over the total number of cells indicates increased MAP2 positivity on poly-D-lysine substrates. (B) Average value for maximal distance a neurite reached during Sholl analysis for MAP2-positive cells. Histogram values are means ± SEM (n ~ 20; ANOVA). *Statistical significance set at $p < 0.05$. (C-E) Sholl analysis of the average neurite crossings in neurons (MAP2-positive) derived from rNPCs (n ~ 15).

electrophysiology, (2) that Geltrex induced a bipolar morphology in attached cells, (3) that poly-D-lysine coated substrates resulted in increased MAP2 expression (which was not necessarily indicative of electrically mature neurons), and (4) that gelatin, although cost-effective, was an inefficient coating strategy for producing neurons following differentiation.

2.5.1 Substrate-dependent effects on structural maturity and cell type-specific marker expression

Each of the substrates selected elicited a distinctive phenotype pattern of neuronal differentiation growth, indicative of a substrate-dependent effect on morphology. Few studies have compared the role that culture substrate plays on the morphological and functional maturity of neurons differentiated from rNPCs. Nonetheless, previously published studies have underscored the importance of the cell culture substrate in determining cell fate. It has been shown that poly-lam promoted differentiation of rNPCs into neurons via the ERK pathway, as opposed to poly-L-lysine and fibronectin (Ge et al., 2015). Specifically, Poly-L-ornithine substrate for neural progenitor cells differentiation has shown that ERK 1/2 is required for polyornithine-induced preferred neuronal differentiation (Ge et al., 2015).

Laminin, as a major ECM component, promotes adherence through its binding domains, which have been shown to increase cell expansion, differentiation, and neurite outgrowth of NPCs-derived neurons in combination with polyornithine (Flanagan et al., 2006). Researchers have found that laminin promoted the proliferation of human neural stem cells via the integrin β1-dependent manner (Hall et al., 2008) and can interact with cells via various integrins such as (α7β1, α6β1, α3β1) (Arulmoli et al., 2016). Although gelatin may be an adequate substrate for neuronal

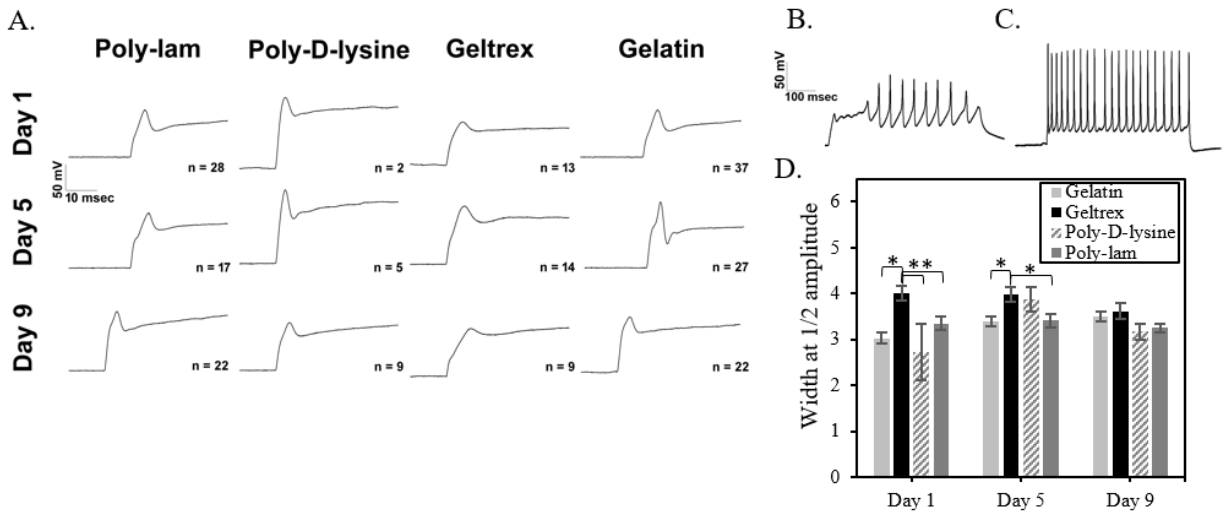

Figure 13. Electrophysiological recordings via patch-clamp. (A) Representative spikes for each substrate per time point. (B) Poly-lam at D9 exhibited a spike train from one cell (the only substrate to yield an observation of a spike train). (C) Spike trains of a primary rat cortical neuron are shown for comparison. (D) Half-amplitude values (ms) were calculated for each cell that spiked and averaged. *Statistical significance was defined at $p < 0.05$ (ANOVA).

differentiation in certain contexts (e.g., differentiation of murine embryonic stem cells via induction of proneural factors) (Purcell et al., 2013; Tong et al., 2010), it has also been reported that gelatin is not an ideal substrate candidate for promoting NPCs neurite outgrowth or homogeneous differentiation (Haque et al., 2015). Our results, which indicate superior induction of neuronal fate with laminin and inferior results with gelatin, largely align with published literature. These results for gelatin might be related to variations in the expression levels of integrins on the cell surface (Komura et al., 2015) which can also explain how gelatin has showed in some cases to be ineffective for adhesion of neural stem cells (Nakajima et al., 2007).

An unexpected result of the current study was that Geltrex, as a substrate for rNPCs, promotes the development of bipolar neurons with enhanced neurite elongation in comparison to the other substrates tested. Geltrex has been referred to be an analog of Matrigel, which has commonly been used for stem cell culture due to its potential to retain self-renewal and

differentiation capabilities (Hughes et al., 2010). Typically, Geltrex is used for seeding microglia or astrocytic cells since this substrate resembles the extracellular matrix of astrocytes (Sellgren et al., 2017) and has also been used for stem cell cultures (Akopian et al., 2010). Geltrex has shown to be also be effective in promoting neurite outgrowth, but the axons of these human stem cells showed low packing density (Song et al., 2019). Although the underlying mechanism is currently unclear, it may be the case that it has extrinsic cues that influence the polarity of the cells by promoting the transition to a bipolar stage during development given that polarization is known to be dependent upon cell-to-cell and cell-to-ECM interactions (Yogev and Shen, 2017).

Likewise, poly-D-lysine was associated with reduced arborization and unanticipated expression of MAP2, which is a marker typically associated with dendrites in differentiated, mature neurons (Izant and McIntosh, 1980; Ming and Song, 2005). Poly-D-lysine is a very commonly used cell adhesion molecule (CAM) due to its positive charge, which allows for neural adhesion (Harnett et al., 2007; Y. H. Kim et al., 2011). It works by attracting negatively charged cell membranes by electrostatic interaction responsible for facilitating neurite outgrowth (Y. H. Kim et al., 2011). However, poly-L-lysine is also likely to produce or enhance inflammatory cell responses (Strand et al., 2002) due to potential cellular toxicity at high concentrations (Yamamoto and Hirata, 1995). In our data, poly-D-lysine coating resulted in blunted neurite crossings and branches closer to the soma, inhibiting neurite growth and maturity, potentially due to toxicity.

When interpreting the higher expression of MAP2 in poly-D-lysine cultures, it is important to note that MAP2 has at least three isoforms and, while it is commonly used as a neuronal marker, can be associated with cells either in early development or mature neurons (Garner and Matus,

1988). The three isoforms are regulated during development and include a low molecular weight (70 kd) form, MAP2c, which is an early stage marker, and two high molecular weight (280 kd) forms, MAP2a and MAP2b, which are found in mature neurons (Johnson and Jope, 1992; Soltani et al., 2005). MAP2 was present in rNPCs after only 24 hours of starting the differentiation protocol, suggesting that staining was likely indicative of precursor cells or the result of spontaneous differentiation of neurons from NPCs. It has been reported that rat EGF-responsive neuronal precursor cells express MAP2 in a sort of bimodal time course, appearing at both an immature and a mature stage when seeded on poly-D-lysine coating (Rosser et al., 1997). MAP2c has also been present during early development in cells that have small and rounded morphology (Blümcke et al., 2001; Doll et al., 1993) and in neurons after ischaemic damage (Saito et al., 1995). This early detection of MAP2 is may not be an indication of maturity, but rather to provide support for neurite formation (Riederer, 1995). It has been reported that glial cells may also express MAP2 during development and early differentiation (Blümcke et al., 2001). Additional experiments will be needed to clearly identify what type of cells are present in the rNPCs population that identify positively for MAP2.

2.5.2 Dichotomy of structural versus functional maturity, and future strategies for improvements

Results suggest differential effects of substrates on the morphology and structural maturity of rNPCs-derived neurons; however, these differences did not translate to changes in functional maturity based on electrophysiology results. Functional maturity requires a proper repertoire of voltage-gated ion channels to be expressed in the cell membrane, and amongst other factors, involves the expression of neurotransmitter receptors prior to synaptic activity and the presence of excitatory GABA (Lledo et al., 2006). Here, the characterization of rNPC-derived neurons could

be improved by investigating cellular proliferation, GABA markers, oxidative stress, and cell-specific phenotype markers. The difficulties associated with producing structurally and functionally mature neurons from progenitor and stem cells is an ongoing challenge in the field (Gage and Temple, 2013). A possible future strategy to improve maturity in rNPCs-derived neurons is to maintain three-dimensional (3D) multicellular structures during all steps from differentiation to maturation, which has been shown to enhance the function of iPSCs-derived neural cells (Illes et al., 2009; Y. Li et al., 2013) and long-term expansion (Li et al., 2016) compared to monolayer cultures. Likewise, induction of specified proneural factors in combination with substrate-associated cues may further enhance results in a synergistic fashion (Purcell et al., 2012).

2.5.3 Conclusions and Future Improvements

This study characterizes and compares the impact of four distinct, commonly used cell culture substrates on the neuronal differentiation of riPSC-derived rNPCs on the functional and structural maturity of the cells. Results suggest that specific substrate coatings can be chosen to produce neurons with unique morphologies. Simple changes in substrate coating methods, therefore, may be used to enrich differentiating rNPCs for the desired level of neuronal maturation and morphology, tailored to the objectives of a specific study. Our results revealed that poly-lam promotes neural differentiation of arborized, TUJ1-positive cells from rNPCs, while Geltrex produces neurons with a bipolar morphology. Geltrex also exhibited very wide single spikes, suggesting dominant calcium-dependent activity which may be a sign of immaturity (Johnson et al., 2011; Zhou and Hablitz, 1996). Poly-D-lysine favored the evolution of immature neurons with unexpected MAP2 labeling, and gelatin resulted in unfavorable growth and differentiation

efficiency over the nine-day time course. A need remains to further understand the interaction of progenitor cells with their microenvironment and signaling to promote functional maturation of these cells. Nonetheless, our results indicate that the fate of rat NPCs, which are less well-understood and characterized than their counterparts from mice, can be manipulated through simple modification to surface coating conditions. Future work is aimed at exploring the differentiation of rNPCs via optically-induced proneural factors to increase the preciseness of spatiotemporal control and integration with neural networks (Khan et al., 2018; Winter et al., 2017).

2.6 Acknowledgments/Funding

The authors would like to thank Dr. Marie-Claude Senut and Biomilab for their expert training on stem cell cultures, guidance, and use of their facilities. Melinda Frame for confocal microscopy training. Research reported in this publication was supported by the National Institutes of Health (NIH) under award number [1 R03 NS095202-01] and by the Discretionary Funding Initiative (DFI) by the Michigan State University Foundation.

3. CHAPTER 3 | A blue light-inducible system for spatial gradient control of mammalian gene expression

3.1 Introduction

Inducible gene expression systems are highly desirable tools in biomedical research for their ability to regulate cellular signaling pathways in a controlled fashion. Traditionally, gene expression systems utilized exogenous chemical inducers to achieve transcription factor binding for artificial control of gene expression. However, the efficacy of chemical systems is limited due to their potential off-target effects, transport delays, toxicity, and lack of reversibility (Kolar and Weber, 2017). Likewise, the relative lack of spatiotemporal control is a critical limitation to this approach. Through recent advances in optogenetics, light-inducible systems derived from naturally photosensitive organisms have been identified to provide enhanced spatial and temporal control in comparison to chemically induced approaches. Over the past decade, the variety of photoactivatable proteins used for inducible gene expression has expanded, including Light-Oxygen-Voltage-Sensing (LOV) domains (Strickland et al., 2012; Tischer and Weiner, 2014; Wu et al., 2009), phytochromes (PHY) (Beyer et al., 2015; Buckley et al., 2016; Muller et al., 2013) and cryptochromes (CRY) (Kennedy et al., 2010; Konermann et al., 2013; Polstein et al., 2017; Polstein and Gersbach, 2015; Taslimi et al., 2016). All these systems share a common objective: identify a protein for signaling domain coupling to regulate gene expression efficiently and robustly in a light-dependent manner.

Light is an ideal tool for controlling gene expression given its high spatiotemporal precision, tunability, and potential for multichromatic control. Nonetheless, opportunities remain to further improve response characteristics, particularly for blue light-activated systems. Many naturally occurring photosensitive systems have evolved to preferentially respond to blue or red

wavelengths (reflecting green light) (Nishio, 2000), and blue light activation is particularly common amongst available optogenetic systems. However, blue light is particularly prone to diffraction in tissue (Yizhar et al., 2011), creating a precipitous decline in optical power density as a function of distance from the light source and severely limiting the depth of penetration for effective activation. Two possible avenues to circumvent this issue are: (1) to explore photoactivatable systems which are responsive to longer wavelengths of light (red and infrared), which display reduced scatter and improved tissue penetration, or (2) to genetically modify naturally occurring systems to enhance sensitivity to blue light (i.e., to allow blue light-activated systems to respond to a lower optical power density). In this study, we explored a recently described blue-light activated gene expression system (EL222, Motta-Mena et al., 2014) to achieve quantifiable induction of gene expression with minimal applied optical power. EL222 is one of four signaling proteins that are part of the light-oxygen-voltage (LOV) domain derived from *E. litoralis* that undergoes a conformational change when exposed to blue light, ultimately favoring dimerization, DNA binding, and expression of a downstream gene (Motta-Mena et al., 2014; Rivera-Cancel et al., 2012). Since EL222 has gone through optimization efforts including photochemistry for various lifetime ranges (Zoltowski et al., 2013, 2011), signal propagation (Rivera-Cancel et al., 2012) and faster on/off kinetics (Motta-Mena et al., 2014), we first explored various versions of the construct to assess the potential to reduce the optical power density required for activation. With limited optical power requirements, EL222 could more effectively penetrate tissue and possibly be used in combination with red light-activated systems (Beyer et al., 2015; Tischer and Weiner, 2014) to enable multichromatic control of gene expression.

Our first goal was to explore the EL2222 variants, understand their activation requirements (which, in turn, would provide design parameters for an implanted LED array), and explore the potential to achieve spatial control of gene expression along a gradient of optical power. Transient transfections were used to initially optimize and understand the system; we tested various versions of the EL222 sequence for an initial characterization of reporter gene induction in response to a low-cost, macro-scale blue LED panel. However, for repeatability between trials, a more controlled expression system was required, as well as an LED light source micro-scaled for implantation. For this, the EL222 system was successfully utilized to develop a stable cell line for optimizing induction of gene expression in mammalian cells. This system enabled the exploration of a variety of stimulation conditions (duration and intensity of light exposure, and their interaction effects) in response to a micro-LED light source. Lastly, we produced spatial gradients of gene expression along an applied gradient of optical power. The spatial gradient of gene expression could be controlled either through modified stimulation parameters (intensity and duration of exposure) or via a custom engineering the micro-LED light source with a coupled micromirror system. Photo-patterning of gene expression is expected to facilitate new approaches for tissue engineering and regeneration, including reconstruction of damaged neural circuitry and restoration of function following central nervous system injury. It may also enable control of gene expression and cell fate at an implanted optoelectrode interface.

3.2 Results encompassing initial EL222 characterization with transient transfection protocol

3.2.1 Initial validation and optimization of system under transient transfection.

Our first task was to derive the EL222 system and validate its ability to induce gene expression in response to blue light. In these early experiments, we explored an EL222 sequence

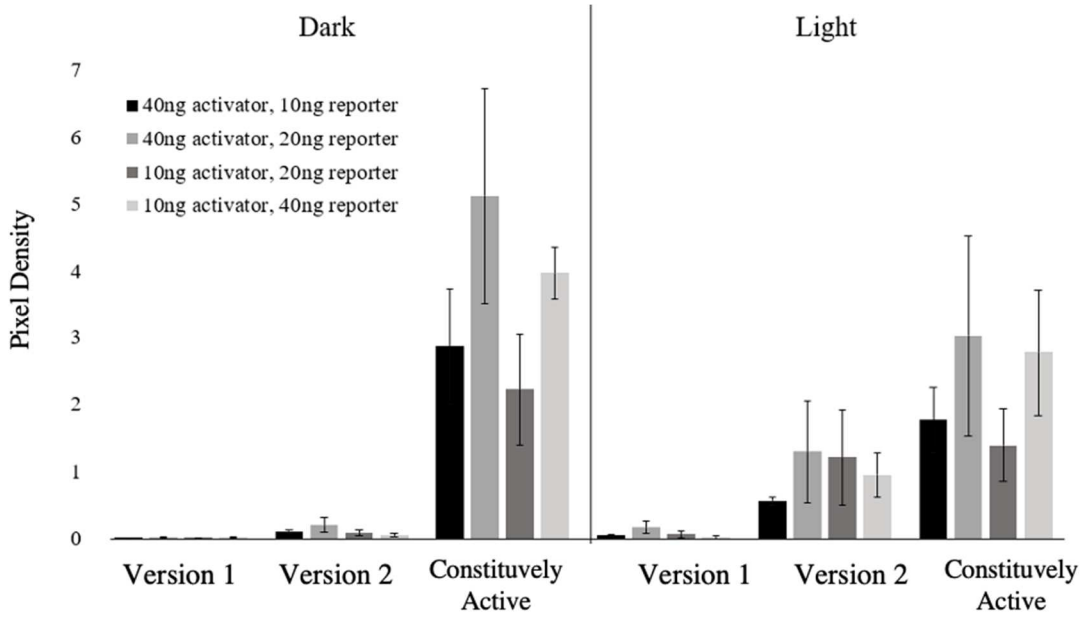

Figure 14. Comparison of original, enhanced and constitutively active EL222 systems under dark and light conditions. Four ratios of activator and reporter (YFP) are shown for the various EL222 systems.

designed to replicate the original version reported by Motta-Mena ('version 1', 'v1') and a modified version predicted to enhance light-responsiveness ('version 2', 'v2') to induce downstream expression of a fluorescent reporter (red fluorescent protein, "RFP", or yellow fluorescent protein, "YFP"). We used a rudimentary, inexpensive commercially available blue LED panel for induction, and used two levels of intensity of exposure by adjusting the proximity to the light source. We also tested various ratios of activator and reporter constructs for transient transfection alongside the different power intensities to determine the optimal conditions for light-induced gene expression. While variable, the data show that a 40ng activator and 20ng reporter combination registered the most robust results (Figure 14 and Figure 15 bottom panel, Linear Mixed Models test: $p<0.05$); thus, this ratio was chosen for the rest of the experiments outlined in this section. Results demonstrate that both intensity levels of blue light exposure (0.004 W/cm^2 and 0.006 W/cm^2) resulted in significant induction of gene expression in comparison to unexposed cells, as evidenced by increased pixel density values (Figure 15B-C, Linear Mixed Models test:

$p<0.05$; n=3 biological replicates). However, pixel density values for the cells exposed to 0.004 W/cm^2 of power were higher than that for cells exposed to 0.006 W/cm^2 (Figure 15B and 2C), where improved viability and cellular attachment in response to reduced exposure and heat generation are potential underlying reasons (EL222 reportedly activates under minimal optical power, 0.0008 W/cm^2 (Motta-Mena et al., 2014)) . Version 2 proved to be more sensitive compared to v1 suggesting successful development of a more robust gene expression system (Figure 14 and 15), although it also exhibited increased dark state activation (background). However, while reducing the intensity of exposure negated the ability of the original EL222 system to respond to light (to ~67% of the 0.006 W/cm^2 exposure condition), the v2 version delivered observable light-induced reporter expression in response to the relatively weaker stimulus (Figure 14 and 15). As a control for comparison, the constitutively active version developed yielded higher pixel density values than v1 and v2, validating the induction efficiencies of these versions relative to a system which is "always on" (Figure 15). While these results initially validated the function of the system, it was also evident that further refinement was needed to optimize the construct, reduce variability, and determine optimal optical stimulation parameters.

3.2.2 Refinement of light source and initial validation of spatial patterning of gene expression.

The future vision of our use of these systems is to couple optogenetic induction of gene expression to implanted microelectrode arrays. To better inform the light exposure conditions necessary to spatially pattern gene expression using a microscale light source for implantation, we replaced the large scale ~ 28 x 10 cm LED panel with a single micro-LED 270 x 220 um under each culture well. Each micro-LED was assembled into a custom 3D-printed tray designed for use with a 24-well cell culture plate, and exposure conditions were controlled with an Arduino

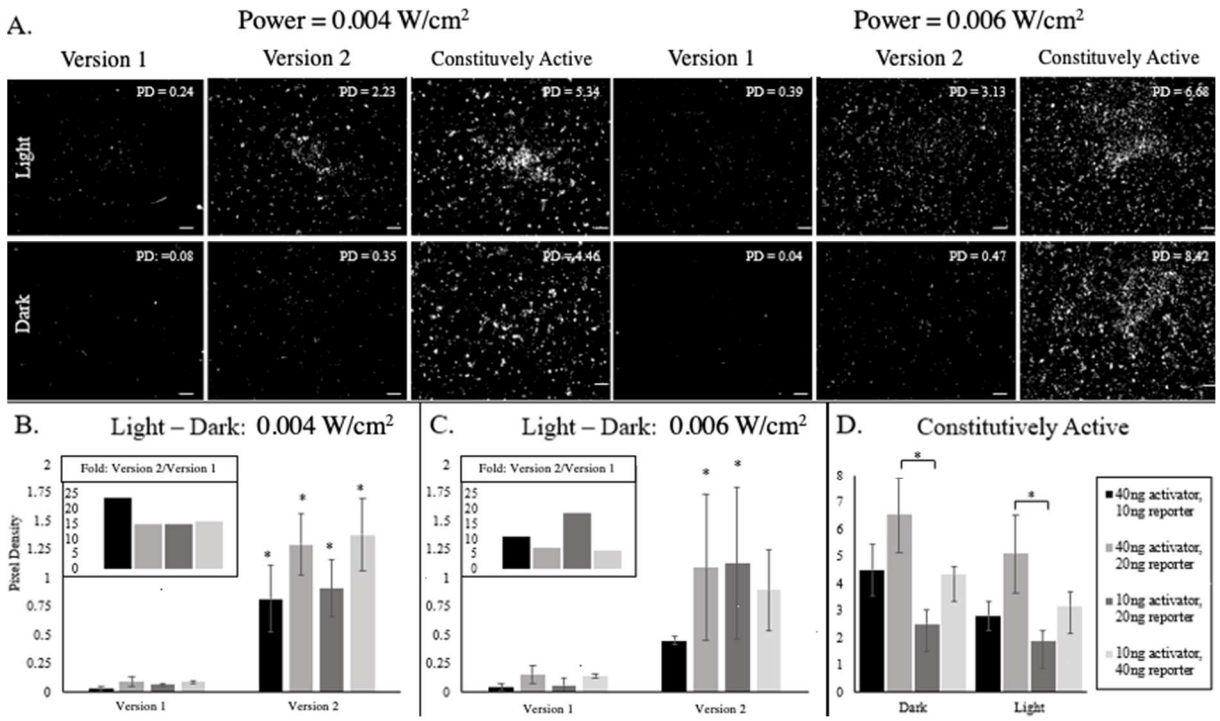

Figure 15. Comparison of v1, v2 and constitutively active EL222 systems for various power settings. (a) Light inducible expression of RFP reporter under blue-light (top) and dark (bottom) conditions for the original, enhanced and constitutively active systems. Blue-light power at 0.004 W/cm^2 (left) and at 0.006 W/cm^2 (right). (b) Fold-change of RFP expression of light minus dark pixel density values of v1 (left) and v2 (right) for 0.004 W/cm^2. (c) Fold-change of RFP expression of light minus dark pixel density values of v1 (left) and v2 (right) for 0.006 W/cm^2. (d) Pixel density values for constitutively active activator under dark and light conditions. Conditions with an asterisk (*) are statistically significant as determined by a Linear Mixed Models test (v2 vs v1 in panels B and C and as indicated in panel D; $p<0.05$; n=3 biological replicates.

microcontroller and micro-LED driver (see Methods). For these experiments, we studied the stimulus-response characteristics of version 2, because it delivered increased reporter expression in early experiments. V2 was tested for various blue-light exposure times (0, 5, 30, 60, 120, 240, and 480 minutes) at various power intensities adjusted using the power source to the micro-LED (as measured at the LED source: 100%= 1.3 *W/cm^2*, 65%= 0.8 *W/cm^2*, 45%=0.6 *W/cm^2*) utilizing the micro-LED setup described in the Methods section. Note that although it was not possible to directly measure the optical power in the culture setting, the optical power density received at the cell surface is estimated to be a small fraction (<1/40) of the source power.

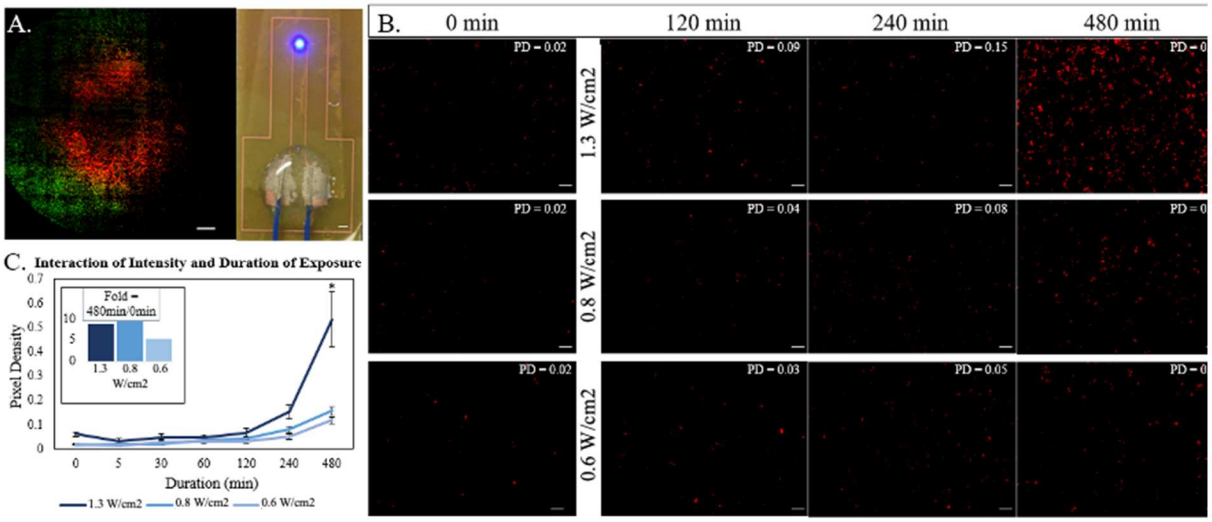

Figure 16. Enhanced activation in relation to time and power intensity. (a) Expression of RFP reporter (red) and YFP activator (green) (left) and micro-LEDs used for reference (right); scale=1mm. (b) RFP reporter expression for enhanced EL222 activator under various times: 0 min, 120 min, 240 min, ad 480 min (left to right) as well as blue-light intensities: 100%, 65% and 45% (from top to bottom); scale=0.5mm. Images are exemplary. (c) Pixel density in relation to blue-light exposure duration. Inset indicates fold-change of 480 min to 0 min.

A nonlinear interaction between intensity level and exposure duration was evident, where longer exposure durations revealed synergistic increases in induced gene expression with increased exposure intensity (Figure 3C). Increased power did not lead to a significant increase in pixel density for durations ≤120 minutes; however, increased power markedly increased pixel density for longer exposure durations (Figure 3C, Linear Mixed Models test: $p<0.05$; n=6 biological replicates). For all power levels, a minimum 4-hour exposure period was required to register increased pixel density values in comparison to non-exposed samples. Blue-light exposure of 480 minutes indicated, in all cases, significantly higher pixel density values (Linear Mixed Models test: $p<0.05$; n=6 biological replicates) than any other duration of exposure. Pixel density values were statistically higher at a duration of 480 minutes (Figure 16C, Linear Mixed Models test: $p<0.05$; n=6 biological replicates). Additionally, pixel density results exhibited relatively low

variability at various power levels as demonstrated by images in Figure 16B and error bars in Figure 16C.

3.2.3 Refinement of sequence and creation of a stable cell line to reduce experimental variability.

From previous results herein, the EL222 variant created with three amino acid modifications ("v2") was found to confer approximately ~10-15-fold increased light sensitivity on average over our "v1" (Figure 15). Modification at a fourth amino acid was found to convert v2 to a constitutive activator ("CA") with equal activity in either light or dark for purposes of testing and development of future variants. However, neither of these versions achieved the desired level of induction, suggesting a need to revisit the sequence. Sequencing performed by the MSU RTSU Genomics Core indicated that v1 was a truncated version of EL222 with eight missing bases. In addition, the transient transfection protocol led to a high inter-trial variability suggesting a need to control for cell density homogeneity and fine-tuning of variability between replicates. We next reexamined our optogenetic system by developing a cell line which stably expressed the EL222 system (Biomilab, LLC). Furthermore, we needed to normalize the images to cell density in order to assess spatial gradients of induction (normalization would correct for inhomogeneous cell density). The results that follow here represent this phase of this project, which show similar methodology but take advantage of utilizing a stable cell line while also providing an internal control for cell density and reporter expression.

3.3 Results utilizing a stable cell line

3.3.1 Pilot test indicates EL222 'v3' has superior light-responsive characteristics

The first step in troubleshooting our optogenetic system was to examine various mutations and combinations to understand the optical induction results. A pilot test was conducted with specific mutations as variants to the original EL222 system. Table 1 describes these eight specific variants utilizing four different mutations performed to the original EL222 system (shown first). After blue-light exposure, a trend towards an increased overall reporter expression was revealed for mutation 1 (Mut 1) and combinations containing Mut 1 for cells exposed to light as well as those kept in the dark (Figure 17). Mut 1 closely resembled "CA" which is the constitutively active mutation we developed that allows gene expression to be kept *on* irrelevant of light exposure. Mutation 2 (Mut 2), mutation 3 (Mut 3), Mut 2 & 3, as well as the version 3 ("v3") EL222 system with 8 missing bases revealed a baseline that was lower than their light-exposed counterparts. Overall the v3 system most closely replicated the one developed by Motta-Mena et al., 2014, featuring a lower baseline and a higher reporter light-induction compared to the rest of the mutations tested for the pilot (Figure 17). The successful creation of this optical gene expression system was verified via genetic sequencing (data not shown).

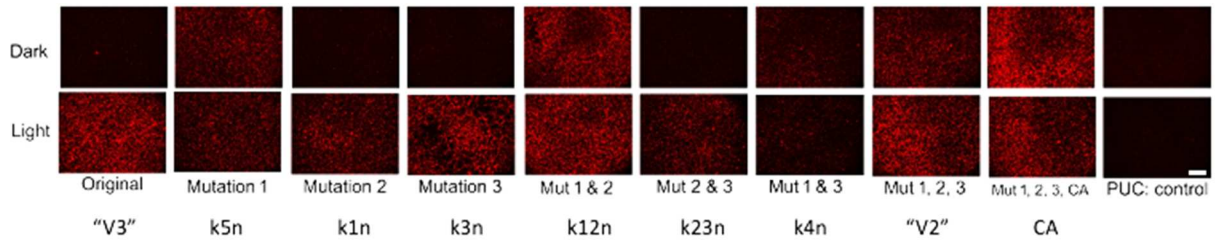

Figure 17. Blue-light induction utilizing transient transfection to test for various mutation separately and in combination. Scale = 0.1mm.

Table 1. Properties of substrates tested for neural differentiation of rNPCs.

SUBSTRATE	POLY-D-LYSINE	POLY-L-ORNITHINE-LAMININ	GELATIN	GELTREX
DESCRIPTION	Poly-D-lysine is a positively charged synthesized extracellular matrix for non-specific attachment of cells to plastic and glass surfaces.	Poly-L-ornithine is positively charged polycationic amino acid polymer. Laminin is a structural protein that forms the extracellular matrix component.	Gelatin is a mixture of water-soluble proteins with high molecular weights that are present in collagen.	Geltrex is composed of basement membrane with major components such as laminin, collagen IV, entactin, and heparin sulfate proteoglycan.
MOLECULAR WEIGHT	~70-150 kD	~78 kD (Poly-L-ornithine); ~400-900 kDa (Laminin).	~300 kD	Not provided.
MECHANISM OF CELL ATTACHMENT	Positive charge enhances electrostatic interaction between negative charges presented by the cell membrane and the culture substrate. Increases number of positively charged sites for cell binding.	Acts by positive charge enhanced electrostatic interaction between negative charges presented by the cell membrane and the culture substrate. It increases the number of positively charged sites for cell binding. Laminin has active domains for collagen binding and cell adhesion and is used to support neural differentiation.	Improves cell-interactive properties and attachment.	Provides physical support and compartmentalization of tissues and influences cell function.
PROTOCOL FOR CELL SEEDING	Coat the surface of the culture vessel with a working solution of poly-D-lysine. Incubate at RT for 1 hour. Remove and rinse with PBS. Let dry.	Coat the surface of the culture vessel with a working solution of poly-L-ornithine. Let sit at RT overnight. Aspirate any residual the next day and rinse with sterile water. Laminin is then used to coat the surface of the culture vessel which is kept overnight in a humidified incubator at 37°C, 5% CO_2. Aspirate any residual the next day, rinse twice with PBS.	Coat the surface of the culture vessel with a working solution of gelatin. Allow to dry for two hours.	Coat the surface of the culture vessel with a working solution of Geltrex. Incubate at 37C for 1 hour and aspirate.
COST	$$	$$	$	$$$
SUPPLIER	Advanced Biomatrix	Sigma-Aldrich	Sigma-Aldrich	ThermoFisher

*Information for each substrate was obtained from supplier's website.

Table 2. Description of mutations created from original EL222 system.

Transactivators	Description	Specific Mutation
"V3"	Original (Motta-Mena 2014)	NLS VP16 EL222
K5n	Mut 1	NLS VP16 EL222 Mut 1 aa 41: Val to Ile
K1n	Mut 2	NLS VP16 EL222 Mut 2 aa 52: Leu to Ile
K3n	Mut 3	NLS VP16 EL222 Mut 3 aa 79: Ala to Gin
K12n	Mut 1 & 2	NLS VP16 EL222 Mut 2 aa 52: Leu to Ile Mut 1 aa 41: Val to Ile
K23n	Mut 2 & 3	NLS VP16 EL222 Mut 3 aa 79: Ala to Gin Mut 2 aa 52: Leu to Ile
K4n	Mut 1 & 3	NLS VP16 EL222 Mut 3 aa 79: Ala to Gin Mut 1 aa 41: Val to Ile
"V2"	Mut 1, 2 & 3	NLS VP16 EL222 Mut 3 aa 79: Ala to Gin Mut 2 aa 52: Leu to Ile Mut 1 aa 41: Val to Ile
"CA"	Mut 1, 2 & 3 Constitutively Active	NLS VP16 EL222 Mut 4 aa 120: Leu to Ly Mut 3 aa 79: Ala to Gin Mut 2 aa 52: Leu to Ile Mut 1 aa 41: Val to Ile

3.3.2 Stimulus light-responsive characteristics utilizing micro-LEDs demonstrate a 'dose'-dependent effect of intensity and duration of light exposure

Our motivation behind exploring the stimulus-response characteristics is to to adapt this system for our purpose of brain electrodes, which represents a novel use of optical induction of gene expression. Therefore, similar to results shown earlier, we studied the stimulus response characteristics of the optimized EL222 system, version 3 ("v3") with micro-LEDs. We tested the version 3 for various blue-light exposure times (0, 5, 30, 60, 120, 240, and 480 minutes) at three different power intensities (100%=1.18 W/cm^2, 75%=0.88 W/cm^2, 50%=0.59 W/cm^2). Again,

longer durations of blue-light exposure led to a synergistic effect which revealed an increase in gene expression. Likewise, higher power intensities led to an increase in gene expression encompassing all power intensities. Representative images for all powers are shown below (Figure 18, Figure 19, Figure 20). Qualitatively, a Hoechst nuclear counterstain, which was used to control for cell density, is similar throughout power trials as well as inter-trials. Reporter induction for the 50% power trial is difficult to see by eye (Figure 18), however an increase is shown for the 75% power trial (Figure 19), and an even higher expression is visible at 100% power (Figure 20). Pixel density values were calculated via MATLAB program discussed in the Methods section. Light over dark values (fold) were calculated as an average for each trial (shown in Table 3).

Increased power led to a significant increase in pixel density for durations ≥ 120 minutes; however, for durations below 120 minutes no significant difference was shown (Figure 21A, Linear Mixed Models test: $p<0.05$; n=6 biological replicates). Induction was normalized to Hoechst density. Blue-light exposure of 480 minutes indicated higher pixel density values than any other duration of exposure and was significant for 50% and 70% powers (Figure 21B, Linear Mixed Models test: $p<0.05$; n=6 biological replicates).

Table 3. Pixel density fold values averaged for each trial (n=2 wells/trial).

Trial number	0	5	30	60	120	240	480
50% (1)	0.28	0.51	0.42	1.20	0.51	1.46	1.92
50% (2)	0.99	0.91	0.42	1.61	1.08	4.51	2.89
50% (3)	0.31	1.24	14.99	4.77	1.27	5.76	2.47
75% (1)	0.28	0.79	1.28	2.16	3.27	3.41	8.39
75% (2)	0.37	0.43	0.27	1.62	4.62	21.07	19.67
75% (3)	0.26	1.91	1.20	1.85	7.41	12.30	16.32
100% (1)	0.51	3.13	2.67	5.08	11.92	32.13	42.17
100% (2)	0.14	1.20	1.18	2.56	2.56	13.26	10.77
100% (3)	0.38	11.74	0.75	3.19	21.19	34.28	35.57

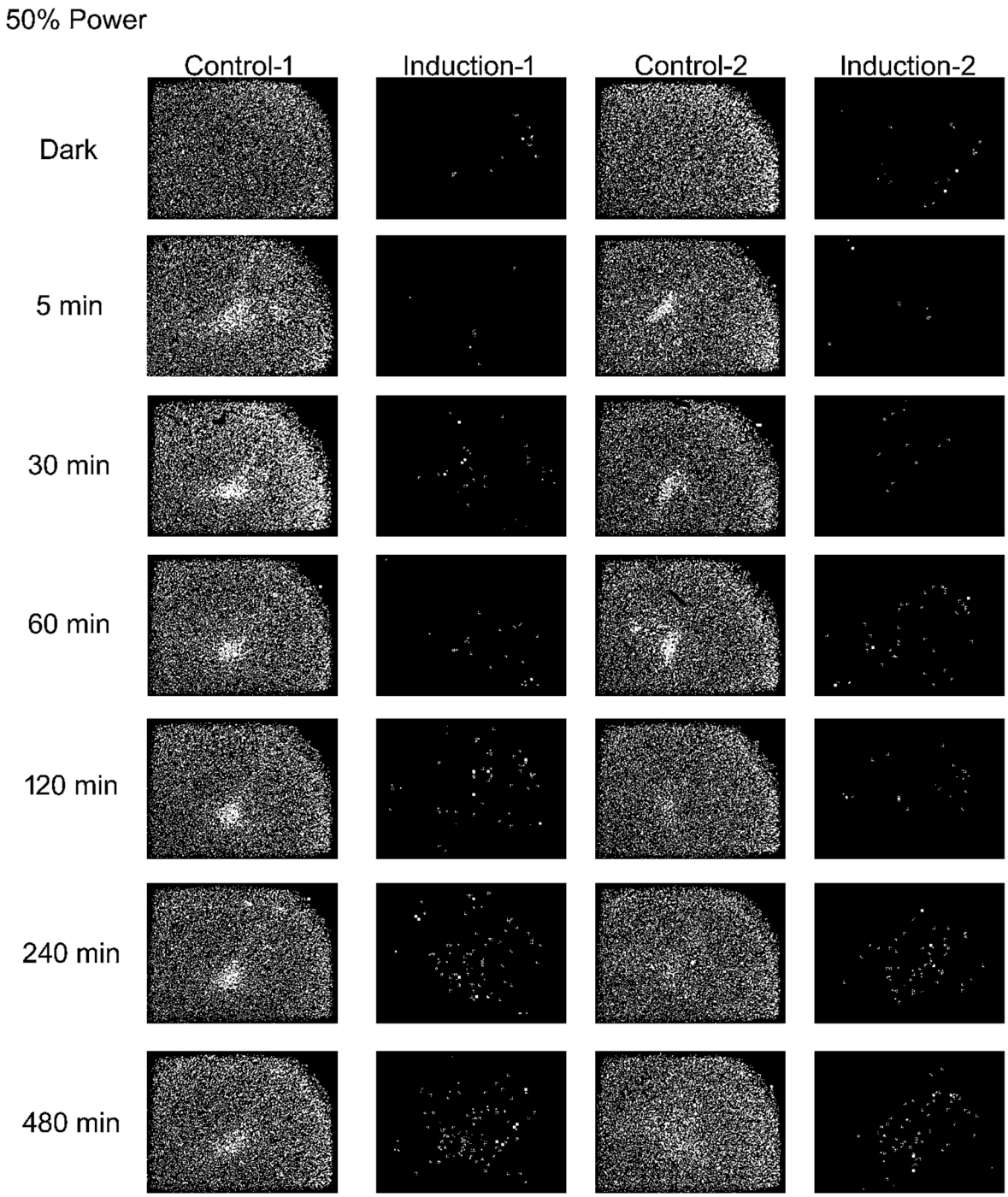

Figure 18. Representative images of micro-LEDs experiment at 50% power. Control column show Hoechst stain (total cell population) and induction columns shown reported expression due to light-induction.

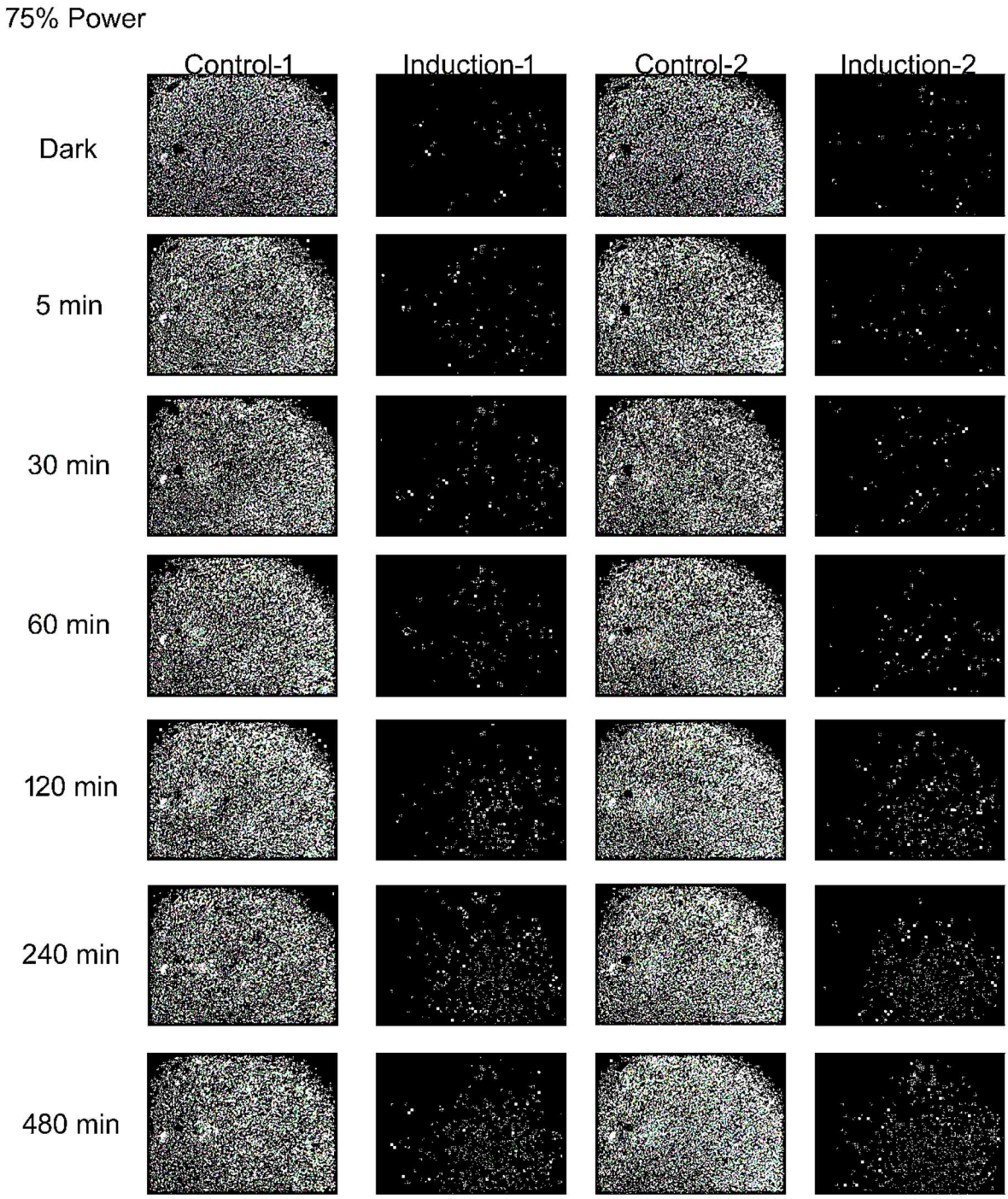

Figure 19. Representative images of micro-LEDs experiment at 75% power. Control column show Hoechst stain (total cell population) and induction columns shown reported expression due to light-induction.

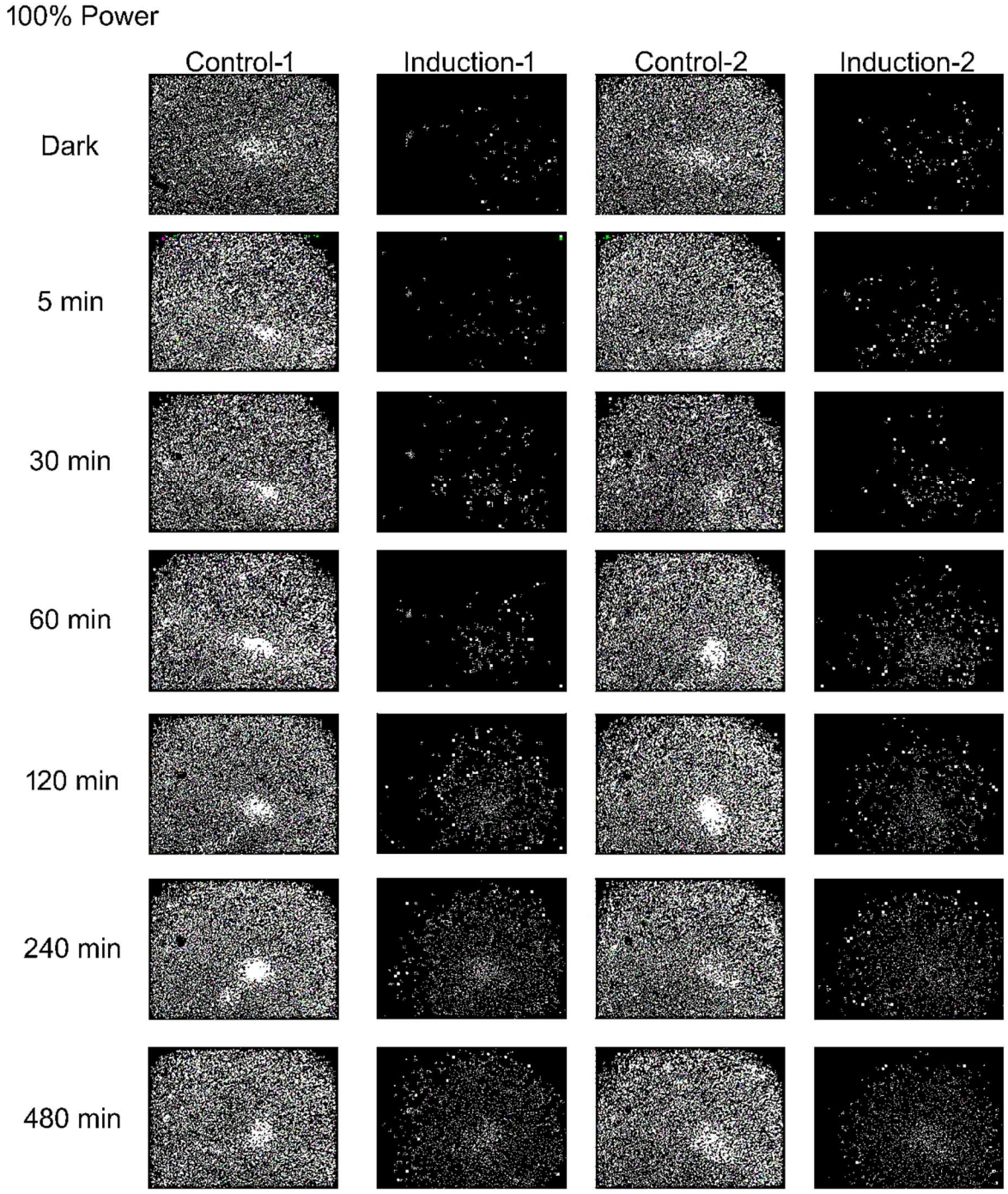

Figure 20. Representative images of micro-LEDs experiment at 100% power. Control column show Hoechst stain (total cell population) and induction columns shown reported expression due to light-induction.

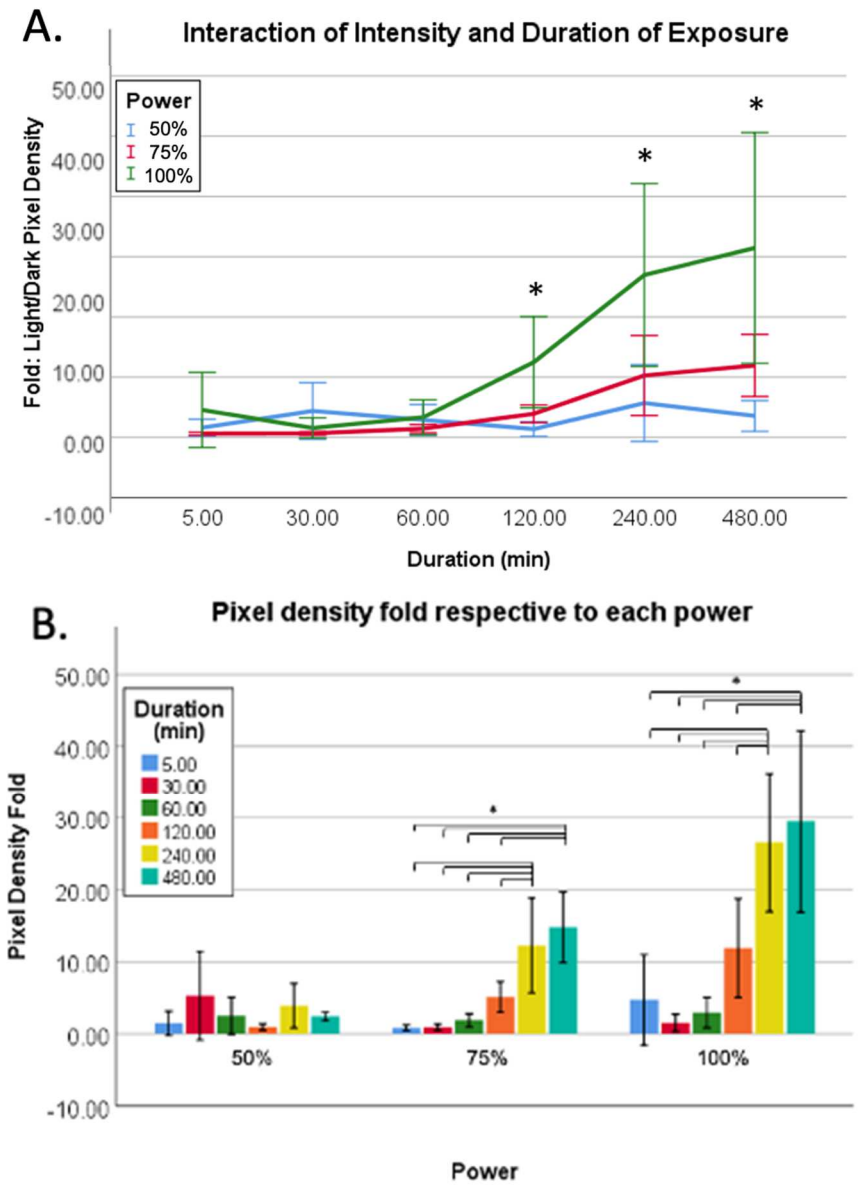

Figure 21. Pixel density in relation to blue-light exposure duration (A) and power level (B).

3.3.3 Spatial Patterning of Reporter Gradient Expression

We analyzed spatially the gene expression from the center of the well which had the most direct exposure to light. We analyzed whether patterning of gene expression could be achieved by analyzing images by various bins radiating from the center of the image, indicating center of emission from the blue-light micro-LED (Figure 22A). Binning analysis was performed on every well that was exposed to the various time settings and power intensities of blue light. MATLAB

analysis data demonstrates that cells that are at a closer distance from the center (0-1200μm) are higher in pixel density than the rest of the bins (1200-4800μm), indicating that a gradient of gene expression could be achieved along a gradient of applied optical power (Linear Mixed Models test: $p<0.05$; n=6 biological replicates). Importantly, these data were normalized to nuclear staining (Hoechst) to correct for inhomogeneous cell density across the cell culture surface. As expected, the data showed increased pixel density values with longer durations of exposure (Figure 18C). The steepest spatial gradient of gene expression was evident with exposure periods of 4 and 8 hours (Figure 23B, 23C) for intermediate and high-power levels. Briefer exposure periods resulted in insufficient induction and a longer duration of exposure (8 hours) did not significantly indicate a significant increase in gradient from the 4-hour timepoint. These data reinforce the interaction between intensity and duration of exposure.

3.4 Discussion

In this study, we explored the sensitivity of a naturally occurring blue-light inducible gene expression system in relation to its sequence, characterized its response characteristics, and identified two routes to achieve controlled spatial patterns of gene expression (control of stimulus characteristics or modification of the design of the light source itself). In an effort to optimize the EL222 system, we tested various amino acid variants predicted to modulate sensitivity and responsiveness, but ultimately identified that the original EL222 system provided a higher fold increased light sensitivity over the modified EL222 variants explored (Figure 15). Modification at a fourth amino acid was found to convert v2 to a constitutive activator ("CA") with equal activity in either light or dark for purposes of testing and development of future variants. Key advantages of the EL222 system are the tunability of spatial gene expression profiles by modifying stimulus

conditions, as well as the very low optical power requirements, which are orders of magnitude lower than thresholds required for channelrhodopsin activation (<0.01 mW/mm^2 versus ~1 mW/mm^2). This feature could be particularly advantageous for gene induction in the *in vivo* setting, where optical power dissipates rapidly over distance through tissue, and heat generation by the activating light source has the potential to damage adjacent tissue. Likewise, the enhanced response characteristics reduce the optical power requirements for effective gene expression, reducing the performance burden for the implanted light source and enabling further miniaturization and flexibility in its design.

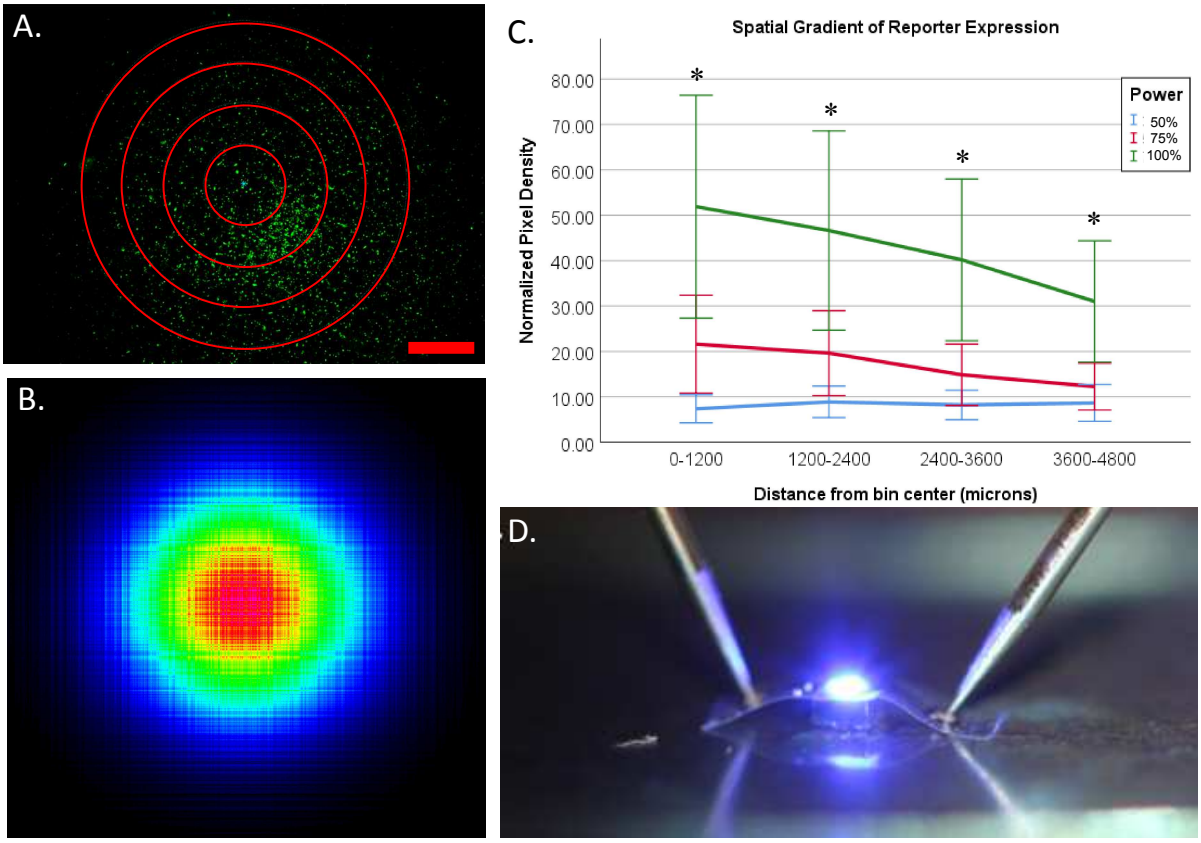

Figure 22. Spatial gradient expression of enhanced EL222 system. (a) Representative image showcasing how binning analysis is performed. Bins show a r = 200µm. (b) Heat map showing intensity variation of micro-LED using a beam profiler at 2mm from source sensor. (c) Pixel density values in relation to distance from the center of the image fir each power intensity. (d) Micro-LEDs with reflector. Image reproduced with permission from Jia et al., 2017.

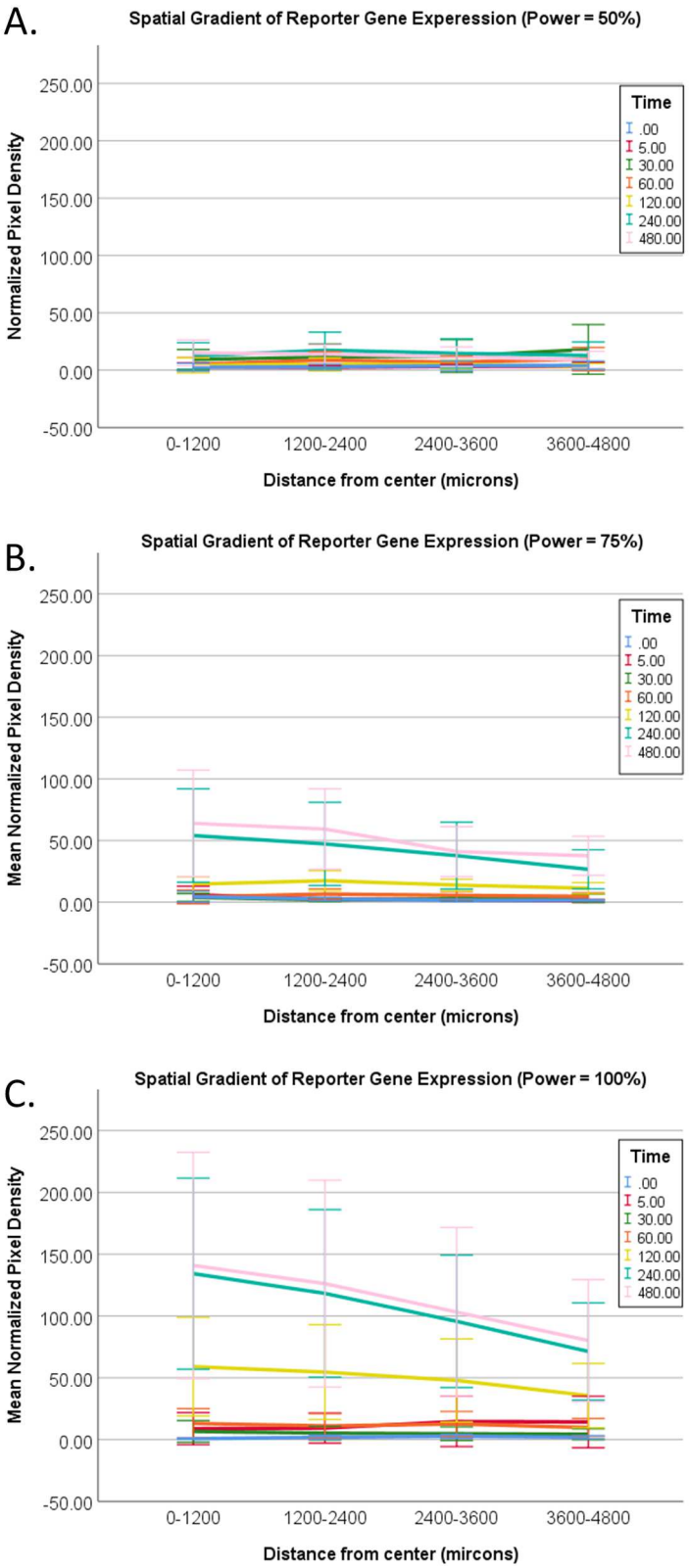

Figure 23. Normalized pixel density values in relation to distance from the center of the image for (a) 50% power, (b) 75% power, and (c) 100% power.

Our results illustrate an interaction between light intensity and exposure duration in the activation of the EL222 system and the spatial pattern of resulting gene induction (Figure 22). The synergy between duration and intensity of exposure could be linked to a mechanistic understanding of the EL222 system. Awareness of this mechanistic interaction can inform the generation of defined spatial gradients of gene expression (Figure 23): greater exposure intensity will activate gene expression more broadly, abolishing gradient formation, while reduced intensity is ineffective at inducing gene expression below a certain threshold. As such, the results reveal a "happy medium" in exposure conditions for effectively generating a spatial gradient of gene expression.

The ability to spatially pattern gene expression with light potentially could be leveraged for regeneration and tissue engineering applications. Just as chemical gradients of signaling factors can guide cellular movement and polarization ("chemotaxis") (Cai and Devreotes, 2011; Iijima et al., 2002; Roca-Cusachs et al., 2013; Swaney et al., 2010; Wang, 2009), contact-mediated guidance cues are powerful surface-mediated cues which control cell migration and maturation (Guo and Anton, 2014; Wellman and Kozai, 2017). In the brain, neural cell migration is a critical mechanism that underlies development of neural tissues into adulthood. Brain development during early embryogenesis engages in a complex migration pattern of cortical interneurons trying to reach their targets. This process is known to be mediated by various chemokines including CXL12 which is factor that plays a major role in embryogenesis, angiogenesis, and inflammation, due to its abilities to activate migration of some progenitor and stem cells and others (Janssens et al., 2018; Yang et al., 2013). Neuroblasts in adult mammals can migrate from the subventricular zone of the lateral ventricles of the olfactory bulb via the rostral migration stream. During development, and extending into adulthood, neural precursor cells leave the subventricular zone and migrate

tangentially through the rostral migratory stream to the olfactory bulb, where they start to move radially to their target location for differentiation (Murase and Horwitz, 2004; Sun et al., 2010). Cell migration regulation is very complex and involves a highly organized interaction between intracellular and extracellular signals (Iijima et al., 2002; Wang, 2009) (Iijima, Huang & Devreotes, 2002; Wang, 2009). By understanding the response characteristics of the system (Figure 22C) and coupling that knowledge with engineered solutions for controlling the stimulus delivered (Figure 22D), controlled spatial gradients of gene expression can be generated with the capability of co-opting these naturally occurring systems for artificially induced regeneration.

In future work, this optogenetic system has the additional potential to be used in regenerating the implanted electrode interface by utilizing light directed stimulus to control neuronal identity. An opportunity to do this is through coupling it to light-activated transcription factors such as proneural genes: NeuroD and Neurogenin-2 (Winter et al., 2017). Likewise, our recent collection of RNAseq data at the electrode interface has identified novel genetic targets for intervention in future work (data not shown). In the future, this optogenetics system may be activated by an optoelectrode array or "optrode" (Kwon et al., 2015; McAlinden et al., 2019; Welkenhuysen et al., 2016a) that is implanted in the brain for cell fate control. Optrodes have the potential to be optimized as well, which is the case for the single channel optical stimulator from Dr. Li's group which consists of a micro-LED coupled with a reflective silicon cavity (Khan and Li, 2017) that assess optical induction. This work in this chapter is an important step toward optimizing the light-inducible system as well as the light source to promote ideal conditions for implantation.

In this work, we describe the development and characterization of a newly optimized blue-light activated system for gene expression control *in vitro*. The characterization of this system has enabled the proof-of-concept for gene expression profile as a light gradient demonstrated by the binning analysis. Taken together, our tools can facilitate the implementation of programmed gene expression profiles to match desired outcomes and will complement current mammalian optogenetic systems for eventual application *in vivo*. Advantages of this system include gene expression regulation with minimal light intensity and exposure duration, which can minimize any possible damage to cells and/or tissue while allowing expression of the gene of interest to turn on permanently. Additionally, we achieved a tailored regulation of expression gradient by fine-tuning the stimulus characteristics or the design of the stimulus source.

3.5 Methods

3.5.1 Generation of EL222 system and plasmid construction.

Development of the EL222 system for use in our laboratory at MSU began with the purchase of a synthetic DNA (IDT corp, Coralville, Iowa) encoding the EL222 open reading frame (ORF) with N-terminal nuclear localization signal and VP16 transactivation domain as described by Motta-Mena et al., 2014. This approximate 1kB DNA termed NVE, for NLS-VP16-EL222, was inserted into MMLV or HIV-based retroviral vectors or plasmid expression vectors for use in individual experiments. After initial experiments indicating that the EL222 activator worked essentially as described in Motta-Mena et al., 2014, the EL222 ORF construct was re-engineered to contain restriction sites flanking the LOV domain that allowed the insertion of synthetic DNA fragments to produce mutant variants with potential to alter the light-responsiveness and sensitivity of the transactivator. To allow us to distinguish between the original NVE and the re-built NVE

with silent restriction sites to facilitate construction of mutants, the new version was termed "MB", although MB and NVE encode precisely the same amino acids and are functionally equivalent.

An EL222-responsive promoter was constructed by inserting four different ELRE sequences (based on the published ELRE consensus in Motta-Mena et al., 2014) upstream of a minimal CMV promoter to test for activation by NVE/MB. After validation of this initial reporter construct, four additional reporter constructs were created, each with the original 4 ELRE variants followed by duplicates of each of the individual ELREs (1-4) for a total of 6 ELREs in the responsive promoter. The variant with the 4 individual ELREs plus a dimer of ELRE 2 with the core sequence GGGCTTTGGTCT termed "E21" was found to be the most robust and was used for all reporter constructs after pilot experiments. A schematic of the E21 reporter promoter is shown in Figure 24. The responsive promoter and different reporter genes such as eYFP and RFP were utilized in different retroviral or plasmid vectors depending on experimental objectives.

Three primary expression vectors were used depending on experimental objectives. The MMLV-based retroviral vector LPCX, the lentiviral vector pSIN-EF-X, and the plasmid vector AXR-CMV-X-PA (Biomilab LLC, Lansing MI) were modified to insert the E21 promoter-reporter cassette or NVE/MB and all variants as described for individual experiments below.

3.5.2 Generation of EL222 stable cell line.

Retroviral vectors were packaged using 3-way transfection of HEK293 cells with the viral vector plasmid, a GAG-POL expressing plasmid, and a VSV-g expressing plasmid. This packaging methodology used world-wide for decades, creates recombinant virus particles that are

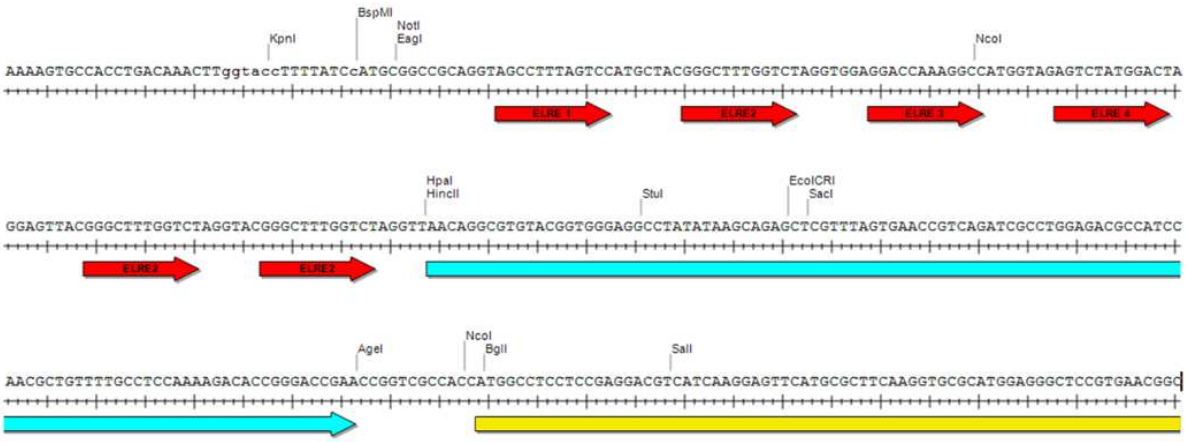

Figure 24. Schematic and sequence of the EL222 responsive promoter E21. ELREs are depicted in red, the minimal CMV basal promoter is shown in blue, and an example of the start of a reporter gene ORF is shown in yellow.

not replication competent, are self-inactivating (for the pSIN vector), but are capable of stable integration and expression in target cells. Packaged and concentrated viral vectors were stored at -70ºC until use. Plasmid vectors (variants of AXR) were transfected into target cells using calcium-phosphate co-precipitation or Lipofectamine reagent for transient-transfection assay in HEK cells.

3.5.3 Cell culture and transfection.

Human Embryonic Kidney (HEK293) cells were used for testing the three light-responsive activators (v1, v2, CA) and reporter (E21) vectors. HEKs were maintained under Dulbecco's modified Eagle's medium (DMEM; Life Technologies) supplemented with 10% fetal bovine serum (FBS, Sigma) and 1% penicillin/streptomycin (Life Technologies) in 5% CO2 at 37°C. HEKs were grown in 15-cm tissue culture treated plates and passaged by chemical dissociation using TrypLE (Life Technologies) every 3-4 days. In preparation for light induction experiments, cells were passaged to 24-well plates (68,000 cells/well) for transient transfection assays. Transfection with Lipofectamine 3000 (Invitrogen) was performed according to manufacturer's

protocol 4-6 hours after plating into 24-well plates. For LED exposure, cells were transfected with 200 ng of DNA at varying activator/reporter concentration ratios (4:1, 2:1, 1:2, 1:4) and an empty plasmid (PUC). For micro-LED experiments the activator/reporter ratio was kept consistent at 40ng of activator and 20ng of reporter vector. The media was exchanged for fresh medium 15-17 hours post-transfection.

3.5.4 Light induced constructs for proneural genes NeuroD1 and Neurogenin-2

Four retroviral vectors were packaged using 3-way transfection of HEK293 cells with the viral vector plasmid, a GAG-POL expressing plasmid, and a VSV-g expressing plasmid. Viral supernatant was harvested and filtered to remove cells and debris. It was then ultracentrifuged to concentrate the virus and resuspended in PBS. Aliquots were stored at -70ºC until use. MMLV plasmid vectors included 1) SCNIT-K6 with high level expression of V2 EL222; 2) LP-ELRE21-YFP with puromycin resistance, the ELRE minimal promoter, and YFP reporter; 3) LP-ELRE21-YND1 with puromycin resistance, the ELRE minimal promoter, and YFP-NeuroD1 reporter; and 4) LP-ELRE21-YNGN2 with puromycin resistance, the ELRE minimal promoter, and YFP-Nuerogenin-2 reporter. Cultured growing rat NPCs seeded in 12-well plates were infected with all vectors at an estimated multiplicity of infection of five for each vector in the following combinations: K6+YFP, K6+ND, K6+NGN. This was done in duplicates, one plate for light treatment for 12 hours (1 min on/5 min off), and one plate for dark condition. Since factor expression was accompanied by a fluorescent reporter (YFP) produced either in tandem (using a 2A element) or by direct fusion to the N-terminus of the factor open reading frame (ORF) it allowed for direct visualization and localization of the expressed protein. Results are shown in Figure 28F.

3.5.5 Micro-LED physical properties and integration on 3D printed base

We used commercially available micro-LEDs (CREE TR2227tm) with a central wavelength of illumination is at 465 nm. To generate a robust and stable optical induction and to analyze the pixel density by binning, the single channel stimulators were attached on a 3D printed base (from Gerhardt et al., 2016). The base had an array of grooves, same as the distance from the micro-LEDs to the bottom surface of the 24-well plates, 2.3 mm. The micro-LEDs were placed in the center of the groove, and two wires were bonded with the interconnect pads of the stimulator using low melting temperature solder and the pads were later packaged with epoxy for protection from the heat and humidity present in the incubator. These two wires were connected with an external power source to illuminate the micro-LEDs. The stimulators were firmly fixed on the 3D printed base by using double side adhesive tapes. For this study, single channel stimulators coupled with a silicon cavity reflector was compared with a similar stimulator without a coupled reflector.

3.5.6 Illumination setup and light delivery protocol.

Twelve (12) to sixteen (16) hours after DNA transfection, cells were illuminated either by a blue LED panel at 67% or 100% power, 0.004 W/cm^2 or 0.006 W/cm^2 respectively, measured with a handheld power meter (843-R, Newport) and Si metal wand detector (818-ST2/DB, Newport) held above LEDs or by a custom-built micro-LED array at 100%, 75%, and 50% power measurements 1.18 W/cm^2, 0.88 W/cm^2, 0.59 W/cm^2 respectively, measured using a Newport Power Meter held directly above micro-LEDs). These exposure conditions were empirically defined following observations of improved cell culture attachment at lower power levels and maximal induction efficiency at higher levels. For LED experiments, blue light was delivered for 8 hours. For micro-LED experiments, cells were exposed to light for 5, 30, 60, 120, 240, or 480

minutes. An array of twelve micro-LEDs (as described in section 3.3) were mounted individually on a 3D printed plate holder (See Supplemental Information for images). The micro-LEDs were then connected to an Arduino Uno microcontroller, interfaced with an LED driver, allowing the current at each micro-LED to be regulated and the stimulus duration to be user controlled. The 3D printed plate holder provided a consistent means of positioning 24-well plates over the array of twelve micro-LEDs (Gerhardt et al., 2016). Plates containing cells under dark conditions were covered with aluminum foil or kept in a separate incubator.

3.5.7 Imaging Procedure and Quantitative Characterization.

A similar plate holder and corresponding microscope sample stage were 3D printed to hold 24-well plates and center the well of interest during fluorescence imaging. This was facilitated by a mating mechanism between an elevated ring on the microscope sample stage and the holes underneath each well of the plate holder. Images were collected 72 hours post-light stimulation utilizing a Leica MZ10 F Fluorescent Microscope (Leica MZ10 F) with a QImaging Retiga R1 CCD camera (QImaging) to assess optical induction of the RFP reporter. Raw images received manual thresholding to eliminate background fluorescence and were then captured with Ocular image acquisition software (QImaging). Then, images were analyzed with an in-house MATLAB script (Supplemental info (Winter et al., 2017)). To assess optical induction, pixel density values were obtained by normalizing the number of non-zero pixels by the total number of pixels. This was done over the entirety of each raw image, in addition to being done based on a binning analysis. To assess the spatial gradient of reporter gene expression, the MATLAB script was used to parse the fluorescence image data into bins that extend out radially from the center of the well.

Images were analyzed by implementing 12 bins per image (r=200μm/bin), excluding corners, followed by normalizing each bin's pixel density value to the first bin.

3.5.8 Statistical Analysis

The degree of statistical significance between groups was determined by a linear mixed- model ANOVA using the SPSS software (IBM Corp.). Statistical significance was defined at $p \leq 0.05$ level.

4. CHAPTER 4 | Controlling Cell Fate, Structure, and Function of Neural Cells

4.1 Material effects on electrode device and integration to brain tissue

4.1.1 Review of electrode materials and future outlook

Traditionally, electrode devices utilize materials such as metal and silicon. Michigan arrays typically consist of primary silicon with electrode sites made from platinum or iridium for which metal sites are deposited onto conductive traces and then embedded in the silicon shank (Vetter et al., 2004), while Utah arrays are composed of a doped silicon body etched into 100 microneedles with silicone dioxide channels, Parylene-C as an insulating layer, and tips metalized with platinum or iridium (Bhandari, 2009; Nordhausen et al., 1996). These traditional probes demonstrate to have a negative immune response (Polikov et al., 2005; Salatino et al., 2017a), thus to overcome challenges faced in the electrode-tissue interface, strategies to stabilize and/or regenerate the interface have been reported and new methods continue to arise including material modifications. Methods involve the redesign of electrode array materials and the incorporation of bioactive molecules, polymer coatings, scaffolds for cell-seeding, and others.

Newer materials for electrode devices have emerged including polymer, mesh, and carbon-based arrays. Polymer-based arrays include probes composed of parylene materials such as a flexible Parylene-C probe (Hara et al., 2016) and a polyamide probe (Chung et al., 2019), which show good tissue integration and biocompatibility when implanted. Mesh technologies include a syringe injectable probe that is composed of planar ribbons of polymer and metal, mainly SU-8 photoresist alongside chromium, gold interconnects, and platinum recording sites (Hong and Lieber, 2019; Liu et al., 2015), demonstrating improved biocompatibility when compared to planar

polymer probes. Carbon-based devices include materials such as glassy carbons (Sharma, 2018), carbon fibers (Wei et al., 2018), and micro-nanocrystalline diamonds (Rusinek et al., 2018).

Diamond is an emerging material for electrode arrays as it can serve as a neurochemical sensor while having electrophysiological recording capabilities. Boron-doped diamond (BDD) is especially attractive as it offers low capacitance and background noise, as well as a wide potential window which can aid in dopamine sensing. BDD has many benefits, although a mismatch exists between Young's modulus of BDD ($\sim 10^3$ GPa) and soft tissue (Schiavone et al., 2009). Hence, a modified method of fabrication was achieved by exposing the growth side of a BDD film as electrode sites for neural recording. We conducted an *in vitro* study to assess the growth and attachment of neurons on the diamond, Parylene, and control materials.

Materials and Methods. E18 embryonic rat cortical neurons (ThermoFisher; #A1084002) were cultured on the surface of planar substrates fabricated from these materials following poly-D-lysine coating according to the supplier's protocol (ThermoFisher; #A3890401). Neurons plated on Nunc Thermanox plastic coverslips (ThermoFisher; #174950) were used as a control. Neurons were fixed with 4% paraformaldehyde in phosphate-buffered saline (PBS) at the 7-day time point and stained for beta III-tubulin (TUJ1) and caspase-3 to assess neurite outgrowth and viability, respectively. Immunohistochemistry was performed using previously reported methods (Thompson et al., 2017); the primary antibodies used were a monoclonal mouse anti-beta III-tubulin antibody ("TUJ1", Abcam; #ab78078) at a 1:500 dilution and a rabbit cleaved caspase-3 antibody (Cell Signaling; #9661S) at a 1:400 dilution. Similarly, secondary antibodies used were Alexa fluor goat anti-rabbit 594 (ThermoFisher; #A-11037) at a 1:200 dilution and Alexafluor

anti-mouse 488 (ThermoFisher; #A-11001) at a 1:200 dilution. Sholl analysis was performed to assess neurite outgrowth according to published protocols (Senut et al., 2014). Briefly, concentric circles with defined radii of 10μm were centered on the neuronal soma and used to manually benchmark the length, branching, and intersection of neurite outgrowth. "Maximal distance" is defined as a measurement of the maximum distance that any individual neurite extends from the soma. "Number of branching" is defined as a measurement of how many branches are formed in each bin. An average of ~60 neurons for each condition was randomly selected and analyzed if neurites were clearly identifiable.

Results for in vitro assessment of device biocompatibility. The Pilot Trial conducted initially, showcased that neurons seeded on polycrystalline diamond (PCD) have high levels of Caspase-3 stain, indicating cell death present compared to control (Figure 25A, 25B). This issue was resolved by rinsing the PCD substrate before cell seeding, which led to similar results to our control in terms of immunocytochemistry (Figure 25C, 25D) and electrophysiology (Figure 25E, 25F). Neurons seeded on PCD and Parylene C appeared qualitatively similar to the control substrate in terms of adhesion, health, and neurite outgrowth (Figure. 26E). To assess more nuanced effects on morphology, Sholl analysis was performed on ~60 cells per substrate. The results revealed that the number of neurites that crossed the boundary of the concentric circles (positioned at incrementally increasing 10 μm distances from the center of each soma) was significantly higher on PCD than Parylene C and control substrates (Figure 26F, Linear Mixed Models test: $p<0.05$). The "maximal distance" measurement likewise indicated that neurons plated on PCD extended longer neurites than cells cultured on control and Parylene substrates (data not shown; Linear Mixed Models test: $p<0.05$). The average "number of branching" was statistically

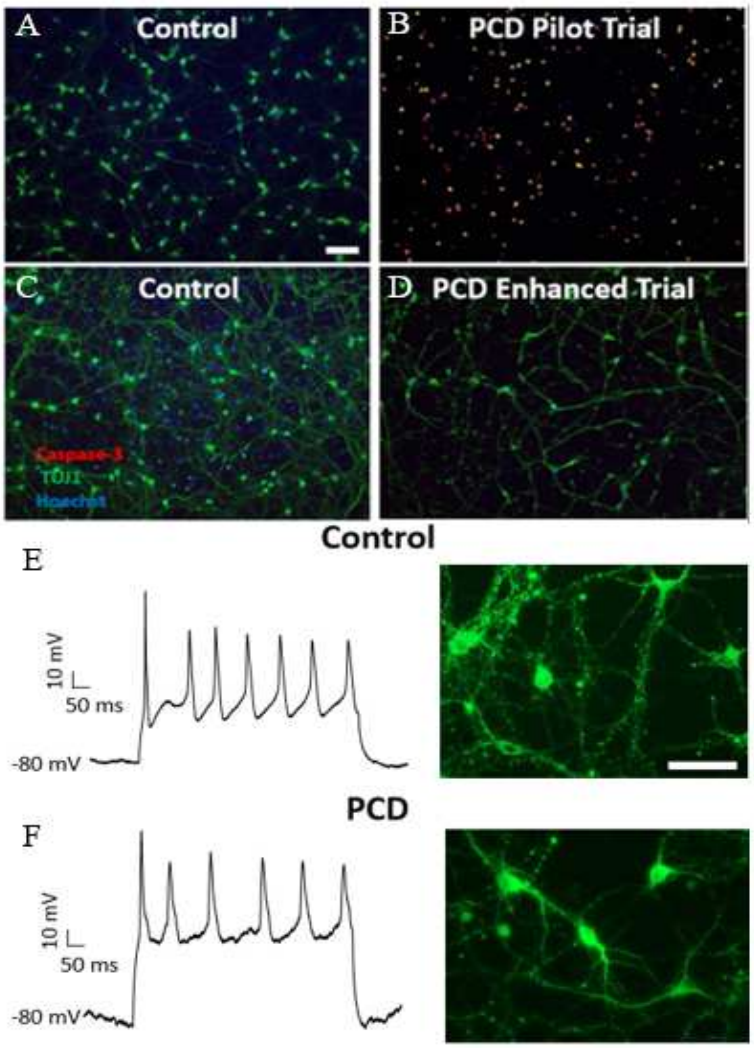

Figure 25. Immunocytochemistry and electrophysiology of neurons grown on control and diamond materials. Immunocytochemistry of primary rat cortical neurons before optimization (Pilot Trial) for control (A) and PCD (B) and after material optimization (Enhanced Trial) for control (C) and PCD (D) show neuronal growth on both substrates. Spike trains obtained via patch-clamp electrophysiology for neurons seeded on control (E) and PCD (F) substrates. (Scale bars = 100μm).

higher for Parylene and PCD than for control, where PCD facilitated the most robust arborization (Figure 26G, Linear Mixed Models test: $p<0.001$). Lastly, the average sum of crossing and average sum of branching showed no statistical significance between the substrates (data not shown; Linear Mixed Models test: $p>0.05$). Additionally, positive caspase-3 staining was not detected in any of the substrates tested, indicating similar support of viability (antibody was validated in preliminary tests, data not shown). While the underlying mechanism has yet to be determined, possibly the

topographical cues presented by the granular PCD surface may promote neuronal maturation and neurite elongation (Purcell et al., 2012; Rusinek et al., 2018). Overall, the PCD and Parylene C substrates performed as expected *in vitro* and supported neuronal growth and maturation similarly to control conditions.

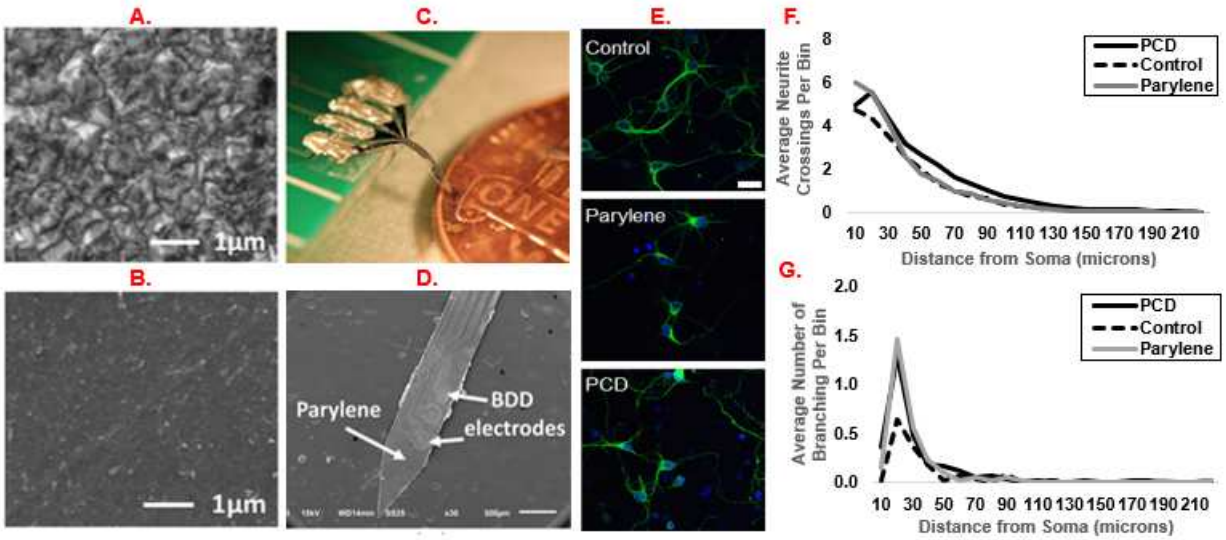

Figure 26. Design of diamond neural probe and Sholl analysis results. SEM images are shown to compare surface topology of the (A) BDD growth side and (B) nucleation side. (C) Photo of the fabricated device against a penny. (D) SEM image showing the device. (E) Rat cortical neurons plated on Parylene C and PCD substrates extended neurites and displayed morphologies that appeared similar to cells plated on control substrates (TUJ1 in green, Hoechst nuclear counterstain in blue). Quantification of morphological effects via Sholl analysis illustrates similar responses on all substrates, with a slight increase in neurite extension (F) and branching (G) over longer distances (>40 microns) registered by PCD substrates (n=~60 neurons/substrate). Scale in (E) = 20 μm.

4.1.2 Coatings and other methods to increase the biocompatibility of implanted electrodes

In addition to novel materials, surface material coatings as a modification method for electrode arrays are a potential tool for increasing neural cell adhesion and for patterning neural cells. To guide cellular growth and improve adhesion, two main strategies are utilized including, topographical surface modifications as well as chemical surface modifications. Techniques to achieve topographical modifications include photolithography, wet etching, laser fabrication, and

reactive ion etching for roughening the surface and developing arrays of different features. On the other hand, chemical modifications work by primarily chemically binding different proteins or cell adhesive molecules to the surface.

A common strategy from improving the biocompatibility of the electrode-tissue interface is to utilize polymers, either synthetic or natural in origin, to restore functions in damaged neural tissue due to the versatility they provide in shape and mechanical properties, as well as their high biocompatibility (Boni et al., 2018). Natural polymers provide the benefit of being highly biocompatible and offering natural biodegradation in combination with malleable chemical properties. Natural polymers have been the most researched and include extracellular matrix components (e.g. collagen) and marine life polymers (e.g. alginate). Issues arise with natural polymers such as complex chemical structures, thermal sensitivity, and processing. Synthetic polymers utilized for neural applications include aqueous hydrogels and soft polymers. The use of synthetic polymers is beneficial since they can be highly tailored to meet high mechanical strength and flexibility, however, toxic residuals can be present therefore extensive testing needs to be in place before translation.

Electroconductive polymers as coatings allow smaller electrodes to be manufactured with high tunable characteristics, such as low impedance and high stability, by providing a high surface area of a material that is favorable to cellular integration. Due to polymers being softer materials, inflammation surrounding the electrode could be reduced due to a lesser mismatch between tissue and electrode material (Green and Abidian, 2015; Green et al., 2008). Some conductive polymers used for this purpose include polypyrrole (PPy), polythiophene (PTh), and its byproducts such as

poly-3,4-ethylene dioxythiophene (PEDOT). PEDOT has an optically transparent quality which has been shown to provide high stability as an electrode material (Castagnola et al., 2015; KA et al., 2011) in addition to increasing neurite outgrowth in neural stem cell differentiation *in vitro* (Pires et al., 2015). Also, hydrogel layers added to conductive polymer nanoparticles provide nanostructured surfaced to microelectrode arrays which help by improving charge transfer and reducing impedance (Abidian et al., 2010, 2009; Abidian and Martin, 2009).

Other polymer materials used in neural engineering include carbon-based materials, in particular, graphene and carbon and carbon nanotubes (CNT) because of their conductive properties, flexibility, and biocompatibility. Graphene nanogrids have been developed to promote neural to glial cell ratio (Akhavan and Ghaderi, 2013), while 3D scaffolds stimulate the differentiation and propagation of neural stem cells. CNTs for wire electrodes implants have shown improvement in stimulation, signal recording, and impedance in *in vivo* and *in vitro* testing (Keefer et al., 2008; N. Li et al., 2013). Polymers in general do offer great potential for their use in probes and electrodes, thus further advances will need to aim at developing natural/synthetic combinations that can provide ideal properties to the tissue-electrode interface.

In addition to polymer coatings, bioactive treatments such as neurotrophic factors, bioactive peptides, and anti-inflammatory drugs can provide an additional avenue for stabilizing the tissue-electrode interface. Nerve growth factor (NGF) is a promising candidate for electrode surface enhancement due to its innate characteristic of promoting neuronal survival and neurite outgrowth. Furthermore, anti-inflammatory coatings have been developed to release over time and have shown an improvement on reducing the foreign body response, but unfortunately do

create a recorded signal of lesser quality (Bezuidenhout et al., 2013; Gutowski et al., 2015; Mercanzini et al., 2010). The implementation and use of these polymer coatings and bioactive treatments can lead to lower impedance and a lessened tissue response (Fattahi et al., 2014; Green and Abidian, 2015). Adhesion molecules (such as L1) as coatings can lead to diminished gliosis due to its capabilities of promoting axonal growth, and neural survival while promoting cellular attachment to electrode device (Eles et al., 2017).

Aqueous hydrogels or soft polymers can be used to create neural scaffolds to enhance the interaction of supporting cells. Scaffolds nowadays can be seeded with neural stem cells or progenitor cells to be integrated with electrode arrays. Stem cells and progenitor cells have shown promise to repair the injury in the central nervous system (Rejali et al., 2007; Stieglitz et al., 2002) and to improve the integration of implanted devices with brain tissue. One method was done by hydrogel scaffolding were neural stem cells were encapsulated in the scaffold. Data demonstrated that neural loss and gliosis associated with implantation showed an improvement likely due to neuroprotective and neurotrophic factors being released by the cells in the graft (E K Purcell et al., 2009). Another approach was developed by utilizing laminin as the surface for neural progenitor cells on a silicon probe, which resulted in an improved astrocytic reaction surrounding the implant site (Azemi et al., 2010). Cell-seeding scaffolds provide two unique benefits; first, they have the potential of gaining additional control over a specific neuronal population that is interfaced with specific electrode sites, and secondly, they have the opportunity to repopulate the device with new neurons, therefore enhancing recording capabilities and sensitivity over time. After initial timepoints graft cells for implant devices become difficult to identify over longer periods as is the survival of these cells (Dimmeler et al., 2014).

4.2 Proneural gene expression control in the brain

Basic helix-loop-helix (bHLH) transcription factors (TFs), called proneural factors, control the cell cycle exit (Bertrand et al., 2002; Lacomme et al., 2012) and also intervene in deciphering the neuronal subtype identity of neural precursor cells (Wilson and Rubenstein, 2000). Proneural factors are the primary regulators for neurogenesis in the embryonic brain, where Ascl1 (also known as Mash1), Neurogenin-1 (Neurog1), and Neurogenin-2 (Neuorg2) have been shown to promote cell cycle completion and neuronal differentiation in many progenitor populations (Bertrand et al., 2002; Ross et al., 2003). Proneural factors have shown to regulate early steps of neurogenesis including commitment and subtype specification (Fode et al., 2000; Nieto et al., 2001) as well as late-stages including migration and axon growth orientation (Ge et al., 2006; Hand et al., 2005; Seibt et al., 2003).

Expression of specific neuronal TFs needs to be tightly regulated to ensure that the spatial and temporal patterning of neuronal populations is correct (Badea et al., 2003). Notch signaling is the main pathway by which this patterning is regulated alongside lateral inhibition which allows the number of neural progenitor cells to be maintained by controlling the number of nearby cells that can exit the cell cycle and differentiate (Formosa-Jordan et al., 2013). Efforts to understand the molecular mechanisms by which different proneural factors control and manipulate neurogenesis and neuronal specification have started to be investigated (Guillemot and Hassan, 2017), however, a need remains to better understand these mechanisms for research and clinical applications (Aydin et al., 2019).

4.2.1 Prospective of reconstructing damaged neural circuitry and restoring function by controlling proneural gene expression

Ascl1 and Neurog-2 are two main proneural factors that oversee regulating and starting neurogenesis for vertebrate animals. Neurog-1 and -2 can activate Notch signaling and inhibit neurogenesis in adjacent cells (Castro et al., 2006). Additionally, Ascl1 can produce GABAergic neurotransmission phenotype through regulation of Dlx1 and Dlx2 genes (Heinrich et al., 2010; Poitras et al., 2007) and overall plays an important role in synchronizing neurogenesis by controlling neural progenitor advancing through the cell cycle (Castro et al., 2011). It has been demonstrated that Neurog-2 can compensate for Ascl1-dependent neurons and rescue their development (McNay et al., 2006). Ascl1 and Neurog1 and -2 play a central role in choosing neuronal subtypes for progenitor cells (Augustyn et al., 2014; Parras et al., 2002; Ware et al., 2016).

Controlling the identity of the cells at the tissue-electrode interface can lead to understanding and mitigating the reactive tissue response. Previous studies have shown that in mice, Ascl1 is required for specification of GABAergic neurons in the forebrain and sympathetic neurons in the peripheral nervous system (PNS), while and Neurog-2 aids in the specification of glutamatergic neurons in the forebrain and sensory neurons of the PNS (Fode et al., 2000; Lo et al., 2002; Ma et al., 1999; Parras et al., 2002). It was shown that Ascl1 and Neurog-2 can generate neurons by binding to different genomic sites which could increase the number of neuronal subtypes produced during development, therefore, Ascl1 and Neurog-2 are key factors in mediating neuronal diversity in the nervous system (Aydin et al., 2019). Also, glutamatergic neurons can be generated from astroglia by overexpressing Neurog-2 (Heinrich et al.,

2010) or NeuroD1 (Guo et al., 2014), while Ascl1 overexpression can produce GABAergic neurons via Dlx2 regulation (Heinrich et al., 2010).

Furthermore, it has been proposed that in astrocyte-to-neuron reprogramming, Ascl1 and Neurog-2 also contribute to neuron-specific programs by conserving the memory of the first neurogenesis elicited by Ascl1 or Neurog-2 binding (Aydin et al., 2019). Hence, TFs should be explored with a focus on neuronal subtype identity specification, especially those widely expressed, like the ones mentioned here. Choosing the correct proneural factor for a given differentiation strategy is key in being successful with the desired neuronal population (Masserdotti et al., 2015).

4.2.2 Novel methods for regulating gene expression following an injury

Many research groups have developed methods for overexpression of proneural genes or for reprogramming to induce neural repair following an injury, with varying degrees of success. For example, Dlx2 overexpression although partially, was able to overcome a glial environment that enhanced neuroblast recruitment after an injury in rodents (Jones and Connor, 2016). On the other hand, Ascl1 overexpression was able to drive reactive astrocytes and glioblastoma stem cells toward neuronal differentiation after damage caused by stoke, and Ascl1 enhanced neurite growth of neurons that remained damaged (Faiz et al., 2015). Repression of Olig2 and Pax6 overexpression have also shown capabilities of reprogramming striatum glia toward a functional neuronal differentiation path after an ischemic lesion in mice (Kronenberg et al., 2010).

In a study performed in our lab group, rat astrocyte cells where successfully reprogramed into functional neurons via overexpression of fate-specifying genes and an optical induction system to

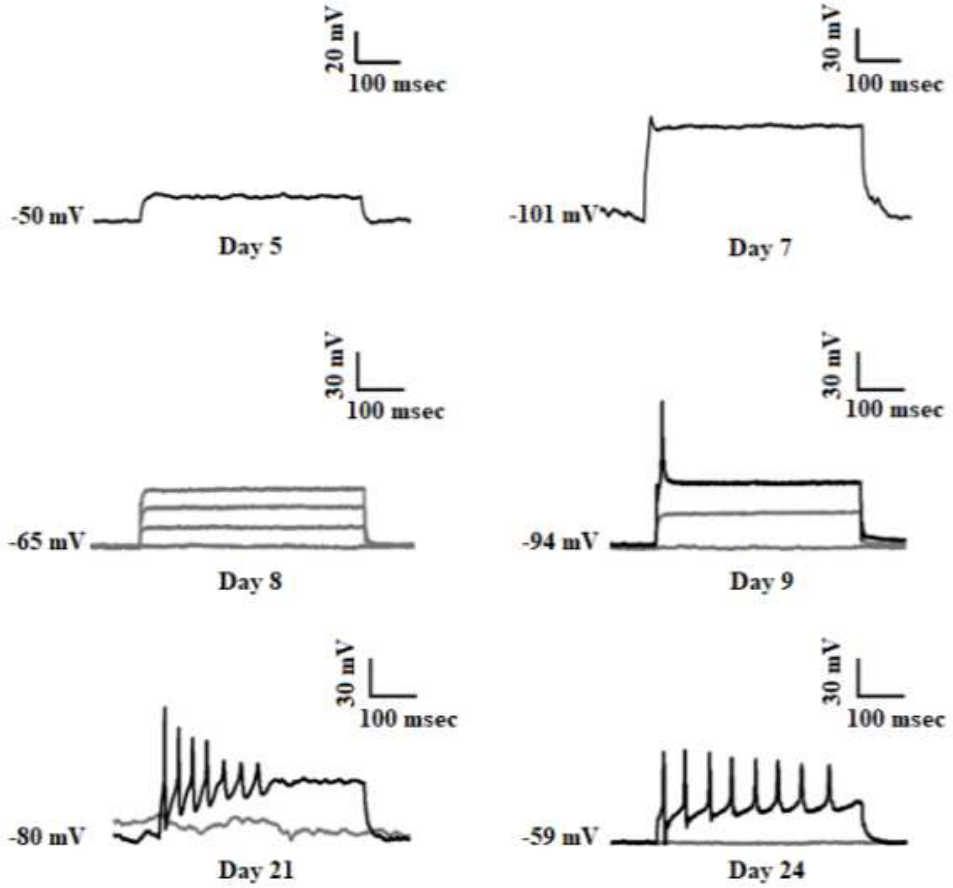

Figure 27. Electrophysiological evidence of successful reprogramming of glia into neurons. Reprogrammed glia elicited single spikes in response to injected current by Day 9 post-infection, spike trains by Day 21, and mature spiking activity by Day 24 (representative traces). Control cultures of glial cells displayed no response to stimulation (data not shown). Reproduced form Winter at al., 2018.

drive proneural gene expression (Winter et al., 2018). Ascl1 was assayed as the key factor in reprogramming in conjunction with NeuroD1 and Neurog-2, based on previous work (Purcell et al., 2013; Tong et al., 2010) (Figure 27). Around the one- to two-week time point, these reprogrammed cells demonstrated single spikes were present; by week three, mature trains developed, and they also responded to injected current, which is indicative of mature neuronal function (Figure 27).

The EL222 optogenetic system produced in our lab was expressed in transduced HEK cells, which produced a robust expression of the light-induced reporter genes (Figure 28). Cells exposed to light at a closer distance showed an increase in reporter expression as well as cells exposed to light for longer periods (Figure 28A). Due to the response of the system, spatial patterning was achieved via the use of micro-LEDs (Figure 28B-C) or a photomask (Figure 28D). Furthermore, we validated the use of the EL222 system coupled with proneural genes and its capabilities in response to light. The system was implemented in NPCs to drive the expression of NeuroD and Neurog-2 for enhancing the morphological and electrical maturity of the cells (Figure 28E-F). These preliminary results yield a successful proneural gene expression induction after 12 hours of blue light, however, future experiments need to be developed to assess electrical activities of the cells for a specific timeline after NeuroD or Neurog-2 is delivered to the NPCs.

4.2.3 Future Work: Synergistic control of the electrode-tissue interface

Microelectrode arrays as implanted prosthetics used for research and clinical settings have demonstrated the potential to reform studies for neurological diseases and for furthering the understanding of the brain-tissue response that occurs after implantation. Future directions will need to aim at controlling cell types that are localized around the implanted electrode array which interface electrode sites. This can be achieved via two main routes including (1) coupling proneural gene expression with light and (2) novel delivery of light and viral delivery of proneural gene

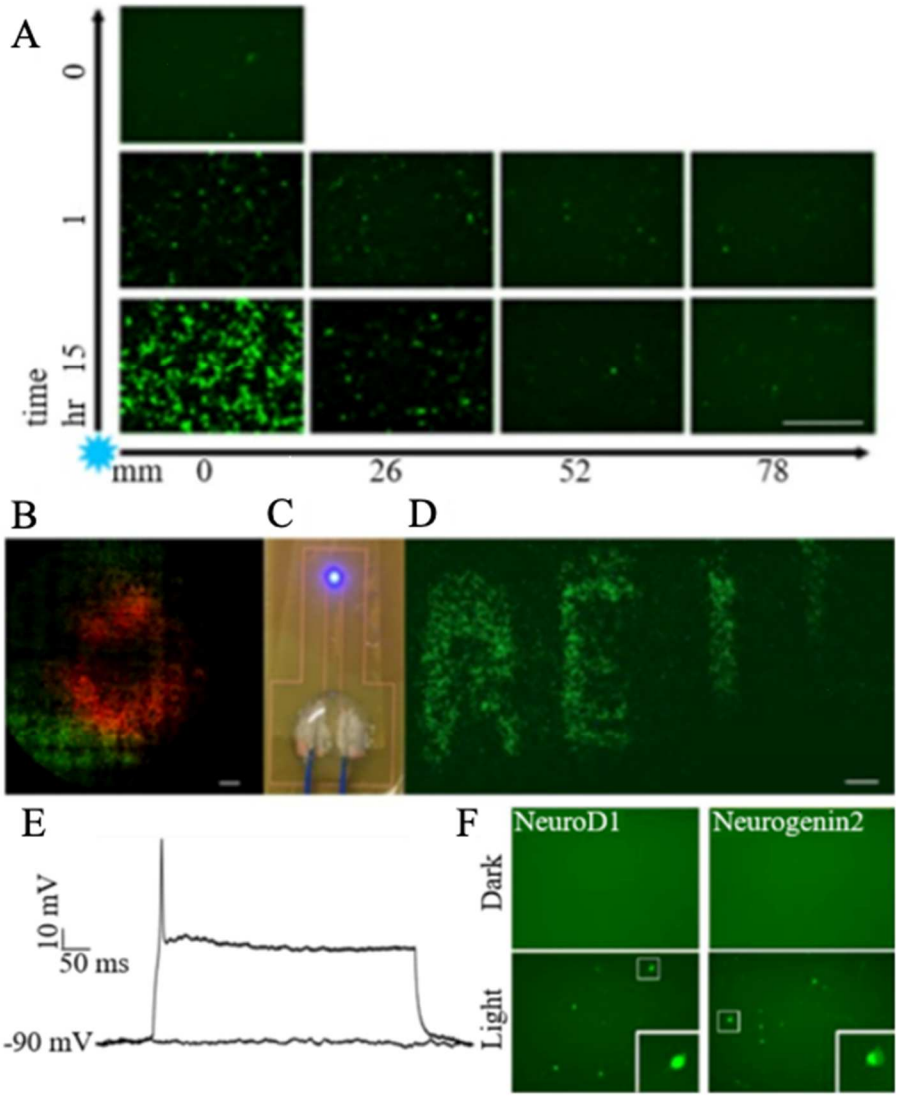

Figure 28. Successful light-induced gene expression with EL222 system and proneural gene control. Increased light source proximity and longer exposure time led to a dose-dependent increase in reporter gene expression (YFP, green) (A). Two methods of spatial patterning of gene expression were achieved with the EL222 system: a spatially defined "spot" of RFP reporter induction (red, B) occurs in response to blue light delivered by a micro-LED (C), while a photomask "spells" the acronym for the lab (REIL) in YFP in response to blue light (D). Scales = 300 μm in (A), = 1mm in (B) and (D). Representative spike of a progenitor cell at day 9 of differentiation into neuron demonstrates limited excitability (E), which may be enhanced by proneural gene delivery. EL222 can drive proneural gene expression (YFP-tagged NeuroD1 or Neurogenin2 exposure, green) following 12 hrs of blue light exposure. Methods are detailed in Ch. 3 (F). Reproduced from Winter et al., 2018.

expression control to the area of interest. In addition to these methods, as discussed beforehand, the optimization of the electrode material is key to bettering the outcome of the tissue-electrode

response. By reprogramming damaged neurons or non-neuronal cells, the identity of the cells that are at a recording distance of the electrode device could be optimized, therefore leading to a fully seamless interface where the user is able to extract electrical signals generated by the manipulatedcell population. By rewiring the electrode interface, the information we can obtain will be of higher resolution and stability, allowing this data to be utilized for understanding the interface and creating long-term solutions for patients who require implanted electrodes. Light provides high spatiotemporal control and the use of an optoelectrode array (Welkenhuysen et al., 2016b) will provide tight control over the cells nearby the device. The long-term goal aims at creating an integrated abiotic-biotic interface that provides seamless integration of the device with the neural tissue, mediated by optogenetic control, electrode material optimization, and cellular reprogramming via proneural gene delivery for cell-type specificity (Figure 29).

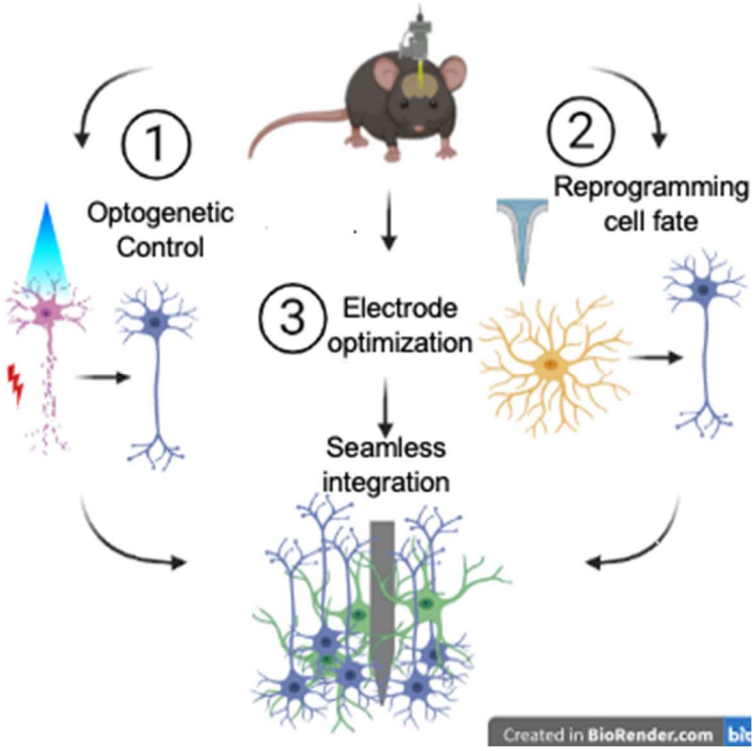

Figure 29. Future work for controlling the tissue-electrode interface. Future work can aim at combining three areas to seamlessly integrate the electrode to the brain tissue, including (1) light-inducible control of the pathways for neural reprogramming, (2) delivering proneural genes to the cells surrounding the implanted device which can be controlled via light (see #1), and (3) utilized next-generation materials that have been optimized to improve tissue response.

5. CHAPTER 5 | Conclusions and future directions

5.1 Conclusions

This dissertation describes in vitro genetic and optical approaches for modifying and controlling the tissue-electrode interface. The studies presented herein used a variety of techniques that encompassed study areas such as neural engineering, molecular biology, neuroscience, and biomaterials. Results obtained from our data collection demonstrate progress towards the control and modification of the interface by successfully differentiating and characterizing rat iPSCs-derived neurons in four substrates, optimizing a blue-light gene expression system and characterizing electrode materials for future use in vivo.

Chapter 2 describes the effects of four substrates on the differentiation of rat iPSC derived-neural progenitor cells. By utilizing these substrates, our aim was to find which candidate (if any) was superior for enriching the differentiating process of progenitor cell environment for promoting maturity in terms of electrical capabilities and morphology. Our results utilizing electrophysiology, immunofluorescence staining, and Sholl analysis demonstrated that there is an influence in polarity and arborization of differentiating neurons in regard to substrate used. Ultimately, gelatin was the least favorable substrate for the growth and differentiation of our cells. This result provides evidence for utilizing a specific substrate to produce a desired unique morphology. More research needs to be done in this area to understand biological mechanisms behind morphological changes in differentiating neural progenitors due to material composition. Key questions for future research include: how does the mechanical properties of the substrate materteral directly affect cell growth patterns? What makes gelatin the better component of the ones tested for NPCs differentiation? How can we modify the substrates further to improve longevity and vitality of NPCs? How does material properties affect potential for action potential firing of NPCs?

In Chapter 3, the optimization of a blue-light gene inducible system is presented. The EL222 system, presented first on Motta-Mena et al., 2014, was successfully utilized for the creation of various mutations and ultimately led to the development of a stably expressing mammalian cell line. The system's response characteristics were explored with respect to different durations and intensities of light exposure, where an interaction was observed. While we did not identify a mutation to optimize light induction, this is a potential area of future inquiry, and the initial results may guide future iterations of the sequence. This data provided a basis for effective generation of a spatial gradient of gene expression, which could be coupled with an implanted micro-LED array. This chapter provides a proof-of-concept for generating a spatial profile of gene expression derived from a light gradient, where future work could leverage this tool to program gene expression profiles. Key steps remain for moving forward into *in vivo* testing, including the addition of new data collection utilizing mammalian primary cells, specifically rat cells for our lab's purpose. Challenges such as delivery of light in a timely fashion and with an effective radius of effect will need to be explored beforehand. *In vivo* experiments should follow after testing on primary cells is successful.

Chapter 4 described various materials for electrode devices including surface coatings and next-generation materials. It also explores of proneural genes to control expression in an injured brain. The EL222 system discussed in Chapter 3 was utilized to robustly express light-induced reporter genes and spatial patterning was also achieved here. The protocol was applied to neural progenitor cells for the expression of NeuroD and Neurog-2 to enhance morphological and electrical maturity of the cells. Results showed successful induction of gene expression which

paves the way for innovative experimentation. Likewise, next-generation flexible arrays incorporating diamond-based sensors have the potential for becoming comparable if not superior to silicon devices due to their high sensitivity, selectivity, and stability. The biocompatibility of a diamond film was assed via an *in vitro* study with primary rat cortical neurons (Fan et al., 2020). These studies, which demonstrate proof-of-concept, provide a foundation for the use of genetic and materials-based engineering to seamlessly integrate implanted electrodes with surrounding brain tissue.

5.2 Future work

The studies shown in this dissertation encompass basic science research required to advance into *in vivo* experiments at the tissue-electrode interface for improvement of neural network formation, excitability, and maturity of cells at the tissue-electrode interface. We are developing techniques derived from molecular biology and biomaterials that can aid in the successful collection of neural signals for long-term purposes. Future research is needed to combine and optimize techniques shown here for them to work most effectively.

5.2.1 Approaches for gene activation control with light

A potential area of future interest is to integrate light-activated gene expression with the use of reprogramming factors. There are possible applications and modifications which could be explored in the future. First, these systems could be activated at the electrode interface using an implanted micro-LED, in order to neighboring cell types. A second or third wavelength of light can be added to enhance to our optogenetic system's capabilities to enhance the range of control and modifications that can be tailored to unique cell types of interest. Various routes can be taken as possible next steps. Firstly, neurons and neural progenitor cells can be targeted with proneural

genes for control (Azemi et al., 2010; E K Purcell et al., 2009). Secondly, reactive astrocytes can be targeted with different reprogramming factors which have been shown to return astrocytes to a reparative or neuronal state at the tissue-electrode interface (Heinrich et al., 2010; Liddelow et al., 2017).

Recent work in the field has guided the utilization of genes such as ASCL1 for reactive astrocyte neuronal reprogramming, NeruoD1 for microglia direct neuronal reprogramming, therefore, an endogenous transcription factor expression can be targeted with light. Additionally, CRISPR-Cas9 system can be utilized to target derived gene activators, similar to Ochoa-Fernandez et al., 2020. A stepwise analysis of the single cell transcriptome and epigenetic profiles of reactive astrocytes and neurons at the electrode-brain interface can shed light on reprogramming paths and mechanisms behind conversion alignment. With this, our engineered optogenetic system can be utilize together by targeting specific genes of interest to study complex cellular processes such as stress response due to electrode implantation, as well as mechanisms behind reactivity. Additionally, while light dissipation through tissue is a concern, new developments have aimed at developing optrodes to successfully achieve the extent light exposure needed for light-inducible gene expression experiments (Khan et al., 2018). Efforts to develop a wireless optoelectode device are underwayand can be adapted to have necessary capabilities for neural simulation (Jia et al., 2020; Stocking et al., 2019).

5.2.2 Methods for delivery of optogenetic system in vivo

Delivery of genetic material or viruses to an in vivo setting has many challenges, particularly in the context of targeting to an implanted electrode array. One alternative to deliver genetic material is by the use of microfluidic channels. It has been shown that at chronic

timepoints issues like biofouling and tissue ingrowth negatively impact the infusion microfluidic channel leading to difficulties for repeated delivery at future timepoints (Jeong et al., 2015). However, our lab has explored various strategies to enable this approach, including the use of a microfluidic device (Winter et al., 2018) custom-fabricated by NeuroNexus. This device has a microfluidic channel along the shank of the electrode that allows for higher delivery precision with lesser damage the tissue. An opportunity to develop new tools to understand tissue-device interactions exist to further efforts for developing next-generation devices which are contingent on manipulating the tissue-electrode interface to revert to their pre-implantation functionality. Even more so, having the ability to track cells in vivo would facilitate our understanding of the tissue-electrode interface. A recent study, by van Dongen et al. shows how positron emission tomography (PET) can be used to detect a single cell and track it over time *in vivo* via intravenous delivery (van Dongen et al., 2020). Similarly, at the time of electrode implantation, optogenetic system can be delivered via optofluidic device or injection and can be tracked over time. We can directly target neurons, reactive astrocytes, and/or microglia and understand their migrating/shifting patterns. By enabling tacking, it would help researchers understand the reasoning behind the effects that take place: loss of recording capabilities, silent neurons, neuronal loss, astrocytic reactivity, etc. This idea, again echoes the possibility of furthering knowledge of how the brain reacts to an electrode, enabling further study.

5.2.3 Utilization of 3D cell culture models, brain in a dish, to bench test prior to animal experiments

An ideal scenario will be for us to obtain an in vitro model of the tissue-electrode interface to have the ability to set many experiments at once and test for many variables. We first will need to assess and perform a gene sequencing analysis to determine genes that are present pre- and post-

implantation (acute and chronic) and understand which genes are being targeted in the neurons for cell health (e.g. find a gene that is downregulated/upregulated after implantation). Additionally, the reactive astrocytes should also be analyzed to obtain knowledge on the factors that induce their reactivity to minimize this. A combination of fluorescence-activated cell sorting (FACS) and RNA sequencing (RNA-seq) can be used to both isolate cells of interest and identify genes that are most strongly differentially expressed. Developing a three-dimensional cell culture model as well as a computational model that mimics the tissue-electrode device environment will be highly beneficial for better understanding what pathways are occurring during implantation and beyond. These techniques could open the door to screening material- and genetic-based modifications in a high-throughput manner.

5.3 Concluding remarks

Based on the developments reported in this dissertation, the development and implementation of these genetic and biomaterial tools can potentially lead to the merging of humans and machines for those who are in need and/or suffer from many neurodegenerative diseases or acquired trauma. These tools can intervene in preventing or minimizing the reactive tissue response to implanted electrodes in the brain as well as improve their functionality, therefore, obtaining stable neural recordings over time is achievable. Here, two approaches were used: a genetic tool to modify gene expression using light and the characterization of various materials for future use in brain electrodes and beyond.

REFERENCES

REFERENCES

Aarum, J., Sandberg, K., Haeberlein, S.L.B., Persson, M.A.A., 2003. Migration and differentiation of neural precursor cells can be directed by microglia. Proc. Natl. Acad. Sci. U. S. A. 100, 15983–15988. https://doi.org/10.1073/pnas.2237050100

Abidian, M.R., Corey, J.M., Kipke, D.R., Martin, D.C., 2010. Conducting-polymer nanotubes improve electrical properties, mechanical adhesion, neural attachment and neurite outgrowth of neural electrodes. Small 6, 421–429. https://doi.org/10.1002/smll.200901868

Abidian, M.R., Ludwig, K.A., Marzullo, T.C., Martin, D.C., Kipke, D.R., 2009. Interfacing conducting polymer nanotubes with the central nervous system: chronic neural recording using poly(3,4-ethylenedioxythiophene) nanotubes. Adv. Mater. 21, 3764–3770. https://doi.org/10.1002/adma.200900887

Abidian, M.R., Martin, D.C., 2009. Multifunctional Nanobiomaterials for Neural Interfaces. Adv. Funct. Mater. 19, 573–585. https://doi.org/10.1002/adfm.200801473

Adewole, D.O., Struzyna, L.A., Harris, J.P., Nemes, A.D., Burrell, J.C., Petrov, D., Kraft, R.H., Chen, H.I., Serruya, M.D., Wolf, J.A., Cullen, D.K., 2018. Optically-Controlled "Living Electrodes" with Long-Projecting Axon Tracts for a Synaptic Brain-Machine Interface. bioRxiv 333526. https://doi.org/10.1101/333526

Ajiboye, A.B., Willett, F.R., Young, D.R., Memberg, W.D., Murphy, B.A., Miller, J.P., Walter, B.L., Sweet, J.A., Hoyen, H.A., Keith, M.W., Peckham, P.H., Simeral, J.D., Donoghue, J.P., Hochberg, L.R., Kirsch, R.F., 2017. Restoration of reaching and grasping movements through brain-controlled muscle stimulation in a person with tetraplegia: a proof-of-concept demonstration. Lancet 389, 1821–1830. https://doi.org/10.1016/S0140-6736(17)30601-3

Akhavan, O., Ghaderi, E., 2013. Differentiation of human neural stem cells into neural networks on graphene nanogrids. J. Mater. Chem. B 1, 6291–6301. https://doi.org/10.1039/c3tb21085e

Akopian, V., Andrews, P.W., Beil, S., Benvenisty, N., Brehm, J., Christie, M., Ford, A., Fox, V., Gokhale, P.J., Healy, L., Holm, F., Hovatta, O., Knowles, B.B., Ludwig, T.E., McKay, R.D.G., Miyazaki, T., Nakatsuji, N., Oh, S.K.W., Pera, M.F., Rossant, J., Stacey, G.N., Suemori, H., 2010. Comparison of defined culture systems for feeder cell free propagation of human embryonic stem cells. Vitr. Cell. Dev. Biol. - Anim. 46, 247–258. https://doi.org/10.1007/s11626-010-9297-z

Aloisi, F., 2001. Immune function of microglia. Glia 36, 165–179. https://doi.org/10.1002/glia.1106

Aregueta-Robles, U.A., Woolley, A.J., Poole-Warren, L.A., Lovell, N.H., Green, R.A., 2014. Organic electrode coatings for next-generation neural interfaces. Front. Neuroeng. 7. https://doi.org/10.3389/fneng.2014.00015

Arulmoli, J., Wright, H.J., Phan, D.T.T., Sheth, U., Que, R.A., Botten, G.A., Keating, M., Botvinick, E.L., Pathak, M.M., Zarembinski, T.I., Yanni, D.S., Razorenova, O. V., Hughes, C.C.W., Flanagan, L.A., 2016. Combination scaffolds of salmon fibrin, hyaluronic acid, and laminin for human neural stem cell and vascular tissue engineering. Acta Biomater. 43, 122–138. https://doi.org/10.1016/j.actbio.2016.07.043

Augustyn, A., Borromeo, M., Wang, T., Fujimoto, J., Shao, C., Dospoy, P.D., Lee, V., Tan, C., Sullivan, J.P., Larsen, J.E., Girard, L., Behrens, C., Wistuba, I.I., Xie, Y., Cobb, M.H., Gazdar, A.F., Johnson, J.E., Minna, J.D., Vogt, P.K., 2014. ASCL1 is a lineage oncogene providing therapeutic targets for high-grade neuroendocrine lung cancers. Proc. Natl. Acad. Sci. U. S. A. 111, 14788–14793. https://doi.org/10.1073/pnas.1410419111

Avior, Y., Sagi, I., Benvenisty, N., 2016. Pluripotent stem cells in disease modelling and drug discovery. Nat. Rev. Mol. Cell Biol. 17, 170–182. https://doi.org/10.1038/nrm.2015.27

Aydin, B., Kakumanu, A., Rossillo, M., Moreno-Estellés, M., Garipler, G., Ringstad, N., Flames, N., Mahony, S., Mazzoni, E.O., 2019. Proneural factors Ascl1 and Neurog2 contribute to neuronal subtype identities by establishing distinct chromatin landscapes. Nat. Neurosci. 22, 897–908. https://doi.org/10.1038/s41593-019-0399-y

Azemi, E., Gobbel, G.T., Cui, X.T., 2010. Seeding neural progenitor cells on silicon-based neural probes: Laboratory investigation. J. Neurosurg. 113, 673–681. https://doi.org/10.3171/2010.1.JNS09313

Baaske, J., Gonschorek, P., Engesser, R., Dominguez-Monedero, A., Raute, K., Fischbach, P., Müller, K., Cachat, E., Schamel, W.W.A., Minguet, S., Davies, J.A., Timmer, J., Weber, W., Zurbriggen, M.D., 2018. Dual-controlled optogenetic system for the rapid down-regulation of protein levels in mammalian cells. Sci. Rep. 8. https://doi.org/10.1038/s41598-018-32929-7

Badea, T.C., Wang, Y., Nathans, J., 2003. A noninvasive genetic/pharmacologic strategy for visualizing cell morphology and clonal relationships in the mouse. J. Neurosci. 23, 2314–2322. https://doi.org/10.1523/jneurosci.23-06-02314.2003

Bahmad, H., Hadadeh, O., Chamaa, F., Cheaito, K., Darwish, B., Makkawi, A.-K., Abou-Kheir, W., 2017. Modeling Human Neurological and Neurodegenerative Diseases: From Induced Pluripotent Stem Cells to Neuronal Differentiation and Its Applications in Neurotrauma. Front. Mol. Neurosci. 10, 50. https://doi.org/10.3389/fnmol.2017.00050

Bedell, H.W., Schaub, N.J., Capadona, J.R., Ereifej, E.S., 2020. Differential expression of genes involved in the acute innate immune response to intracortical microelectrodes. Acta Biomater. 102, 205–219. https://doi.org/10.1016/j.actbio.2019.11.017

Bernstein, J., 1868. Ueber den zeitlichen Verlauf der negativen Schwankung des Nervenstroms. Pflüger, Arch. für die Gesammte Physiol. des Menschen und der Thiere 1, 173–207. https://doi.org/10.1007/BF01640316

Bertrand, N., Castro, D.S., Guillemot, F., 2002. Proneural genes and the specification of neural

cell types. Nat. Rev. Neurosci. https://doi.org/10.1038/nrn874

Beyer, H.M., Naumann, S., Weber, W., Radziwill, G., 2015. Optogenetic control of signaling in mammalian cells. Biotechnol. J. 10, 273–283. https://doi.org/10.1002/biot.201400077

Bezuidenhout, D., Oosthuysen, A., Davies, N., Ahrenstedt, L., Dobner, S., Roberts, P., Zilla, P., 2013. Covalent incorporation and controlled release of active dexamethasone from injectable polyethylene glycol hydrogels. J. Biomed. Mater. Res. - Part A 101 A, 1311–1318. https://doi.org/10.1002/jbm.a.34438

Bhandari, R., 2009. A novel masking method for high aspect ratio penetrating microelectrode arrays Related content. https://doi.org/10.1088/0960-1317/19/3/035004

Biran, R., Martin, D.C., Tresco, P.A., 2005. Neuronal cell loss accompanies the brain tissue response to chronically implanted silicon microelectrode arrays. Exp. Neurol. 195, 115–126. https://doi.org/10.1016/j.expneurol.2005.04.020

Blümcke, I., Becker, A.J., Normann, S., Hans, V., Riederer, B.M., Krajewski, S., Wiestler, O.D., Reifenberger, G., 2001. Distinct expression pattern of microtubule-associated protein-2 in human oligodendrogliomas and glial precursor cells. J. Neuropathol. Exp. Neurol. 60, 984–93. https://doi.org/10.1093/jnen/60.10.984

Boni, R., Ali, A., Shavandi, A., Clarkson, A.N., 2018. Current and novel polymeric biomaterials for neural tissue engineering. J. Biomed. Sci. https://doi.org/10.1186/s12929-018-0491-8

Boyden, E.S., Zhang, F., Bamberg, E., Nagel, G., Deisseroth, K., 2005. Millisecond-timescale, genetically targeted optical control of neural activity. Nat. Neurosci. 8, 1263–1268. https://doi.org/10.1038/nn1525

Buckley, C.E., Moore, R.E., Reade, A., Goldberg, A.R., Weiner, O.D., Clarke, J.D.W., 2016. Reversible Optogenetic Control of Subcellular Protein Localization in a Live Vertebrate Embryo. Dev. Cell 36, 117–126. https://doi.org/10.1016/j.devcel.2015.12.011

Buehr, M., Meek, S., Blair, K., Yang, J., Ure, J., Silva, J., McLay, R., Hall, J., Ying, Q.-L., Smith, A., 2008. Capture of authentic embryonic stem cells from rat blastocysts. Cell 135, 1287–98. https://doi.org/10.1016/j.cell.2008.12.007

Buffo, A., Rolando, C., Ceruti, S., 2010. Astrocytes in the damaged brain: Molecular and cellular insights into their reactive response and healing potential. Biochem. Pharmacol. https://doi.org/10.1016/j.bcp.2009.09.014

Cai, H., Devreotes, P.N., 2011. Moving in the right direction: How eukaryotic cells migrate along chemical gradients. Semin. Cell Dev. Biol. 22, 834–841. https://doi.org/10.1016/J.SEMCDB.2011.07.020

Carlson, C., Devinsky, O., 2009. The excitable cerebral cortex. Fritsch G, Hitzig E. Über die elektrische Erregbarkeit des Grosshirns. Arch Anat Physiol Wissen 1870;37:300-32. Epilepsy Behav. 15, 131–132. https://doi.org/10.1016/j.yebeh.2009.03.002

Carter, M.E., De Lecea, L., 2011. Optogenetic investigation of neural circuits in vivo. Trends Mol. Med. 17, 197–206. https://doi.org/10.1016/j.molmed.2010.12.005

Castagnola, V., Descamps, E., Lecestre, A., Dahan, L., Remaud, J., Nowak, L.G., Bergaud, C., 2015. Parylene-based flexible neural probes with PEDOT coated surface for brain stimulation and recording. Biosens. Bioelectron. 67, 450–457. https://doi.org/10.1016/j.bios.2014.09.004

Castro, D.S., Martynoga, B., Parras, C., Ramesh, V., Pacary, E., Johnston, C., Drechsel, D., Lebel-Potter, M., Garcia, L.G., Hunt, C., Dolle, D., Bithell, A., Ettwiller, L., Buckley, N., Guillemot, F., 2011. A novel function of the proneural factor Ascl1 in progenitor proliferation identified by genome-wide characterization of its targets. Genes Dev. 25, 930–945. https://doi.org/10.1101/gad.627811

Castro, D.S., Skowronska-Krawczyk, D., Armant, O., Donaldson, I.J., Parras, C., Hunt, C., Critchley, J.A., Nguyen, L., Gossler, A., Göttgens, B., Matter, J.M., Guillemot, F., 2006. Proneural bHLH and Brn Proteins Coregulate a Neurogenic Program through Cooperative Binding to a Conserved DNA Motif. Dev. Cell 11, 831–844. https://doi.org/10.1016/j.devcel.2006.10.006

Chang, M.-Y., Kim, D., Kim, C.-H., Kang, H.-C., Yang, E., Moon, J.-I., Ko, S., Park, J., Park, K.-S., Lee, K.-A., Hwang, D.-Y., Chung, Y., Lanza, R., Kim, K.-S., 2010. Direct Reprogramming of Rat Neural Precursor Cells and Fibroblasts into Pluripotent Stem Cells. PLoS One 5, e9838. https://doi.org/10.1371/journal.pone.0009838

Chen, S., Weitemier, A.Z., Zeng, X., He, L., Wang, X., Tao, Y., Huang, A.J.Y., Hashimotodani, Y., Kano, M., Iwasaki, H., Parajuli, L.K., Okabe, S., Loong Teh, D.B., All, A.H., Tsutsui-Kimura, I., Tanaka, K.F., Liu, X., McHugh, T.J., 2018. Near-infrared deep brain stimulation via upconversion nanoparticle–mediated optogenetics. Science (80-.). 359, 679–684. https://doi.org/10.1126/science.aaq1144

Chung, J.E., Joo, H.R., Fan, J.L., Liu, D.F., Barnett, A.H., Chen, S., Geaghan-Breiner, C., Karlsson, M.M.P., Karlsson, M.M.P., Lee, K.Y., Liang, H., Magland, J.F., Pebbles, J.A., Tooker, A.C., Greengard, L.F., Tolosa, V.M., Frank, L.M., 2019. High-Density, Long-Lasting, and Multi-region Electrophysiological Recordings Using Polymer Electrode Arrays. Neuron 101, 21-31.e5. https://doi.org/10.1016/j.neuron.2018.11.002

Churchland, M.M., Shenoy, K. V., 2007. Temporal complexity and heterogeneity of single-neuron activity in premotor and motor cortex. J. Neurophysiol. 97, 4235–4257. https://doi.org/10.1152/jn.00095.2007

Crick, F., 1999. The impact of molecular biology on neuroscience. Philos. Trans. R. Soc. B Biol. Sci. 354, 2021–2025. https://doi.org/10.1098/rstb.1999.0541

Deisseroth, K., 2011. Optogenetics. Nat. Methods 8, 26–29. https://doi.org/10.1038/nmeth.f.324

Demers, S.-P., Yoo, J.G., Lian, L., Therrien, J., Smith, L.C., 2007. Rat Embryonic Stem-Like (ES-Like) Cells Can Contribute to Extraembryonic Tissues *In Vivo*. Cloning Stem Cells 9, 512–522. https://doi.org/10.1089/clo.2007.0029

Dimmeler, S., Ding, S., Rando, T.A., Trounson, A., 2014. Translational strategies and challenges in regenerative medicine. Nat. Med. https://doi.org/10.1038/nm.3627

Doll, T., Meichsner, M., Riederer, B.M., Honegger, P., Matus, A., 1993. An isoform of microtubule-associated protein 2 (MAP2) containing four repeats of the tubulin-binding motif. J. Cell Sci. 106 (Pt 2), 633–9.

Eles, J.R., Vazquez, A.L., Kozai, T.D.Y., Cui, X.T., 2018. In vivo imaging of neuronal calcium during electrode implantation: Spatial and temporal mapping of damage and recovery. Biomaterials 174, 79–94. https://doi.org/10.1016/J.BIOMATERIALS.2018.04.043

Eles, J.R., Vazquez, A.L., Snyder, N.R., Lagenaur, C., Murphy, M.C., Kozai, T.D.Y., Cui, X.T., 2017. Neuroadhesive L1 coating attenuates acute microglial attachment to neural electrodes as revealed by live two-photon microscopy. Biomaterials 113, 279–292. https://doi.org/10.1016/j.biomaterials.2016.10.054

Ereifej, E.S., Rial, G.M., Hermann, J.K., Smith, C.S., Meade, S.M., Rayyan, J.M., Chen, K., Feng, H., Capadona, J.R., 2018. Implantation of neural probes in the brain elicits oxidative stress. Front. Bioeng. Biotechnol. 6. https://doi.org/10.3389/fbioe.2018.00009

Faiz, M., Sachewsky, N., Gascón, S., Bang, K.W.A., Morshead, C.M., Nagy, A., 2015. Adult Neural Stem Cells from the Subventricular Zone Give Rise to Reactive Astrocytes in the Cortex after Stroke. Cell Stem Cell 17, 624–634. https://doi.org/10.1016/j.stem.2015.08.002

Fan, B., Rusinek, C.A., Thompson, C.H., Setien, M., Guo, Y., Rechenberg, R., Gong, Y., Weber, A.J., Becker, M.F., Purcell, E., Li, W., Li wenli, W., 2020. Flexible, Diamond-based Microelectrodes Fabricated Using the Diamond Flexible, Diamond-based Microelectrodes Fabricated Using the Diamond Growth Side for Neural Sensing. https://doi.org/10.1038/s41378-020-0155-1

Fattahi, P., Yang, G., Kim, G., Abidian, M.R., 2014. A Review of Organic and Inorganic Biomaterials for Neural Interfaces. Adv. Mater. 26, 1846–1885. https://doi.org/10.1002/adma.201304496

Ferreira, L.M.R., Mostajo-Radji, M.A., 2013. How induced pluripotent stem cells are redefining personalized medicine. Gene. https://doi.org/10.1016/j.gene.2013.02.037

Ferrier, D., 1873. Experimental researches in cerebral physiology and pathology. Br. Med. J. 1, 457. https://doi.org/10.1136/bmj.1.643.457

Flanagan, L.A., Rebaza, L.M., Derzic, S., Schwartz, P.H., Monuki, E.S., 2006. Regulation of human neural precursor cells by laminin and integrins. J. Neurosci. Res. 83, 845–856. https://doi.org/10.1002/jnr.20778

Fode, C., Ma, Q., Casarosa, S., Ang, S.L., Anderson, D.J., Guillemot, F., 2000. A role for neural determination genes in specifying the dorsoventral identity of telencephalic neurons. Genes Dev. 14, 67–80. https://doi.org/10.1101/gad.14.1.67

Formosa-Jordan, P.A.U., Ibañes, M., Ares, S., Frade, J.M., 2013. Lateral inhibition and neurogenesis: Novel aspects in motion. Int. J. Dev. Biol. https://doi.org/10.1387/ijdb.120259jf

Gage, F.H., Temple, S., 2013. Neural Stem Cells: Generating and Regenerating the Brain. Neuron 80, 588–601. https://doi.org/10.1016/j.neuron.2013.10.037

Gagnon-Turcotte, G., LeChasseur, Y., Bories, C., Messaddeq, Y., De Koninck, Y., Gosselin, B., 2017. A Wireless Headstage for Combined Optogenetics and Multichannel Electrophysiological Recording. IEEE Trans. Biomed. Circuits Syst. 11, 1–14. https://doi.org/10.1109/TBCAS.2016.2547864

Garner, C.C., Matus, A., 1988. Different forms of microtubule-associated protein 2 are encoded by separate mRNA transcripts. J. Cell Biol. 106, 779–783. https://doi.org/10.1083/jcb.106.3.779

Ge, H., Tan, L., Wu, P., Yin, Y., Liu, X., Meng, H., Cui, G., Wu, N., Lin, J., Hu, R., Feng, H., 2015. Poly-L-ornithine promotes preferred differentiation of neural stem/progenitor cells via ERK signalling pathway. Sci. Rep. 5, 15535. https://doi.org/10.1038/srep15535

Ge, W., He, F., Kim, K.J., Blanchi, B., Coskun, V., Nguyen, L., Wu, X., Zhao, J., Heng, J.I.T., Martinowich, K., Tao, J., Wu, H., Castro, D., Sobeih, M.M., Corfas, G., Gleeson, J.G., Greenberg, M.E., Guillemot, F., Sun, Y.E., 2006. Coupling of cell migration with neurogenesis by proneural bHLH factors. Proc. Natl. Acad. Sci. U. S. A. 103, 1319–1324. https://doi.org/10.1073/pnas.0510419103

Georgopoulos, A.P., Kalaska, J.F., Caminiti, R., Massey, J.T., 1982. On the relations between the direction of two-dimensional arm movements and cell discharge in primate motor cortex. J. Neurosci. 2, 1527–1537. https://doi.org/10.1523/jneurosci.02-11-01527.1982

Georgopoulos, A.P., Schwartz, A.B., Kettner, R.E., 1986. Neuronal population coding of movement direction. Science (80-.). 233, 1416–1419. https://doi.org/10.1126/science.3749885

Gerhardt, K.P., Olson, E.J., Castillo-Hair, S.M., Hartsough, L.A., Landry, B.P., Ekness, F., Yokoo, R., Gomez, E.J., Ramakrishnan, P., Suh, J., Savage, D.F., Tabor, J.J., 2016. An open-hardware platform for optogenetics and photobiology. Sci. Rep. 6, 35363. https://doi.org/10.1038/srep35363

Goding, J., Gilmour, A., Robles, U.A., Poole-Warren, L., Lovell, N., Martens, P., Green, R., 2017. A living electrode construct for incorporation of cells into bionic devices. MRS Commun. 7, 487–495. https://doi.org/10.1557/mrc.2017.44

Gordon, J., Amini, S., White, M.K., 2013. General overview of neuronal cell culture. Methods Mol. Biol. https://doi.org/10.1007/978-1-62703-640-5_1

Gossen, M., Bujardt, H., 1992. Tight control of gene expression in mammalian cells by tetracycline-responsive promoters. Cell Biol. J. Gehring 89, 5547–5551.

Green, J.D., 1958. A simple microelectrode for recording from the central nervous system. Nature 182, 962. https://doi.org/10.1038/182962a0

Green, R., Abidian, M.R., 2015. Conducting Polymers for Neural Prosthetic and Neural Interface Applications. https://doi.org/10.1002/adma.201501810

Green, R.A., Lim, K.S., Henderson, W.C., Hassarati, R.T., Martens, P.J., Lovell, N.H., Poole-Warren, L.A., 2013. Living electrodes: Tissue engineering the neural interface, in: Proceedings of the Annual International Conference of the IEEE Engineering in Medicine and Biology Society, EMBS. pp. 6957–6960. https://doi.org/10.1109/EMBC.2013.6611158

Green, R.A., Lovell, N.H., Wallace, G.G., Poole-Warren, L.A., 2008. Conducting polymers for neural interfaces: Challenges in developing an effective long-term implant. Biomaterials 29, 3393–3399. https://doi.org/10.1016/j.biomaterials.2008.04.047

Griffith, R.W., Humphrey, D.R., 2006. Long-term gliosis around chronically implanted platinum electrodes in the Rhesus macaque motor cortex. Neurosci. Lett. 406, 81–86. https://doi.org/10.1016/j.neulet.2006.07.018

Guillemot, F., Hassan, B.A., 2017. Beyond proneural: emerging functions and regulations of proneural proteins. Curr. Opin. Neurobiol. https://doi.org/10.1016/j.conb.2016.11.011

Guo, J., Anton, E.S., 2014. Decision making during interneuron migration in the developing cerebral cortex. Trends Cell Biol. 24, 342–51. https://doi.org/10.1016/j.tcb.2013.12.001

Guo, Z., Zhang, L., Wu, Z., Chen, Y., Wang, F., Chen, G., 2014. In vivo direct reprogramming of reactive glial cells into functional neurons after brain injury and in an Alzheimer's disease model. Cell Stem Cell 14, 188–202. https://doi.org/10.1016/j.stem.2013.12.001

Gutowski, S.M., Shoemaker, J.T., Templeman, K.L., Wei, Y., Latour, R.A., Bellamkonda, R. V., LaPlaca, M.C., García, A.J., 2015. Protease-degradable PEG-maleimide coating with on-demand release of IL-1Ra to improve tissue response to neural electrodes. Biomaterials 44, 55–70. https://doi.org/10.1016/j.biomaterials.2014.12.009

Hall, P.E., Lathia, J.D., Caldwell, M.A., Ffrench-Constant, C., 2008. Laminin enhances the growth of human neural stem cells in defined culture media. BMC Neurosci. 9, 71. https://doi.org/10.1186/1471-2202-9-71

Hamanaka, S., Yamaguchi, T., Kobayashi, T., Kato-Itoh, M., Yamazaki, S., Sato, H., Umino, A., Wakiyama, Y., Arai, M., Sanbo, M., Hirabayashi, M., Nakauchi, H., 2011. Generation of Germline-Competent Rat Induced Pluripotent Stem Cells. PLoS One 6, e22008. https://doi.org/10.1371/journal.pone.0022008

Hand, R., Bortone, D., Mattar, P., Nguyen, L., Heng, J.I.T., Guerrier, S., Boutt, E., Peters, E., Barnes, A.P., Parras, C., Schuurmans, C., Guillemot, F., Polleux, F., 2005. Phosphorylation of neurogenin2 specifies the migration properties and the dendritic morphology of pyramidal neurons in the neocortex. Neuron 48, 45–62. https://doi.org/10.1016/j.neuron.2005.08.032

Haque, A., Adnan, N., Motazedian, A., Akter, F., Hossain, S., Kutsuzawa, K., Nag, K., Kobatake, E., Akaike, T., 2015. An engineered N-cadherin substrate for differentiation, survival, and selection of pluripotent stem cell-derived neural progenitors. PLoS One 10. https://doi.org/10.1371/journal.pone.0135170

Hara, S.A., Kim, B.J., Kuo, J.T.W., Lee, C.D., Meng, E., Pikov, V., 2016. Long-term stability of intracortical recordings using perforated and arrayed Parylene sheath electrodes. J. Neural Eng. 13, 066020. https://doi.org/10.1088/1741-2560/13/6/066020

Harnett, E.M., Alderman, J., Wood, T., 2007. The surface energy of various biomaterials coated with adhesion molecules used in cell culture. Colloids Surfaces B Biointerfaces 55, 90–97. https://doi.org/10.1016/j.colsurfb.2006.11.021

Hatsopoulos, N.G., Suminski, A.J., 2011. Sensing with the motor cortex. Neuron. https://doi.org/10.1016/j.neuron.2011.10.020

He, W., McConnell, G.C., Schneider, T.M., Bellamkonda, R.V., 2007. A Novel Anti-inflammatory Surface for Neural Electrodes. Adv. Mater. 19, 3529–3533. https://doi.org/10.1002/adma.200700943

Heinrich, C., Blum, R., Gascón, S., Masserdotti, G., Tripathi, P., Sánchez, R., Tiedt, S., Schroeder, T., Götz, M., Berninger, B., 2010. Directing astroglia from the cerebral cortex into subtype specific functional neurons. PLoS Biol. 8, e1000373. https://doi.org/10.1371/journal.pbio.1000373

Hochberg, L.R., Bacher, D., Jarosiewicz, B., Masse, N.Y., Simeral, J.D., Vogel, J., Haddadin, S., Liu, J., Cash, S.S., Van Der Smagt, P., Donoghue, J.P., 2012. Reach and grasp by people with tetraplegia using a neurally controlled robotic arm. Nature 485, 372–375. https://doi.org/10.1038/nature11076

Hochberg, L.R., Serruya, M.D., Friehs, G.M., Mukand, J.A., Saleh, M., Caplan, A.H., Branner, A., Chen, D., Penn, R.D., Donoghue, J.P., 2006. Neuronal ensemble control of prosthetic devices by a human with tetraplegia. Nature 442, 164–171. https://doi.org/10.1038/nature04970

Hodgkin, A.L., Huxley, A.F., 1952. A quantitative description of membrane current and its application to conduction and excitation in nerve. J. Physiol. 117, 500–544. https://doi.org/10.1113/jphysiol.1952.sp004764

Hong, G., Lieber, C.M., 2019. Novel electrode technologies for neural recordings. Nat. Rev. Neurosci. https://doi.org/10.1038/s41583-019-0140-6

Hoogerwerf, A.C., Wise, K.D., 1994. A Three-Dimensional Microelectrode Array for Chronic Neural Recording. IEEE Trans. Biomed. Eng. 41, 1136–1146. https://doi.org/10.1109/10.335862

Hughes, C.S., Postovit, L.M., Lajoie, G.A., 2010. Matrigel: a complex protein mixture required for optimal growth of cell culture. Proteomics 10, 1886–1890.

https://doi.org/10.1002/pmic.200900758

Iannaccone, P.M., Jacob, H.J., 2009. Rats! Dis. Model. Mech. 2, 206–10. https://doi.org/10.1242/dmm.002733

Iijima, M., Huang, Y.E., Devreotes, P., 2002. Temporal and Spatial Regulation of Chemotaxis. Dev. Cell 3, 469–478. https://doi.org/10.1016/S1534-5807(02)00292-7

Illes, S., Theiss, S., Hartung, H.P., Siebler, M., Dihné, M., 2009. Niche-dependent development of functional neuronal networks from embryonic stem cell-derived neural populations. BMC Neurosci. 10. https://doi.org/10.1186/1471-2202-10-93

Izant, J.G., McIntosh, J.R., 1980. Microtubule-associated proteins: a monoclonal antibody to MAP2 binds to differentiated neurons. Proc. Natl. Acad. Sci. U. S. A. 77, 4741–4745. https://doi.org/10.1073/pnas.77.8.4741

Janssens, R., Struyf, S., Proost, P., 2018. The unique structural and functional features of CXCL12. Cell. Mol. Immunol. 15, 299–311. https://doi.org/10.1038/cmi.2017.107

Jeong, J.-W., McCall, J.G., Shin, G., Zhang, Y., Al-Hasani, R., Kim, M., Li, S., Sim, J.Y., Jang, K.-I., Shi, Y., Hong, D.Y., Liu, Y., Schmitz, G.P., Xia, L., He, Z., Gamble, P., Ray, W.Z., Huang, Y., Bruchas, M.R., Rogers, J.A., 2015. Wireless Optofluidic Systems for Programmable In Vivo Pharmacology and Optogenetics. Cell 162, 662–674. https://doi.org/10.1016/j.cell.2015.06.058

Jia, Y., Gong, Y., Weber, A., Li, W., Ghovanloo, M., 2020. A mm-Sized Free-Floating Wireless Implantable Opto-Electro Stimulation Device. Micromachines 11, 621. https://doi.org/10.3390/mi11060621

Johnson, S.L., Eckrich, T., Kuhn, S., Zampini, V., Franz, C., Ranatunga, K.M., Roberts, T.P., Masetto, S., Knipper, M., Kros, C.J., Marcotti, W., 2011. Position-dependent patterning of spontaneous action potentials in immature cochlear inner hair cells. Nat. Neurosci. 14, 711–717. https://doi.org/10.1038/nn.2803

Johnson, G. V, Jope, R.S., 1992. The role of microtubule-associated protein 2 (MAP-2) in neuronal growth, plasticity, and degeneration. J. Neurosci. Res. 33, 505–12. https://doi.org/10.1002/jnr.490330402

Jones, K.S., Connor, B.J., 2016. The Effect of Pro-Neurogenic Gene Expression on Adult Subventricular Zone Precursor Cell Recruitment and Fate Determination After Excitotoxic Brain Injury. J. Stem Cells Regen. Med. 12, 25–35.

Jun, J.J., Steinmetz, N.A., Siegle, J.H., Denman, D.J., Bauza, M., Barbarits, B., Lee, A.K., Anastassiou, C.A., Andrei, A., Aydın, Ç., Barbic, M., Blanche, T.J., Bonin, V., Couto, J., Dutta, B., Gratiy, S.L., Gutnisky, D.A., Häusser, M., Karsh, B., Ledochowitsch, P., Lopez, C.M., Mitelut, C., Musa, S., Okun, M., Pachitariu, M., Putzeys, J., Rich, P.D., Rossant, C., Sun, W., Svoboda, K., Carandini, M., Harris, K.D., Koch, C., O'Keefe, J., Harris, T.D., 2017. Fully integrated silicon probes for high-density recording of neural activity. Nature 551, 232–

236. https://doi.org/10.1038/nature24636

KA, L., NB, L., MD, J., SM, R.-B., JL, H., DR, K., 2011. Poly(3,4-ethylenedioxythiophene) (PEDOT) Polymer Coatings Facilitate Smaller Neural Recording Electrodes. J. Neural Eng. 8. https://doi.org/10.1088/1741-2560/8/1/014001

Keefer, E.W., Botterman, B.R., Romero, M.I., Rossi, A.F., Gross, G.W., 2008. Carbon nanotube coating improves neuronal recordings. Nat. Nanotechnol. 3, 434–439. https://doi.org/10.1038/nnano.2008.174

Kennedy, M.J., Hughes, R.M., Peteya, L.A., Schwartz, J.W., Ehlers, M.D., Tucker, C.L., 2010. Rapid blue-light–mediated induction of protein interactions in living cells. Nat. Methods 7, 973–975. https://doi.org/10.1038/nmeth.1524

Khan, W., Setien, M., Purcell, E., Li, W., 2018. Micro-Reflector Integrated Multichannel μLED Optogenetic Neurostimulator With Enhanced Intensity. Front. Mech. Eng. 4, 17. https://doi.org/10.3389/fmech.2018.00017

Khodagholy, D., Gelinas, J.N., Thesen, T., Doyle, W., Devinsky, O., Malliaras, G.G., Buzsáki, G., 2015. NeuroGrid: recording action potentials from the surface of the brain. Nat. Neurosci. 18, 310–315. https://doi.org/10.1038/nn.3905

Kim, J., Efe, J. a, Zhu, S., Talantova, M., Yuan, X., Wang, S., Lipton, S. a, 2011. Direct reprogramming of mouse fibroblasts to neural progenitors Normal and neoplastic nonstem cells can spontaneously convert to a stem-like state. Pnas 108, 7838–7843. https://doi.org/10.1073/pnas.1103113108/-/DCSupplemental.www.pnas.org/cgi/doi/10.1073/pnas.1103113108

Kim, S.U., de Vellis, J., 2009. Stem cell-based cell therapy in neurological diseases: A review. J. Neurosci. Res. 87, 2183–2200. https://doi.org/10.1002/jnr.22054

Kim, T., McCall, J.G., Jung, Y.H., Huang, X., Siuda, E.R., Li, Y., Song, J., Song, Y.M., Pao, H.A., Kim, R.-H., Lu, C., Lee, S.D., Song, I.-S., Shin, G., Al-Hasani, R., Kim, S., Tan, M.P., Huang, Y., Omenetto, F.G., Rogers, J.A., Bruchas, M.R., 2013. Injectable, cellular-scale optoelectronics with applications for wireless optogenetics. Science 340, 211–6. https://doi.org/10.1126/science.1232437

Kim, Y.H., Baek, N.S., Han, Y.H., Chung, M.A., Jung, S.D., 2011. Enhancement of neuronal cell adhesion by covalent binding of poly-d-lysine. J. Neurosci. Methods 202, 38–44. https://doi.org/10.1016/j.jneumeth.2011.08.036

Kipke, D.R., Vetter, R.J., Williams, J.C., Hetke, J.F., 2003. Silicon-substrate intracortical microelectrode arrays for long-term recording of neuronal spike activity in cerebral cortex. IEEE Trans. Neural Syst. Rehabil. Eng. 11, 151–155. https://doi.org/10.1109/TNSRE.2003.814443

Kolar, K., Weber, W., 2017. Synthetic biological approaches to optogenetically control cell signaling. Curr. Opin. Biotechnol. 47, 112–119.

https://doi.org/10.1016/J.COPBIO.2017.06.010

Kolarcik, C.L., Bourbeau, D., Azemi, E., Rost, E., Zhang, L., Lagenaur, C.F., Weber, D.J., Cui, X.T., 2012. In vivo effects of L1 coating on inflammation and neuronal health at the electrode-tissue interface in rat spinal cord and dorsal root ganglion. Acta Biomater. 8, 3561–3575. https://doi.org/10.1016/j.actbio.2012.06.034

Komura, T., Kato, K., Konagaya, S., Nakaji-Hirabayashi, T., Iwata, H., 2015. Optimization of surface-immobilized extracellular matrices for the proliferation of neural progenitor cells derived from induced pluripotent stem cells. Biotechnol. Bioeng. 112, 2388–2396. https://doi.org/10.1002/bit.25636

Konermann, S., Brigham, M.D., Trevino, A., Hsu, P.D., Heidenreich, M., Le Cong, Platt, R.J., Scott, D.A., Church, G.M., Zhang, F., 2013. Optical control of mammalian endogenous transcription and epigenetic states. Nature. https://doi.org/10.1038/nature12466

Kozai, T.D.Y., Catt, K., Li, X., Gugel, Z. V., Olafsson, V.T., Vazquez, A.L., Cui, X.T., 2015. Mechanical failure modes of chronically implanted planar silicon-based neural probes for laminar recording. Biomaterials 37, 25–39. https://doi.org/10.1016/j.biomaterials.2014.10.040

Kozai, T.D.Y., Langhals, N.B., Patel, P.R., Deng, X., Zhang, H., Smith, K.L., Lahann, J., Kotov, N.A., Kipke, D.R., Yoshida Kozai, T.D., Langhals, N.B., Patel, P.R., Deng, X., Zhang, H., Smith, K.L., Lahann, J., Kotov, N.A., Kipke, D.R., Kozai, T.D.Y., Langhals, N.B., Patel, P.R., Deng, X., Zhang, H., Smith, K.L., Lahann, J., Kotov, N.A., Kipke, D.R., Yoshida Kozai, T.D., Langhals, N.B., Patel, P.R., Deng, X., Zhang, H., Smith, K.L., Lahann, J., Kotov, N.A., Kipke, D.R., 2012. Ultrasmall implantable composite microelectrodes with bioactive surfaces for chronic neural interfaces. Nat. Mater. 11, 1065–1073. https://doi.org/10.1038/nmat3468

Kronenberg, G., Gertz, K., Cheung, G., Buffo, A., Kettenmann, H., Götz, M., Endres, M., 2010. Modulation of fate determinants olig2 and pax6 in resident glia evokes spiking neuroblasts in a model of mild brain ischemia. Stroke 41, 2944–2949. https://doi.org/10.1161/STROKEAHA.110.583039

Krüger, J., Bach, M., 1981. Simultaneous recording with 30 microelectrodes in monkey visual cortex. Exp. Brain Res. 41, 191–194. https://doi.org/10.1007/BF00236609

Kshitiz, Park, J., Kim, P., Helen, W., Engler, A.J., Levchenko, A., Kim, D.H., 2012. Control of stem cell fate and function by engineering physical microenvironments. Integr. Biol. (United Kingdom). https://doi.org/10.1039/c2ib20080e

Kwon, K.Y., Lee, H.M., Ghovanloo, M., Weber, A., Li, W., 2015. Design, fabrication, and packaging of an integrated, wirelessly-powered optrode array for optogenetics application. Front. Syst. Neurosci. 9, 1–12. https://doi.org/10.3389/fnsys.2015.00069

Labno, C., n.d. Two Ways to Count Cells with ImageJ [WWW Document]. URL http://rsbweb.nih.gov/ij/docs/index.html. (accessed 1.2.19).

Lacomme, M., Liaubet, L., Pituello, F., Bel-Vialar, S., 2012. NEUROG2 Drives Cell Cycle Exit of Neuronal Precursors by Specifically Repressing a Subset of Cyclins Acting at the G1 and S Phases of the Cell Cycle. Mol. Cell. Biol. 32, 2596–2607. https://doi.org/10.1128/mcb.06745-11

Laxton, A.W., Tang-Wai, D.F., McAndrews, M.P., Zumsteg, D., Wennberg, R., Keren, R., Wherrett, J., Naglie, G., Hamani, C., Smith, G.S., Lozano, A.M., 2010. A phase I trial of deep brain stimulation of memory circuits in Alzheimer's disease. Ann. Neurol. 68, 521–534. https://doi.org/10.1002/ana.22089

Lebedev, M.A., Nicolelis, M.A.L., 2006. Brain-machine interfaces: past, present and future. Trends Neurosci. https://doi.org/10.1016/j.tins.2006.07.004

Levskaya, A., Weiner, O.D., Lim, W.A., Voigt, C.A., 2009. Spatiotemporal control of cell signalling using a light-switchable protein interaction. Nature 461, 997–1001. https://doi.org/10.1038/nature08446

Li, N., Zhang, Q., Gao, S., Song, Q., Huang, R., Wang, L., Liu, L., Dai, J., Tang, M., Cheng, G., 2013. Three-dimensional graphene foam as a biocompatible and conductive scaffold for neural stem cells. Sci. Rep. 3. https://doi.org/10.1038/srep01604

Li, W., Wei, W., Zhu, S., Zhu, J., Shi, Y., Lin, T., Hao, E., Hayek, A., Deng, H., Ding, S., 2009. Generation of Rat and Human Induced Pluripotent Stem Cells by Combining Genetic Reprogramming and Chemical Inhibitors. Cell Stem Cell 4, 16–19. https://doi.org/10.1016/J.STEM.2008.11.014

Li, Y., Gautam, A., Yang, J., Qiu, L., Melkoumian, Z., Weber, J., Telukuntla, L., Srivastava, R., Whiteley, E.M., Brandenberger, R., 2013. Differentiation of oligodendrocyte progenitor cells from human embryonic stem cells on vitronectin-derived synthetic peptide acrylate surface. Stem Cells Dev. 22, 1497–1505. https://doi.org/10.1089/scd.2012.0508

Li, Z., Araoka, T., Wu, J., Liao, H.K., Li, M., Lazo, M., Zhou, B., Sui, Y., Wu, M.Z., Tamura, I., Xia, Y., Beyret, E., Matsusaka, T., Pastan, I., Rodriguez Esteban, C., Guillen, I., Guillen, P., Campistol, J.M., Izpisua Belmonte, J.C., 2016. 3D Culture Supports Long-Term Expansion of Mouse and Human Nephrogenic Progenitors. Cell Stem Cell 19, 516–529. https://doi.org/10.1016/j.stem.2016.07.016

Liao, J., Cui, C., Chen, S., Ren, J., Chen, J., 2009. Generation of induced pluripotent stem cell lines from adult rat cells. Cell Stem Cell 4.

Liddelow, S.A., Guttenplan, K.A., Clarke, L.E., Bennett, F.C., Bohlen, C.J., Schirmer, L., Bennett, M.L., Münch, A.E., Chung, W.-S., Peterson, T.C., Wilton, D.K., Frouin, A., Napier, B.A., Panicker, N., Kumar, M., Buckwalter, M.S., Rowitch, D.H., Dawson, V.L., Dawson, T.M., Stevens, B., Barres, B.A., 2017. Neurotoxic reactive astrocytes are induced by activated microglia. Nature 541, 481–487. https://doi.org/10.1038/nature21029

Liu, J., Fu, T.-M., Cheng, Z., Hong, G., Zhou, T., Jin, L., Duvvuri, M., Jiang, Z., Kruskal, P., Xie, C., Suo, Z., Fang, Y., Lieber, C.M., 2015. Syringe-injectable electronics. Nat. Nanotechnol.

10, 629–636. https://doi.org/10.1038/nnano.2015.115

Liu, R.-H., Morassutti, D.J., Whittemore, S.R., Sosnowski, J.S., Magnuson, D.S.K., 1999. Electrophysiological Properties of Mitogen-Expanded Adult Rat Spinal Cord and Subventricular Zone Neural Precursor Cells. Exp. Neurol. 158, 143–154. https://doi.org/10.1006/exnr.1999.7078

Lledo, P.-M.M., Alonso, M., Grubb, M.S., 2006. Adult neurogenesis and functional plasticity in neuronal circuits. Nat. Rev. Neurosci. 7, 179–193. https://doi.org/10.1038/nrn1867

Lo, L., Dormand, E., Greenwood, A., Anderson, D.J., 2002. Comparison of the generic neuronal differentiation and neuron subtype specification functions of mammalian achaete-scute and atonal homologs in cultured neural progenitor cells. Development 129, 1553–67. https://doi.org/10.1038/nrn874

Lu, P., Jones, L.L., Snyder, E.Y., Tuszynski, M.H., 2003. Neural stem cells constitutively secrete neurotrophic factors and promote extensive host axonal growth after spinal cord injury. Exp. Neurol. 181, 115–129. https://doi.org/10.1016/S0014-4886(03)00037-2

Luan, L., Wei, X., Zhao, Z., Siegel, J.J., Potnis, O., Tuppen, C.A., Lin, S., Kazmi, S., Fowler, R.A., Holloway, S., Dunn, A.K., Chitwood, R.A., Xie, C., 2017. Ultraflexible nanoelectronic probes form reliable, glial scar–free neural integration. Sci. Adv. 3, e1601966. https://doi.org/10.1126/sciadv.1601966

Ma, Q., Fode, C., Guillemot, F., Anderson, D.J., 1999. NEUROGENIN1 and NEUROGENIN2 control two distinct waves of neurogenesis in developing dorsal root ganglia. Genes Dev. 13, 1717–1728. https://doi.org/10.1101/gad.13.13.1717

Mammadov, B., Sever, M., Guler, M.O., Tekinay, A.B., 2013. Neural differentiation on synthetic scaffold materials. Biomater. Sci. https://doi.org/10.1039/c3bm60150a

Martin, G.R., 1981. Isolation of a pluripotent cell line from early mouse embryos cultured in medium conditioned by teratocarcinoma stem cells. Proc. Natl. Acad. Sci. U. S. A. 78, 7634–7638. https://doi.org/10.1073/pnas.78.12.7634

Masserdotti, G., Gillotin, S., Sutor, B., Drechsel, D., Irmler, M., Jørgensen, H.F., Sass, S., Theis, F.J., Beckers, J., Berninger, B., Guillemot, F., Götz, M., 2015. Transcriptional Mechanisms of Proneural Factors and REST in Regulating Neuronal Reprogramming of Astrocytes. Cell Stem Cell 17, 74–88. https://doi.org/10.1016/j.stem.2015.05.014

Matveev, M. V., Erofeev, A.I., Terekhin, S.G., Plotnikova, P. V., Vorobyov, K. V., Vlasova, O.L., 2015. Implantable devices for optogenetic studies and stimulation of excitable tissue. St. Petersbg. Polytech. Univ. J. Phys. Math. 1, 264–271. https://doi.org/10.1016/J.SPJPM.2015.12.004

McAlinden, N., Cheng, Y., Scharf, R., Xie, E., Gu, E., Reiche, C.F., Sharma, R., Tathireddy, P., Dawson, M.D., Rieth, L., Blair, S., Mathieson, K., 2019. Multisite microLED optrode array for neural interfacing. Neurophotonics 6, 1. https://doi.org/10.1117/1.nph.6.3.035010

McNay, D.E.G., Pelling, M., Claxton, S., Guillemot, F., Ang, S.L., 2006. Mash1 is required for generic and subtype differentiation of hypothalamic neuroendocrine cells. Mol. Endocrinol. 20, 1623–1632. https://doi.org/10.1210/me.2005-0518

Mercanzini, A., Reddy, S.T., Velluto, D., Colin, P., Maillard, A., Bensadoun, J.-C., Hubbell, J.A., Renaud, P., 2010. Controlled release nanoparticle-embedded coatings reduce the tissue reaction to neuroprostheses. J. Control. Release 145, 196–202. https://doi.org/10.1016/j.jconrel.2010.04.025

Merkl, C., Saalfrank, A., Riesen, N., Kühn, R., Pertek, A., 2013. Efficient generation of rat induced pluripotent stem cells using a non-viral inducible vector. PLoS One 8.

Ming, G., Song, H., 2005. Adult neurogenesis in the mammalian central nervous system. Annu. Rev. Neurosci. 28, 223–50. https://doi.org/10.1146/annurev.neuro.28.051804.101459

Moore, D.R., Shannon, R. V., 2009. Beyond cochlear implants: Awakening the deafened brain. Nat. Neurosci. https://doi.org/10.1038/nn.2326

Moshayedi, P., Ng, G., Kwok, J.C.F., Yeo, G.S.H., Bryant, C.E., Fawcett, J.W., Franze, K., Guck, J., 2014. The relationship between glial cell mechanosensitivity and foreign body reactions in the central nervous system. Biomaterials 35, 3919–3925. https://doi.org/10.1016/j.biomaterials.2014.01.038

Moss, J., Ryder, T., Aziz, T.Z., Graeber, M.B., Bain, P.G., 2004. Electron microscopy of tissue adherent to explanted electrodes in dystonia and Parkinson's disease. Brain 127, 2755–63. https://doi.org/10.1093/brain/awh292

Motta-Mena, L.B., Reade, A., Mallory, M.J., Glantz, S., Weiner, O.D., Lynch, K.W., Gardner, K.H., 2014. An optogenetic gene expression system with rapid activation and deactivation kinetics. Nat. Chem. Biol. 10, 196–202. https://doi.org/10.1038/nchembio.1430

Muller, K., Engesser, R., Schulz, S., Steinberg, T., Tomakidi, P., Weber, C.C., Ulm, R., Timmer, J., Zurbriggen, M.D., Weber, W., 2013. Multi-chromatic control of mammalian gene expression and signaling. Nucleic Acids Res. 41, e124–e124. https://doi.org/10.1093/nar/gkt340

Murase, S., Horwitz, A.F., 2004. Directions in Cell Migration Along the Rostral Migratory Stream: The Pathway for Migration in the Brain. Curr. Top. Dev. Biol. 61, 135–152. https://doi.org/10.1016/S0070-2153(04)61006-4

Nakajima, M., Ishimuro, T., Kato, K., Ko, I.K., Hirata, I., Arima, Y., Iwata, H., 2007. Combinatorial protein display for the cell-based screening of biomaterials that direct neural stem cell differentiation. Biomaterials 28, 1048–1060. https://doi.org/10.1016/j.biomaterials.2006.10.004

Nash, A.I., McNulty, R., Shillito, M.E., Swartz, T.E., Bogomolni, R.A., Luecke, H., Gardner, K.H., 2011. Structural basis of photosensitivity in a bacterial light-oxygen-voltage/ helix-turn-helix (LOV-HTH) DNA-binding protein. Proc. Natl. Acad. Sci. U. S. A. 108, 9449–

9454. https://doi.org/10.1073/pnas.1100262108

Nicolelis, M.A.L., 2001. Actions from thoughts. Nature. https://doi.org/10.1038/35053191

Nieto, M., Schuurmans, C., Britz, O., Guillemot, F., 2001. Neural bHLH genes control the neuronal versus glial fate decision in cortical progenitors. Neuron 29, 401–413. https://doi.org/10.1016/S0896-6273(01)00214-8

Nishio, J.N., 2000. Why are higher plants green? Evolution of the higher plant photosynthetic pigment complement. Plant, Cell Environ. 23, 539–548. https://doi.org/10.1046/j.1365-3040.2000.00563.x

Nordhausen, C.T., Maynard, E.M., Normann, R.A., 1996. Single unit recording capabilities of a 100 microelectrode array, Brain Research.

Oakes, R.S., Polei, M.D., Skousen, J.L., Tresco, P.A., 2018. An astrocyte derived extracellular matrix coating reduces astrogliosis surrounding chronically implanted microelectrode arrays in rat cortex. Biomaterials 154, 1–11. https://doi.org/10.1016/j.biomaterials.2017.10.001

Ochoa-Fernandez, R., Abel, N.B., Wieland, F.G., Schlegel, J., Koch, L.A., Miller, J.B., Engesser, R., Giuriani, G., Brandl, S.M., Timmer, J., Weber, W., Ott, T., Simon, R., Zurbriggen, M.D., 2020. Optogenetic control of gene expression in plants in the presence of ambient white light. Nat. Methods 17, 717–725. https://doi.org/10.1038/s41592-020-0868-y

Okabe, S., Forsberg-Nilsson, K., Spiro, A.C., Segal, M., McKay, R.D.G., 1996. Development of neuronal precursor cells and functional postmitotic neurons from embryonic stem cells in vitro. Mech. Dev. 59, 89–102. https://doi.org/10.1016/0925-4773(96)00572-2

Ourednik, J., Ourednik, V., Lynch, W.P., Schachner, M., Snyder, E.Y., 2002. Neural stem cells display an inherent mechanism for rescuing dysfunctional neurons. Nat. Biotechnol. 20, 1103–1110. https://doi.org/10.1038/nbt750

Oxley, T.J., Opie, N.L., John, S.E., Rind, G.S., Ronayne, S.M., Wheeler, T.L., Judy, J.W., McDonald, A.J., Dornom, A., Lovell, T.J.H., Steward, C., Garrett, D.J., Moffat, B.A., Lui, E.H., Yassi, N., Campbell, B.C. V, Wong, Y.T., Fox, K.E., Nurse, E.S., Bennett, I.E., Bauquier, S.H., Liyanage, K.A., van der Nagel, N.R., Perucca, P., Ahnood, A., Gill, K.P., Yan, B., Churilov, L., French, C.R., Desmond, P.M., Horne, M.K., Kiers, L., Prawer, S., Davis, S.M., Burkitt, A.N., Mitchell, P.J., Grayden, D.B., May, C.N., O'Brien, T.J., 2016. Minimally invasive endovascular stent-electrode array for high-fidelity, chronic recordings of cortical neural activity. Nat. Biotechnol. 34, 320–327. https://doi.org/10.1038/nbt.3428

Parras, C.M., Schuurmans, C., Scardigli, R., Kim, J., Anderson, D.J., Guillemot, F., 2002. Divergent functions of the proneural genes Mash1 and Ngn2 in the specification of neuronal subtype identity. Genes Dev. 16, 324–338. https://doi.org/10.1101/gad.940902

Perge, J.A., Homer, M.L., Malik, W.Q., Cash, S., Eskandar, E., Friehs, G., Donoghue, J.P., Hochberg, L.R., 2013. Intra-day signal instabilities affect decoding performance in an intracortical neural interface system. J. Neural Eng. 10, 036004.

https://doi.org/10.1088/1741-2560/10/3/036004

Pires, F., Ferreira, Q., Rodrigues, C.A.V., Morgado, J., Ferreira, F.C., 2015. Neural stem cell differentiation by electrical stimulation using a cross-linked PEDOT substrate: Expanding the use of biocompatible conjugated conductive polymers for neural tissue engineering. Biochim. Biophys. Acta - Gen. Subj. 1850, 1158–1168. https://doi.org/10.1016/j.bbagen.2015.01.020

Poitras, L., Ghanem, N., Hatch, G., Ekker, M., 2007. The proneural determinant MASH1 regulates forebrain Dlx1/2 expression through the l12b intergenic enhancer. Development 134, 1755–1765. https://doi.org/10.1242/dev.02845

Polikov, V.S., Tresco, P.A., Reichert, W.M., 2005. Response of brain tissue to chronically implanted neural electrodes. J. Neurosci. Methods 148, 1–18. https://doi.org/10.1016/J.JNEUMETH.2005.08.015

Polstein, L.R., Gersbach, C.A., 2015. A light-inducible CRISPR-Cas9 system for control of endogenous gene activation. Nat. Chem. Biol. 11, 198–200. https://doi.org/10.1038/nchembio.1753

Polstein, L.R., Juhas, M., Hanna, G., Bursac, N., Gersbach, C.A., 2017. An Engineered Optogenetic Switch for Spatiotemporal Control of Gene Expression, Cell Differentiation, and Tissue Morphogenesis. ACS Synth. Biol. 6, 2003–2013. https://doi.org/10.1021/acssynbio.7b00147

Prasad, A., Xue, Q.-S., Sankar, V., Nishida, T., Shaw, G., Streit, W.J., Sanchez, J.C., 2012. Comprehensive characterization and failure modes of tungsten microwire arrays in chronic neural implants. J. Neural Eng. 9, 056015. https://doi.org/10.1088/1741-2560/9/5/056015

Purcell, E.K., Naim, Y., Yang, A., Leach, M.K., Velkey, J.M., Duncan, R.K., Corey, J.M., 2012. Combining Topographical and Genetic Cues to Promote Neuronal Fate Specification in Stem Cells. Biomacromolecules 13, 3427–3438. https://doi.org/10.1021/bm301220k

Purcell, E K, Seymour, J.P., Yandamuri, S., Kipke, D.R., 2009. *In vivo* evaluation of a neural stem cell-seeded prosthesis. J. Neural Eng. 6, 026005. https://doi.org/10.1088/1741-2560/6/2/026005

Purcell, Erin K., Thompson, D.E., Ludwig, K.A., Kipke, D.R., 2009. Flavopiridol reduces the impedance of neural prostheses in vivo without affecting recording quality. J. Neurosci. Methods 183, 149–157. https://doi.org/10.1016/j.jneumeth.2009.06.026

Purcell, E.K., Yang, A., Liu, L., Velkey, J.M., Morales, M.M., Duncan, R.K., 2013. BDNF profoundly and specifically increases KCNQ4 expression in neurons derived from embryonic stem cells. Stem Cell Res. 10, 29–35. https://doi.org/10.1016/j.scr.2012.08.005

Ramón y Cajal, S., 1888. Sobre las fibras nerviosas de la capa molecular del cerebelo. Rev. Trim. Histol. Norm. Patol 1, 33–49.

Reade, A., Motta-Mena, L.B., Gardner, K.H., Stainier, D.Y., Weiner, O.D., Woo, S., 2017. TAEL:

A zebrafish-optimized optogenetic gene expression system with fine spatial and temporal control. Dev. 144, 345–355. https://doi.org/10.1242/dev.139238

Rejali, D., Lee, V.A., Abrashkin, K.A., Humayun, N., Swiderski, D.L., Raphael, Y., 2007. Cochlear implants and ex vivo BDNF gene therapy protect spiral ganglion neurons. Hear. Res. 228, 180–187. https://doi.org/10.1016/j.heares.2007.02.010

Reynolds, B.A., Weiss, S., 1992. Generation of neurons and astrocytes from isolated cells of the adult mammalian central nervous system. Science (80-.). 255, 1707–1710. https://doi.org/10.1126/science.1553558

Richter, A., Kruse, C., Moser, A., Hofmann, U.G., Danner, S., 2011. Cellular modulation of polymeric device surfaces: Promise of adult stem cells for neuro-prosthetics. Front. Neurosci. 5, 114. https://doi.org/10.3389/fnins.2011.00114

Riederer, B.M., 1995. Development of the Axonal and Dendritic Cytoskeleton. Adv. Mol. Cell Biol. 12, 107–142. https://doi.org/10.1016/S1569-2558(08)60261-1

Rivera-Cancel, G., Motta-Mena, L.B., Gardner, K.H., 2012. Identification of natural and artificial DNA substrates for light-activated LOV-HTH transcription factor EL222. Biochemistry 51, 10024–10034. https://doi.org/10.1021/bi301306t

Roca-Cusachs, P., Sunyer, R., Trepat, X., 2013. Mechanical guidance of cell migration: lessons from chemotaxis. Curr. Opin. Cell Biol. 25, 543–549. https://doi.org/10.1016/J.CEB.2013.04.010

Roitbak, T., Syková, E., 1999. Diffusion barriers evoked in the rat cortex by reactive astrogliosis. Glia 28, 40–48. https://doi.org/10.1002/(SICI)1098-1136(199910)28:1<40::AID-GLIA5>3.0.CO;2-6

Rosin, B., Slovik, M., Mitelman, R., Rivlin-Etzion, M., Haber, S.N., Israel, Z., Vaadia, E., Bergman, H., 2011. Closed-loop deep brain stimulation is superior in ameliorating parkinsonism. Neuron 72, 370–384. https://doi.org/10.1016/j.neuron.2011.08.023

Ross, S.E., Greenberg, M.E., Stiles, C.D., 2003. Basic helix-loop-helix factors in cortical development. Neuron. https://doi.org/10.1016/S0896-6273(03)00365-9

Rosser, A.E., Tyers, P., Ter Borg, M., Dunnett, S.B., Svendsen, C.N., 1997. Co-expression of MAP-2 and GFAP in cells developing from rat EGF responsive precursor cells. Dev. Brain Res. 98, 291–295. https://doi.org/10.1016/S0165-3806(96)00189-7

Rousche, P.J., Normann, R.A., 1999. Chronic intracortical microstimulation (ICMS) of cat sensory cortex using the utah intracortical electrode array. IEEE Trans. Rehabil. Eng. 7, 56–68. https://doi.org/10.1109/86.750552

Rousche, P.J., Pellinen, D.S., Pivin, D.P., Williams, J.C., Vetter, R.J., Kipke, D.R., 2001. Flexible polyimide-based intracortical electrode arrays with bioactive capability. IEEE Trans. Biomed. Eng. 48, 361–370. https://doi.org/10.1109/10.914800

Royer, S., Zemelman, B. V., Barbic, M., Losonczy, A., Buzsáki, G., Magee, J.C., 2010. Multi-array silicon probes with integrated optical fibers: light-assisted perturbation and recording of local neural circuits in the behaving animal. Eur. J. Neurosci. 31, 2279–2291. https://doi.org/10.1111/j.1460-9568.2010.07250.x

Rusinek, C.A., Guo, Y., Rechenberg, R., Becker, M.F., Purcell, E., Verber, M., McKinney, C., Li, W., 2018. All-Diamond Microfiber Electrodes for Neurochemical Analysis. J. Electrochem. Soc. 165, G3087–G3092. https://doi.org/10.1149/2.0141812jes

Saito, N., Kawai, K., Nowak, T.S., 1995. Reexpression of Developmentally Regulated MAP2c mRNA after Ischemia: Colocalization with hsp72 mRNA in Vulnerable Neurons. J. Cereb. Blood Flow Metab. 15, 205–215. https://doi.org/10.1038/jcbfm.1995.26

Salatino, J.W., Ludwig, K.A., Kozai, T.D.Y., Purcell, E.K., 2017a. Glial responses to implanted electrodes in the brain. Nat. Biomed. Eng. 1, 862–877. https://doi.org/10.1038/s41551-017-0154-1

Salatino, J.W., Winter, B.M., Drazin, M.H., Purcell, E.K., 2017b. Functional remodeling of subtype-specific markers surrounding implanted neuroprostheses. J. Neurophysiol. 118, 194–202. https://doi.org/10.1152/jn.00162.2017

Schiavone, P., Chassat, F., Boudou, T., Promayon, E., Valdivia, F., Payan, Y., 2009. In vivo measurement of human brain elasticity using a light aspiration device. Med. Image Anal. 13, 673–678. https://doi.org/10.1016/j.media.2009.04.001

Schmidt, E.M., McIntosh, J.S., Durelli, L., Bak, M.J., 1978. Fine control of operantly conditioned firing patterns of cortical neurons. Exp. Neurol. 61, 349–369. https://doi.org/10.1016/0014-4886(78)90252-2

Schneider, C.A., Rasband, W.S., Eliceiri, K.W., 2012. NIH Image to ImageJ: 25 years of image analysis. Nat. Methods. https://doi.org/10.1038/nmeth.2089

Seibt, J., Schuurmans, C., Gradwhol, G., Dehay, C., Vanderhaeghen, P., Guillemot, F., Polleux, F., 2003. Neurogenin2 specifies the connectivity of thalamic neurons by controlling axon responsiveness to intermediate target cues. Neuron 39, 439–452. https://doi.org/10.1016/S0896-6273(03)00435-5

Sellgren, C.M., Sheridan, S.D., Gracias, J., Xuan, D., Fu, T., Perlis, R.H., 2017. Patient-specific models of microglia-mediated engulfment of synapses and neural progenitors. Mol. Psychiatry 22, 170–177. https://doi.org/10.1038/mp.2016.220

Senut, M.-C., Sen, A., Cingolani, P., Shaik, A., Land, S.J., Ruden, D.M., 2014. Lead exposure disrupts global DNA methylation in human embryonic stem cells and alters their neuronal differentiation. Toxicol. Sci. 139, 142–61. https://doi.org/10.1093/toxsci/kfu028

Serruya, M.D., Harris, J.P., Adewole, D.O., Struzyna, L.A., Burrell, J.C., Nemes, A., Petrov, D., Kraft, R.H., Chen, H.I., Wolf, J.A., Cullen, D.K., 2018. Engineered Axonal Tracts as "Living Electrodes" for Synaptic-Based Modulation of Neural Circuitry. Adv. Funct. Mater. 28,

1701183. https://doi.org/10.1002/adfm.201701183

Seymour, J.P., Kipke, D.R., 2007. Neural probe design for reduced tissue encapsulation in CNS. Biomaterials 28, 3594–3607. https://doi.org/10.1016/J.BIOMATERIALS.2007.03.024

Seymour, J.P., Wu, F., Wise, K.D., Yoon, E., 2017. State-of-the-art MEMS and microsystem tools for brain research. Microsystems Nanoeng. 3, 16066. https://doi.org/10.1038/micronano.2016.66

Sharma, S., 2018. Glassy Carbon: A promising material for microand nanomanufacturing. Materials (Basel). https://doi.org/10.3390/ma11101857

Shihabuddin, L.S., Ray, J., Gage, F.H., 1997. FGF-2 is sufficient to isolate progenitors found in the adult mammalian spinal cord. Exp. Neurol. 148, 577–586. https://doi.org/10.1006/exnr.1997.6697

Shin, G., Gomez, A.M., Al-Hasani, R., Jeong, Y.R., Kim, J., Xie, Z., Banks, A., Lee, S.M., Han, S.Y., Yoo, C.J., Lee, J.-L., Lee, S.H., Kurniawan, J., Tureb, J., Guo, Z., Yoon, J., Park, S.-I., Bang, S.Y., Nam, Y., Walicki, M.C., Samineni, V.K., Mickle, A.D., Lee, K., Heo, S.Y., McCall, J.G., Pan, T., Wang, L., Feng, X., Kim, T.-I., Kim, J.K., Li, Y., Huang, Y., Gereau, R.W., Ha, J.S., Bruchas, M.R., Rogers, J.A., 2017. Flexible Near-Field Wireless Optoelectronics as Subdermal Implants for Broad Applications in Optogenetics. Neuron 93, 509-521.e3. https://doi.org/10.1016/j.neuron.2016.12.031

Simeral, J.D., Kim, S.P., Black, M.J., Donoghue, J.P., Hochberg, L.R., 2011. Neural control of cursor trajectory and click by a human with tetraplegia 1000 days after implant of an intracortical microelectrode array, in: Journal of Neural Engineering. https://doi.org/10.1088/1741-2560/8/2/025027

Soltani, M.H., Pichardo, R., Song, Z., Sangha, N., Camacho, F., Satyamoorthy, K., Sangueza, O.P., Setaluri, V., 2005. Microtubule-associated protein 2, a marker of neuronal differentiation, induces mitotic defects, inhibits growth of melanoma cells, and predicts metastatic potential of cutaneous melanoma. Am. J. Pathol. 166, 1841–1850. https://doi.org/10.1016/S0002-9440(10)62493-5

Song, L., Yuan, X., Jones, Z., Griffin, K., Zhou, Y., Ma, T., Li, Y., 2019. Assembly of Human Stem Cell-Derived Cortical Spheroids and Vascular Spheroids to Model 3-D Brain-like Tissues. Sci. Rep. 9. https://doi.org/10.1038/s41598-019-42439-9

Stieglitz, T., Ruf, H., Gross, M., Schuettler, M., Meyer, J.U., 2002. A biohybrid system to interface peripheral nerves after traumatic lesions: Design of a high channel sieve electrode. Biosens. Bioelectron. 17, 685–696. https://doi.org/10.1016/S0956-5663(02)00019-2

Stocking, K.C., Vazquez, A.L., Kozai, T.D.Y., 2019. Intracortical Neural Stimulation with Untethered, Ultrasmall Carbon Fiber Electrodes Mediated by the Photoelectric Effect. IEEE Trans. Biomed. Eng. 66, 2402–2412. https://doi.org/10.1109/TBME.2018.2889832

Strand, B.L., Gåserød, O., Kulseng, B., Espevik, T., Skjåk-Bræk, G., 2002. Alginate-polylysine-

alginate microcapsules: Effect of size reduction on capsule properties. J. Microencapsul. 19, 615–630. https://doi.org/10.1080/02652040210144243

Strickland, D., Lin, Y., Wagner, E., Hope, C.M., Zayner, J., Antoniou, C., Sosnick, T.R., Weiss, E.L., Glotzer, M., 2012. TULIPs: tunable, light-controlled interacting protein tags for cell biology. Nat. Methods 9, 379–384. https://doi.org/10.1038/nmeth.1904

Strumwasser, F., 1958. Long-term recording from single neurons in brain of unrestrained mammals. Science (80-.). 127, 469–470. https://doi.org/10.1126/science.127.3296.469

Suminski, A.J., Tkach, D.C., Fagg, A.H., Hatsopoulos, N.G., 2010. Incorporating feedback from multiple sensory modalities enhances brain-machine interface control. J. Neurosci. 30, 16777–16787. https://doi.org/10.1523/JNEUROSCI.3967-10.2010

Sun, W., Kim, H., Moon, Y., 2010. Control of neuronal migration through rostral migration stream in mice. Anat. Cell Biol. 43, 269. https://doi.org/10.5115/acb.2010.43.4.269

Swaney, K.F., Huang, C.-H., Devreotes, P.N., 2010. Eukaryotic Chemotaxis: A Network of Signaling Pathways Controls Motility, Directional Sensing, and Polarity. Annu. Rev. Biophys. 39, 265–289. https://doi.org/10.1146/annurev.biophys.093008.131228

Szabo, V., Ventalon, C., De Sars, V., Bradley, J., Emiliani, V., 2014. Spatially Selective Holographic Photoactivation and Functional Fluorescence Imaging in Freely Behaving Mice with a Fiberscope. Neuron 84, 1157–1169. https://doi.org/10.1016/j.neuron.2014.11.005

Tabar, V., Studer, L., 2014. Pluripotent stem cells in regenerative medicine: challenges and recent progress. Nat. Rev. Genet. 15, 82–92. https://doi.org/10.1038/nrg3563

Takahashi, K., Tanabe, K., Ohnuki, M., Narita, M., Ichisaka, T., Tomoda, K., Yamanaka, S., 2007. Induction of Pluripotent Stem Cells from Adult Human Fibroblasts by Defined Factors. Cell 131, 861–872. https://doi.org/10.1016/j.cell.2007.11.019

Takahashi, Kazutoshi, Yamanaka, S., 2006. Induction of pluripotent stem cells from mouse embryonic and adult fibroblast cultures by defined factors. Cell 126, 663–676. https://doi.org/10.1016/J.CELL.2006.07.024

Takahashi, K, Yamanaka, S., 2006. Induction of pluripotent stem cells from mouse embryonic and adult fibroblast cultures by defined factors. Cell 126.

Taslimi, A., Zoltowski, B., Miranda, J.G., Pathak, G.P., Hughes, R.M., Tucker, C.L., 2016. Optimized second-generation CRY2–CIB dimerizers and photoactivatable Cre recombinase. Nat. Chem. Biol. 12, 425–430. https://doi.org/10.1038/nchembio.2063

Thompson, C.H., Khan, S.A., Khan, W.A., Li, W., Purcell, E.K., 2017. Neuronal excitability and network formation on optically transparent electrode materials, in: 2017 8th International IEEE/EMBS Conference on Neural Engineering (NER). IEEE, pp. 154–157. https://doi.org/10.1109/NER.2017.8008315

Thompson, C.H., Riggins, T.E., Patel, P.R., Chestek, C.A., Li, W., Purcell, E., 2020. Toward guiding principles for the design of biologically-integrated electrodes for the central nervous system. J. Neural Eng. 17, 021001. https://doi.org/10.1088/1741-2552/ab7030

Tien, L.W., Wu, F., Tang-Schomer, M.D., Yoon, E., Omenetto, F.G., Kaplan, D.L., 2013. Silk as a Multifunctional Biomaterial Substrate for Reduced Glial Scarring around Brain-Penetrating Electrodes. Adv. Funct. Mater. 23, 3185–3193. https://doi.org/10.1002/adfm.201203716

Tischer, D., Weiner, O.D., 2014. Illuminating cell signalling with optogenetic tools. Nat. Rev. Mol. Cell Biol. 15, 551–8. https://doi.org/10.1038/nrm3837

Tong, M., Hernandez, J.L., Purcell, E.K., Altschuler, R.A., Duncan, R.K., 2010. The intrinsic electrophysiological properties of neurons derived from mouse embryonic stem cells overexpressing neurogenin-1. Am. J. Physiol. Physiol. 299, C1335–C1344. https://doi.org/10.1152/ajpcell.00207.2010

Ueda, S., Kawamata, M., Teratani, T., Shimizu, T., Tamai, Y., Ogawa, H., Hayashi, K., Tsuda, H., Ochiya, T., 2008. Establishment of Rat Embryonic Stem Cells and Making of Chimera Rats. PLoS One 3, e2800. https://doi.org/10.1371/journal.pone.0002800

van Dongen, G.A.M.S., Boellaard, R., Vugts, D.J., 2020. In vivo tracking of single cells with PET. Nat. Biomed. Eng. https://doi.org/10.1038/s41551-020-0598-6

Vetter, R.J., Williams, J.C., Hetke, J.F., Nunamaker, E.A., Kipke, D.R., 2004. Chronic neural recording using silicon-substrate microelectrode arrays implanted in cerebral cortex. IEEE Trans. Biomed. Eng. 51, 896–904. https://doi.org/10.1109/TBME.2004.826680

Wang, F., 2009. The signaling mechanisms underlying cell polarity and chemotaxis. Cold Spring Harb. Perspect. Biol. 1, a002980. https://doi.org/10.1101/cshperspect.a002980

Wang, X., Chen, X., Yang, Y., 2012. Spatiotemporal control of gene expression by a light-switchable transgene system. Nat. Methods 9, 266–269. https://doi.org/10.1038/nmeth.1892

Ware, M., Hamdi-Rozé, H., Le Friec, J., David, V., Dupé, V., 2016. Regulation of downstream neuronal genes by proneural transcription factors during initial neurogenesis in the vertebrate brain. Neural Dev. 11, 22. https://doi.org/10.1186/s13064-016-0077-7

Ware, T., Simon, D., Arreaga-Salas, D.E., Reeder, J., Rennaker, R., Keefer, E.W., Voit, W., 2012. Fabrication of Responsive, Softening Neural Interfaces. Adv. Funct. Mater. 22, 3470–3479. https://doi.org/10.1002/adfm.201200200

Ware, T., Simon, D., Liu, C., Musa, T., Vasudevan, S., Sloan, A., Keefer, E.W., Rennaker, R.L., Voit, W., 2014. Thiol-ene/acrylate substrates for softening intracortical electrodes. J. Biomed. Mater. Res. - Part B Appl. Biomater. 102, 1–11. https://doi.org/10.1002/jbmb.32946

Wei, X., Luan, L., Zhao, Z., Li, X., Zhu, H., Potnis, O., Xie, C., 2018. Nanofabricated Ultraflexible Electrode Arrays for High-Density Intracortical Recording. Adv. Sci. 5, 1700625. https://doi.org/10.1002/advs.201700625

Welkenhuysen, M., Hoffman, L., Luo, Z., De Proft, A., Van Den Haute, C., Baekelandt, V., Debyser, Z., Gielen, G., Puers, R., 2016a. An integrated multi-electrode- optrode array for in vitro optogenetics. Nat. Publ. Gr. https://doi.org/10.1038/srep20353

Welkenhuysen, M., Hoffman, L., Luo, Z., De Proft, A., Van Den Haute, C., Baekelandt, V., Debyser, Z., Gielen, G., Puers, R., Braeken, D., 2016b. An integrated multi-electrode-optrode array for in vitro optogenetics. Sci. Rep. 6, 1–10. https://doi.org/10.1038/srep20353

Wellman, S.M., Kozai, T.D.Y., 2017. Understanding the Inflammatory Tissue Reaction to Brain Implants To Improve Neurochemical Sensing Performance. ACS Chem. Neurosci. 8, 2578–2582. https://doi.org/10.1021/acschemneuro.7b00403

Wilson, S.W., Rubenstein, J.L.R., 2000. Induction and dorsoventral patterning of the telencephalon. Neuron. https://doi.org/10.1016/S0896-6273(00)00171-9

Winter, B., Daniels, S., Salatino, J., Purcell, E., 2018. Genetic Modulation at the Neural Microelectrode Interface: Methods and Applications. Micromachines 9, 476. https://doi.org/10.3390/mi9100476

Winter, B.M., Setien, M.B., Salatino, J.W., Blanke, N., Thompson, C.H., Smith, K.R., Khan, W.A., Li, W., Suhr, S.T., Purcell, E.K., 2017. Control of cell fate and excitability at the neural electrode interface: Genetic reprogramming and optical induction, in: 2017 IEEE Life Sciences Conference (LSC). IEEE, pp. 157–161. https://doi.org/10.1109/LSC.2017.8268167

Wu, Y.I., Frey, D., Lungu, O.I., Jaehrig, A., Schlichting, I., Kuhlman, B., Hahn, K.M., 2009. A genetically encoded photoactivatable Rac controls the motility of living cells. Nature 461, 104–108. https://doi.org/10.1038/nature08241

Xu, H., Weltman, A., Hsiao, M.C., Scholten, K., Meng, E., Berger, T.W., Song, D., 2015. Design of a flexible parylene-based multi-electrode array for multi-region recording from the rat hippocampus, in: Proceedings of the Annual International Conference of the IEEE Engineering in Medicine and Biology Society, EMBS. Institute of Electrical and Electronics Engineers Inc., pp. 7139–7142. https://doi.org/10.1109/EMBC.2015.7320038

Yamamoto, H., Hirata, Y., 1995. Biodegradation of the Cross-Linked Cationic Poly(amino acid) Hydrogels by Proteolytic Enzymes. Macromolecules 28, 6701–6704. https://doi.org/10.1021/ma00124a002

Yamanaka, S., 2009. A Fresh Look at iPS Cells. Cell. https://doi.org/10.1016/j.cell.2009.03.034

Yang, S., Edman, L.C., Sánchez-Alcañiz, J.A., Fritz, N., Bonilla, S., Hecht, J., Uhlén, P., Pleasure, S.J., Villaescusa, J.C., Marín, O., Arenas, E., 2013. Cxcl12/Cxcr4 signaling controls the migration and process orientation of A9-A10 dopaminergic neurons. Dev. 140, 4554–4564. https://doi.org/10.1242/dev.098145

Yizhar, O., Fenno, L.E.E., Davidson, T.J.J., Mogri, M., Deisseroth, K., 2011. No Title. Neuron 71, 9–34. https://doi.org/10.1016/j.neuron.2011.06.004

Yogev, S., Shen, K., 2017. Establishing Neuronal Polarity with Environmental and Intrinsic Mechanisms. Neuron 96, 638–650. https://doi.org/10.1016/j.neuron.2017.10.021

Zhou, F.M., Hablitz, J.J., 1996. Postnatal development of membrane properties of layer I neurons in rat neocortex. J. Neurosci. 16, 1131–9.

Zoltowski, B.D., Motta-Mena, L.B., Gardner, K.H., 2013. Blue light-induced dimerization of a bacterial LOV-HTH DNA-binding protein. Biochemistry 52, 6653–61. https://doi.org/10.1021/bi401040m

Zoltowski, B.D., Nash, A.I., Gardner, K.H., 2011. Variations in Protein–Flavin Hydrogen Bonding in a Light, Oxygen, Voltage Domain Produce Non-Arrhenius Kinetics of Adduct Decay. Biochemistry 50, 8771–8779. https://doi.org/10.1021/bi200976a